UNIVERSITY OF BIRMINGHAM

The Mechanical and Tribological Properties of PEEK Gears

By

Thomas James Hoskins

A thesis submitted to the University of Birmingham
for the degree of:

DOCTOR OF PHILOSOPHY

School of Metallurgy and Materials
College of Engineering and Physical Sciences
University of Birmingham

2015

Abstract

This research compares the dynamic performance of injection moulded and laser sintered poly-ether-ether-ketone (PEEK), outlining the potential of laser sintering as a manufacturing method for high performance polymer gears.

It was observed that the mechanical properties of laser sintered PEEK was a significant improvement over previous laser-sintered materials, and comparable with high performance injection-moulded materials. In addition, the coefficient of friction and wear rates were significantly below that of injection moulded PEEK.

However, for direct application of the laser sintered material EOS PEEK HP3 to power transmission gears, the predominant form of failure was bending fatigue, limiting the material to low power transmission levels.

Observation of the fracture surface highlighted limited amounts of plasticity, although regions of intergranular failure and fast fracture could be identified from the failed surface. In addition, the failure stress path, in the region of progressive intergranuar failure, was governed by the partially sintered particle boundaries in the material; showing a similar failure response to flexure testing.

In conclusion, despite the limited amount of plasticity shown in the material failure, the tribological properties of laser sintered PEEK mean that their application to power transmission is still desirable.

Acknowledgements

The author would firstly like to thank Dr. Karl Dearn and Dr. Stephen Kukureka for their continual assistance and supervision throughout this project.

I would also like to thank the late Prof. Doug Walton for introducing me to the world of gears; you will always be an inspiration…

With regards to the collaborating partners in this research project, I would like to express my gratitude to Dr. Yongkang Chen of the University of Hertfordshire for your efforts and hospitality.

Finally, I would like to thank my family, friends (in particular Rob, Ali, Wentao and Danny), and my dear Sarah for your ongoing support… I couldn't have done it without you.

Nomenclature

A	Area	mm^2
a	Semi width of contact	mm
b	Width	mm
C	Centre distance	mm
$\hat{C}$	Maximum sliding velocity (gears)	mm/s
D	Pore diameter	- -
d_p	Pitch circle diameter	mm
E	Elastic modulus	MPa
E^*	Reduced modulus	MPa
E'	In-phase storage modulus	MPa
E''	Out-of-phase loss modulus	MPa
E_f	Flexural modulus	MPa
E_t	Tensile modulus	MPa
F	Force	N
f	Frequency	Hz
G_{IC}	Critical energy release rate	J/m^2
H	Hardness	- -
h	Thickness	mm
I_a	Path of approach	mm
I_r	Path of recess	mm
K_{IC}	Critical stress intensity factor	MPa/m^2
l	Length	mm
L_{ab}	length of contact	mm
m	Gear tooth module	mm
N	Number of gear teeth	- -
P	Pressure	MPa
P_c	Circular pitch	mm
r	Strain rate	$\%/min$
R	Effective radius	mm
T	Torque	Nm
T	Temperature	$^\circ C$
$tan\ \delta$	Loss tangent	- -
T_f	Flash temperature	$^\circ C$
T_g	Glass transition temperature	$^\circ C$
T_i	Interfacial temperature	$^\circ C$

T_m	Melting temperature	$°C$
v	Velocity	mm/s
V_{max}	Maximum sliding velocity (HFRR)	mm/s
α	Plasticity index	- -
β	Asperity tip radius	mm
γ	Surface tension	N/m
ΔH	Change in enthalpy	J
ε	Contact ratio	- -
ε	Strain	- -
ν	Poisson's ratio	- -
ρ	Radius of curvature	mm
σ	Standard deviation of asperity heights	- -
$\sigma_{\_}$	Stress	MPa
ϕ	Pressure angle	$Degrees$
ψ	Working pressure angle	$^{\circ}$
ω	Rotational speed	rpm

Subscripts

$_1$	Pinion (driver)
$_2$	Wheel (driven)
$_0$	Initial value
$_f$	Flexural
$_c$	Compressive
$_t$	Tensile

Abbreviations

ALM	Additive Layer Manufacturing
DMTA	Dynamic Mechanical Thermal Analysis
DSC	Differential Scanning Calorimetry
EDS	Energy Dispersive X-ray Spectroscopy
HFRR	High Frequency Reciprocating Rig
HT-SLS	High Temperature – Selective Laser Sintering
L	Lubricated
LSR	Load Share Ratio
LVDT	Linear Variable differential transformer
PA	Polyamide
PAEK	Poluaryletherketone

PC	Path of Contact
PEEK	Poly-ether-ether-ketone
PLF	Pitch-Line-Fracture
POM	Polyoxymethylene
PTFE	Polytetrafluoroethylene
RTI	Relative Thermal Index
SEM	Scanning Electron Microscopy (Scanning Electron Microscope)
UL	Unlubricated
μCT	Microtomography

Contents

Chapter 1

INTRODUCTION

"Because the circumference of a circular object moves in opposite directions and one end of a diameter, point A, moves forwards while the other, point B, moves backwards, some people devise it that from one movement many wheels are driven simultaneously in opposite directions – as when they make little wheels of bronze and iron which they dedicate in temples. For if there is a second wheel with diameter ΓΔ touching wheel AB, when diameter AB is moved forwards, that of ΓΔ is moved backwards, if the diameter is moved around a single point. That is, the wheel with diameter ΓΔ is moved in the opposite direction from that with diameter AB. And again, for the same reason, it will move the next in series, EZ, in the direction opposite to its own. And in the same way, if there are more wheels, they will act the same when only one is moved. Seizing upon the innate characteristic of the circular body, then, craftsmen prepare a devise whose first principle they conceal, so that only the wonder of the machine is apparent, the cause hidden."

Aristotle, *Mechanical Problems Preface, 848a. 20-38 (4^{th} century B.C.)* [1]

1.1. Polymer Gearing

The use of friction to transmit motion was first described by Aristotle in the 4^{th} century BC [1]. However, modern gear theory, in which the accurate transmission of motion is a central part, was not developed until the 17^{th} century.

In 1673 Christiaan Huygens published "*Horologium oscillatorium: sive, De motu pendulorum ad horologia aptato demonstrationes geometricae*" [2], in which he described a specific method for finding the "*involute*" of a curve based on the motion of a cycloidal pendulum (**Figure 1**).

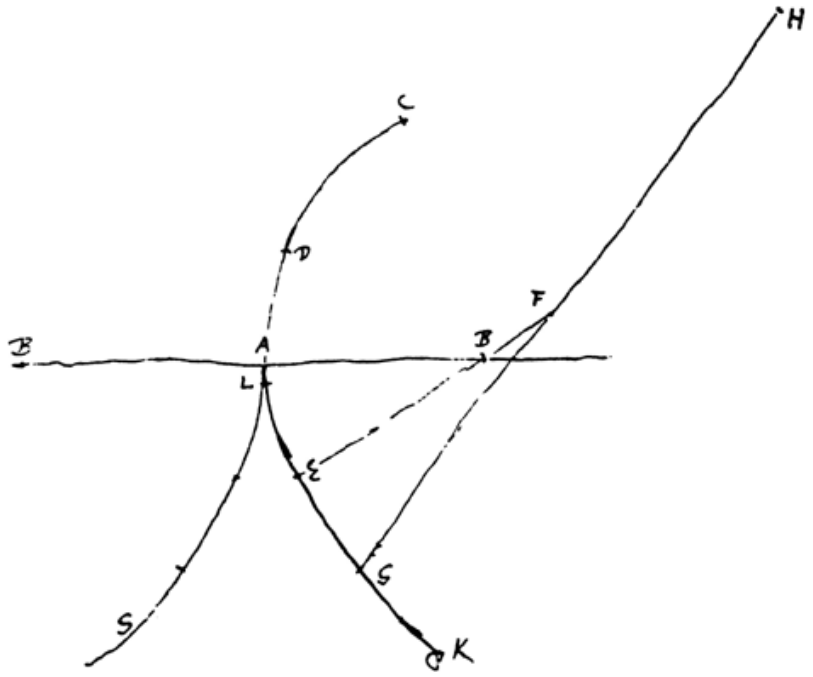

Figure 1: An early sketch by Huygens showing the formation of an involute from the arc of a weighted pendulum, ("*Horologium oscillatorium*") [2]

And since being applied to gearing in 1694 by Philipe de la Hire (*Traité de Mécanique*); the involute has become the standard form for the majority of conformal (constant velocity ratio) gear applications.

For the majority of power transmission gearing applications, the selection of a steel material is governed by the application loads and environmental factors. However, more recently, with developments in materials and design geometry, the application of alternative materials such as polymers has increased.

Traditionally, polymer gear design has been centred on motion and control in applications such as those found in office equipment, automatic telling machines, domestic appliances and small electric motors; where the transmissible loads and running speeds were low.

However, more recently, preliminary investigations into the use of high temperature polymers in automotive mass balance[1] and pump gear applications to reduce system inertia, power consumption and noise levels have re-emphasised their potential benefits for power transmission applications [3,4].

Motivation for further research into polymers for power transmission has been driven by their low cost (when injection moulded), light weight and resilience, coupled with the ability of polymers to operate under dry, un-lubricated, conditions [5]. In addition, in terms of their specific energy consumption, polymerisation of monomeric polymers consumes approximately 60% less oil than that required to produce an equivalent amount of raw steel material [6,7]. These figures are based on 'commodity' plastics; savings are likely to reduce for the production of engineering polymers, but are still likely to be significant [7].

The power transmission laboratory and the polymer tribology group at the University of Birmingham have investigated high performance polymers and their application to machine elements for over 30 years. The primary focus of the work conducted has been to investigate polymer transmission systems, including design optimisation, fatigue and vibration analysis, and tribological studies. This has developed simultaneously with material design.

[1] 68% weight reduction, 78% reduction in inertia, 9% improvement in efficiency, 3db (50% audible) noise reduction for Victrex PEEK based balance shafts

The continued development of polymer gearing has led to the principles governing their design becoming separate from those for steel gears. However, the specific application requirements and the significance of operating conditions on the performance of polymer gears have meant that the only way of confidently specifying a polymer for a gearing application is through physical testing [8].

1.2. Thesis Outline

Polymers and polymer composites are being increasingly applied to engineering applications as non-conformal components such as gears, rolling element bearings and cams. However, the application is primarily to low load transmission.

The purpose of this programme of research is to further the development of polymeric machine elements by improving the understanding (through experimentation and analysis) of a variety of mechanical, material and tribological aspects.

Firstly, the concept of engineering polymers, aspects of polymer manufacture, tribology and wear, and the application of polymers to machine elements are introduced, before then looking more specifically at polymer gear selection for power transmission.

Chapter 5 examines the influence of contact stress, sliding-speed and temperature on the fundamental tribological properties of injection moulded poly-ether-ether-ketone (PEEK) when simulating polymer gear contact. Fretting and twin-disc tests are used to establish and characterise the mechanical properties of the material; providing a benchmark for comparative tests against laser sintered PEEK.

The majority of polymers are injection moulded. However, recent developments in additive manufacturing methods have meant that geometry, that was previously very complicated to manufacture, can now be produced automatically through layer deposition

techniques. Additive layer manufacturing allows for a significant improvement in design flexibility; high complexity bespoke/prototype parts can be produced economically, without the need for expensive tooling.

Chapter 6 looks at the results of physical, mechanical and tribological testing of the high temperature laser sintered polymer EOS PEEK HP3. The significance of these results is then outlined along with specific properties that should be considered in the application of this material to machine elements.

Finally, **chapter 7** investigates the dynamic performance of injection moulded and laser sintered PEEK. These materials will be compared, in an attempt to outline the potential of laser sintering as a manufacturing method for high performance polymer gears. The results of this investigation are then used, in parallel with those obtained in **chapter 6,** to establish an optimised gear geometry for high performance laser sintered polymer gears.

1.3. Aims and Objectives

The main aims of this thesis are to study the dynamic behaviour of injection moulded and laser sintered PEEK for use in power transmission, and to investigate their properties under load and temperature, in an environment comparable with that to which the material would typically be applied.

To do this, the following objectives have been outlined:

- Review the current 'state of the art' of: polymer machine element wear and tribology; laser sintered materials and their application; and, the principles and mechanisms of polymer gear failure

- Investigate the tribological properties of highly loaded polymers; fundamental assessments will be made using fretting and twin-disc tests in an attempt to establish and characterise their properties, and to provide a benchmark for tests comparing laser sintered materials.
- Design and produce test samples to investigate the mechanical and tribological properties of laser sintered PEEK.
- Investigate the mechanical performance, modes of failure and tribological response of laser sintered polymer gears to develop material specific optimised design principles

Figure 2 summarises the development steps to be used in the development of optimised laser sintered PEEK gear geometry.

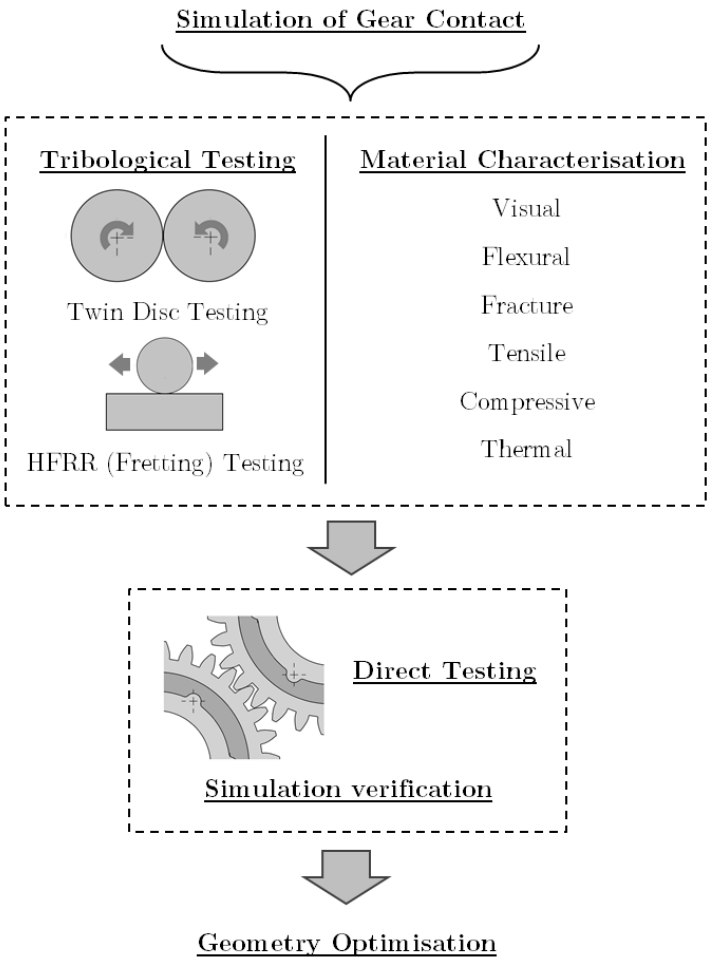

Figure 2: Flowchart showing the development of an optimised laser sintered PEEK gear geometry.

Chapter 2

LITERATURE REVIEW – POLYMER TRIBOLOGY

2.1. Introduction

This chapter presents a survey of literature covering the wear and tribology of polymeric materials. Emphasis is made on specific performance related aspects associated with the mechanical application of polymers.

Firstly, the concept of an "engineering polymer" is introduced, before looking more specifically at aspects of polymer tribology and wear associated with operation at high temperatures and loads.

Finally the use of selective laser sintering as a manufacturing method for high temperature mechanical polymers is discussed.

2.2. Engineering Polymers

Although numerous grades of polymer exist, a mechanical application is most likely to require an '*engineering polymer*'; offering an optimum performance in terms of strength and stiffness [9].

Polymers can be broadly classified into four main types: elastomers, thermoplastic elastomers, thermoplastics and thermosets. In mechanical applications, the use of elastomers and thermosets are limited, as their respective load bearing and wear capabilities, are low. Therefore, the majority of engineering polymers are currently thermoplastics.

Thermoplastics typically behave in an elastic manner; known as viscoelasticity. In addition, a thermoplastic material will react differently in compression to tension. Under tensile stress the macromolecular chains slide past one another, however, in compression the chains become immobile, meaning the observed modulus is higher than in tension; this is desirable for the majority of mechanical applications [10].

The molecules of a thermoplastic are primarily bound by strong covalent bonds forming long molecular chains, and secondarily by much weaker van der Walls forces, governed by the relative position of neighbouring chains. This difference in bonding strengths (the secondary forces typically one hundredth of the primary) is a characteristic of thermoplastics. Consequently, the material will soften when heated, causing the molecular chains slide over one another [10–12].

However, in mechanical applications the need to maintain mechanical properties at high temperatures is essential. **Figure 3** shows the adverse effect of high temperatures on the stiffness of a thermoplastic polymer.

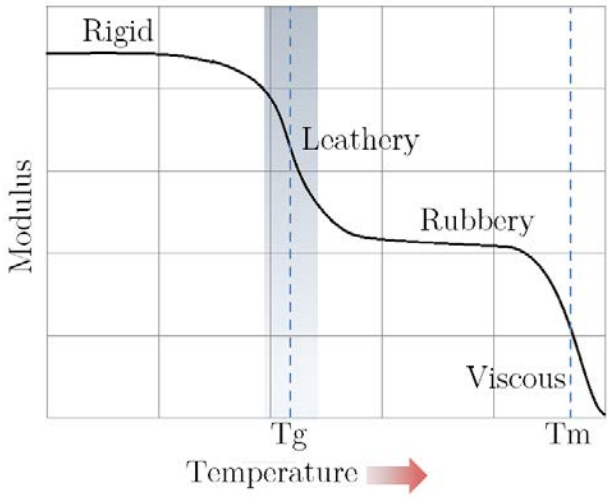

Figure 3: transitional stages of thermoplastic behaviour with respect to temperature [10]

It can be seen that there are two distinct temperature transitions. The first of these is the glass transition temperature (T_g) and the second is the melting point of the material (T_m). The glass transition temperature of a material is the temperature after which the material becomes amorphous (i.e. flexible and showing distinct plastic tendencies), becoming hard, brittle and rigid. In reality, this correlates to the point where the van der Waals forces start to lose their cohesive influence and segments of the polymer chains gain a degree of mobility [10].

Table 1 provides the glass transition temperatures for common engineering thermoplastics.

Table 1: Glass transition temperatures of common engineering thermoplastics [12]

Thermoplastic	Glass Transition Temperature (T_g)
Polyetheretherketone (PEEK)	143 °C
Polyoxymethylene (POM)	-76 °C
Polyamide 66 (PA66)	66 °C
Polytetrafluoroethylene (PTFE)	115 °C

Typically, operation beyond the glass transition temperature is detrimental to the performance of polymers [13]. However, the susceptibility of different polymers to degradation with temperature varies significantly. For example, in contrast to many other engineering polymers, polyoxymethylene (POM) maintains its high toughness down to very low temperatures due to both its high crystallinity and low glass transition temperature. The majority of thermoplastic materials are, however, significantly affected by the transition around the glass transition temperature, with wear mechanisms and wear rates both changing as the material properties change.

The orientation of the macromolecular chains is also a major factor in the behaviour of some plastics [12]. Above the melting temperature there is a liquid state where there is easy movement of the chains. However, below the melting point there exist three different morphologies distinguished by their molecular order and the temperature at which they occur; the amorphous, glassy and crystalline phases. The amorphous and glassy stages possess no orientation or order with regards to their polymer chains, although they are distinguished from each other by the glass transition temperature. However, in the crystalline phase the aligned nature of the polymer chains, in the form of lamellae, form spherulites which have a significant effect on the materials bulk stiffness, strength and dimensional accuracy.

Only a few thermoplastics are capable of forming crystallites (thermoplastic crystals), as the majority of thermoplastics do not lend themselves to close packing, owing to the large side-groups that sprout from the polymer chains. Additionally, a 100% crystalline polymer is unobtainable due to the many entanglements preventing the polymer chains from arranging into a fully crystalline phase; therefore the crystals of highly ordered chains exist in an amorphous matrix as a '*semi-crystalline*' material [12,14].

The physical and mechanical properties of semi-crystalline polymers are highly dependent on their degree of crystallinity. Generally speaking, the effect of crystallinity is to reduce the temperature dependency of a polymer between the glass transition temperature and the melting temperature. When compared with the equivalent amorphous plastic, crystalline thermoplastics tend to be stronger; both the tensile and shear strength of PEEK and Polyethylene have been reported to increase with an increase in crystallinity [15,16]; stiffer, denser, more fatigue resistant and more resistant to chemical attack. However, the material is also more brittle than its amorphous counterpart. Thus crystallinity can have numerous effects on the performance of a thermoplastic polymer; not all of which are beneficial [12].

The selection of an engineering polymer for a specific industrial application is not well understood. The combined influence of application factors such as temperature, wear, friction, and lubrication, means that the only way of confidently specifying a polymer for an industrial application is to physically test them. However, the characteristics of the polymer such as its crystallinity, glass transition temperature and melting points can all give an indication of the material performance and should be used in combination with physical testing to fully understand the limitations of a material.

2.3. Mechanisms of Wear in Thermoplastic Materials

When designing polymer machine elements, their specific limitations when used to transmit load must be considered. The wear of polymers is significantly different to that of metals; they have much lower modulus values, lower strengths and melting points. In addition, lower thermal conductivity often means that thermal effects are more significant [5]. Consequently, the majority of polymer failure mechanisms have been attributed to wear [13,17–19]. The following sections will consider the wear and tribology of polymers

and the requirements of polymer machine elements, specifically gears, when transmitting power.

The wear resistance of a surface was initially considered to be reliant, primarily, on the material hardness [20]. However, despite hard materials often demonstrating a high elastic modulus and low wear, it has been shown that some polymeric materials can provide excellent wear resistance despite possessing a comparatively low elastic modulus. It has therefore been recognised that the characterisation of materials according to their elastic strain to failure, the ratio between their hardness (H) and elastic modulus (E), is fundamental to material wear [20]. Additionally, the ratio between H and E appears in the *'plasticity index - α'* (**Equation 1**), a valuable measure in determining the limit of elastic behaviour in surface contact; and therefore important in the avoidance of wear.

$$\alpha = \frac{E}{H}\left(\frac{\sigma}{\beta}\right)^{\frac{1}{2}} \qquad \textbf{Equation 1}$$

σ: standard deviation of asperity heights
β: Asperity tip radius

It is necessary, however, to also understand the importance of the motions to which the system is subjected and the interaction of the contacting materials; a materials ability to resist wear is not solely dependent on the E/H ratio. For example, H is not clearly defined for polymers, which are usually significantly viscoelastic and rate-dependent in all but their most rigid forms. Any use of H for polymers must be cautious to include time-dependent effects. Also E is usually time dependent for polymers as they exhibit viscoelasticity [10].

Despite the wear of polymers having not been fully understood, certain principles are established and wear is often divided into two categories: Cohesive Wear and Interfacial

Wear (**Figure 4**). "*If the counter-face is smooth, then wear may result from adhesion between the surfaces, and involve deformation only in the surface layers of the polymer. On the other hand, if the counter-face is rough then its asperities will cause deformation in the polymer to a significant depth; wear then results either from abrasion associated with plastic deformation of the polymer, or from fatigue crack growth in the deformed region. These two classes of wear mechanism, involving surface and subsurface deformation respectively, have been termed 'interfacial' and 'cohesive' wear processes*" [21].

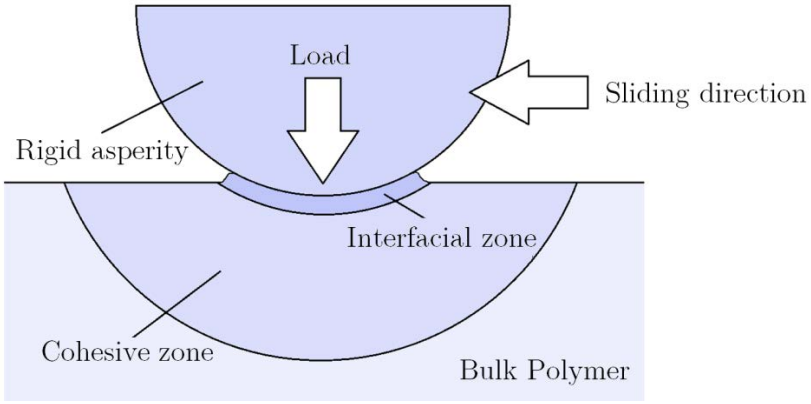

Figure 4: Cohesive and Interfacial zones in polymers [22]

Cohesive wear occurs adjacent to the surface over relatively large volumes. It involves the dissipation of frictional work and resultant damage and is often caused by the passage of an asperity or hard particle over the surface of the polymer. The behaviour depends on the mechanical properties of the polymer (i.e. strength, toughness and fatigue limits) as well as the level of penetration of the surface feature and the stresses occurring over the cohesive zone, in and beneath the contact area [5]. The failure process occurring involves abrasive processes, often associated with permanent plastic deformation or fatigue associated with elastic, recoverable deformation (plus the subsequent cracking) [22].

Interfacial wear occurs when the frictional energy is dissipated in a much thinner region adjacent to the surface (as shown in **Figure 4**). The transfer of material from one body to the other is important here, as are chemical effects at the surface which can reduce adhesion at the interface.

2.3.1. Adhesive Wear

When two contacting surfaces move relative to each other, friction is contributed primarily by adhesion and secondarily by contact asperity deformation [22].

Interfacial wear is related to the adhesion component of sliding friction. When two materials contact the molecular forces may act through the interface causing interfacial bonding and the generation of adhesive junctions. These strong localised adhesive junctions produce elastic and plastic deformations in the upper layer of the material.

The rupture of the cohesive junctions in the bulk of the polymer material following adhesion results in either material transfer or wear debris formation.

The frictional transfer role in the tribological behaviour of polymers is very important. Friction, wear, and self-lubrication depend upon the capability of polymer to form a transfer film on the counterface, as well as upon the thickness and structure of the film.

Laux and Schwarts discussed the influence of sliding on the wear performance and transfer film formation in PEEK. It was shown that lower wear was associated with an increased transfer film as the transferred layer prevented asperity abrasion [23]. However, it has been shown in some instances that large levels of material transfer can have a detrimental influence on the rolling performance of a tribological contact [24].

The rate of this film creation, its structure, durability and lubrication properties depend on forces of adhesion between the transfer layer and the contacting surface, and on the properties of the polymer itself.

The retention of the transferred material has also been shown to be significantly affected by the surface roughness of the counterface, with smooth counter-faces supporting more transfer, and by operating conditions [25,26].

Nunez *et al.* showed that transfer layers were continuous and uniform when testing against the smooth disks. Suggesting that the increased transfer layer was due to the high interfacial adhesion forces when the pin is brought into contact against a smooth surface; leading to more cohesion and a more uniform film compared when testing against a rough surface [27].

Adhesion interactions may often be calculated in terms of free surface energies (γ_n); the energy required in creating a new surface, expressed over an area consisting of many atoms in the surface lattice. The higher the surface energy of a solid surface, the stronger the bonds will form on the mating material [28].

For two surfaces in contact, the interfacial bond may be stronger than the cohesive bond in the cohesively weaker of the two materials. In this case, separation of the two solids results in the transfer of the cohesively weaker material to the cohesively stronger, i.e. a material with a lower surface energy will tend to transfer onto a material with a higher surface energy.

Table 2 provides the surface energy for a number of engineering polymers:

Table 2: Surface energies of polymers[2]

Polymer	Surface Energy (mJ/m²)
PEEK	42.1
Polyamide 6	45.4
Polyamide 6-6	44.3
POM	38.6
PTFE	21.8

It can be seen that polymers such as POM and PTFE have low surface energies. Therefore, when these materials are run in combination with either a polymer or a steel counterface of higher surface energy, adhesive wear and transfer should be significant as the work required to separate two internal surfaces is low.

In this case, material transfer is attributed to the difference in surface energies between the two surfaces. This is supported by twin-disc observations and the conclusions of Hoskins *et al.* (2010) who showed that high frequency acoustic responses from adhesive wear in POM gears when running in unlubricated contact against steel, were less prevalent in Polyamide or PEEK [29]. However, mechanical and thermal effects will also significantly affect the adhesion process.

Other studies on the adhesive properties of PEEK have shown that lower sliding velocities promote increased adhesion; any viscoelastic or viscoplastic deformation (creep) under load increases the real area of contact as a function of duration of the contact, leading to an increase in adhesion [30]. Therefore, slower sliding speeds and higher temperatures should increase the adhesive wear.

[2] http://www.accudynetest.com/polytable_01.html?sortby=sort_name

2.3.2. Abrasive Wear

There is no clear or well-defined distinction between Cohesive and Interfacial wear but the roughness of the counter-face surface, and the nature of the polymer surface together help to determine the overall wear mechanisms. Lancaster and Hutchings attempted to represent these factors diagrammatically (**Figure 5**) [21,22,31,32]. They showed that for elastomers, deformation is often almost entirely elastic due to their low modulus. Cohesive wear in elastomers is dominated by fatigue mechanisms. In contrast, higher modulus thermoplastics and thermosets are often susceptible to abrasive wear by plastic deformation (though if brittle the wear processes may be different).

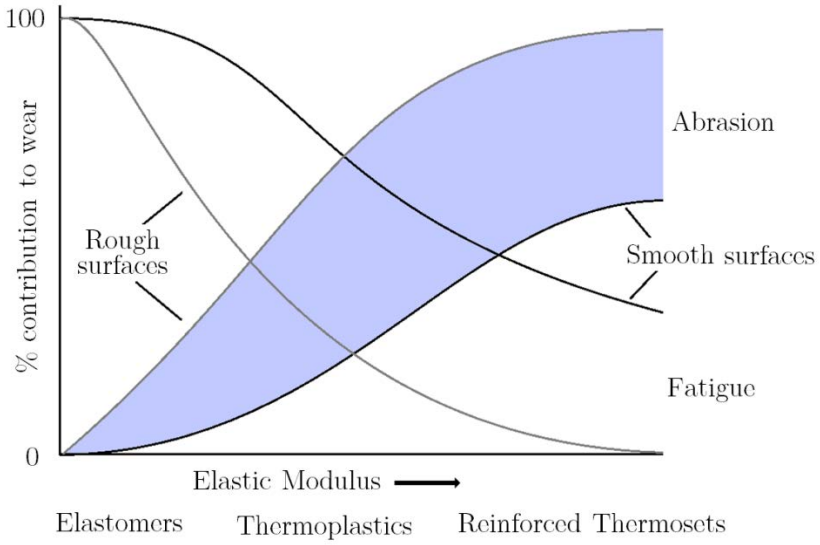

Figure 5: Transitions in Cohesive wear mechanisms (after [21,32])

Typically the abrasive wear of mechanical polymers (thermoplastics and reinforced thermoplastics) is based on one, or a combination of the following processes:

- Two-body abrasion, where hard abrasive particles project from the surface of one body, to cause wear on the second.

- Third body abrasion, where independent hard particles become entrained between two sliding but non-abrasive surfaces.
- Erosion, where fast moving, hard particles strike a surface causing wear.

Generally speaking, the surface roughness of the contacting surfaces and the filler content have been shown to have the most significant effect on the abrasive wear observed in polymers [18,33–36];

The inclusion of reinforcing fillers can alter the wear mechanism. Typically, the exposure of a reinforcing element results in abrasive wear as the filler contacts the softer base matrix. Hooke *et al.* investigated the effect of glass fibre reinforcement on the wear properties of polyamide discs and gears [17]. It was found that the reinforcement was dispersed within the matrix and once an initial layer was removed, they observed the most prolific form of wear was abrasion. However, the orientation of the reinforcement within the polymer has a significant effect on the amount of abrasion observed [37].

Many investigations on the friction and wear properties of the high performance thermoplastic PEEK and its composites have been carried out. It has been reported that the high performance abilities of PEEK have not been entirely realized in practice because PEEK-ferrous metal contacts may fail by scuffing and/or two-three body abrasion for certain tribosystems [36]. Ovaert and Cheng reported that, for PEEK running against steel, a transition from relatively low to high abrasive wear was measured for counterfaces with surface root-mean-square roughness in the range of 0.13 (smooth) to 0.76 (rough) μm respectively [38].

However, it has been shown that for carbon fibre reinforced PEEK blends running against steel, the presence of carbon fibre enhanced protection against abrasion by minimising plastic deformation [36], although the damage observed on the steel counterface increased.

The effect that sliding velocity has on the friction of polymers is dependent on the predominant mechanism of wear and the mechanical properties of the polymer. The behaviour depends on the mechanical properties of the polymer (i.e. strength, toughness and fatigue limits) as well as the level of penetration of the surface feature and the stresses occurring over the cohesive zone, in and beneath the contact area [5]. The failure process occurring involves abrasive processes, often associated with permanent plastic deformation or fatigue associated with elastic, recoverable deformation (plus the subsequent cracking) [22].

2.3.3. Fatigue Wear

In the event that contacting asperities deflect elastically, as for the case of engineering polymers at elevated temperature, then the wear regime tends towards one of fatigue.

Fatigue studies of polymeric materials have primarily been based on rolling contact fatigue. Kukureka *et al.* found that surface fatigue occurred on Acetal running in like/like combinations under unlubricated roll slide conditions [39]. However, it was shown to manifest itself differently depending on the sliding speeds. When the sliding speeds were low, the wear rate was negligible and shallow flakes and pits were observed at the surface of the discs. However, as sliding speeds were increased, lateral surface cracks were observed, aligned normally to the direction of sliding. In a study of surface temperature due to frictional heating Kukureka also found that the onset of this mode of wear coincided with sliding temperatures of around 110C; the onset of thermal softening.

However, the wear of Nylon 66 roll/slide discs, under similar circumstances to those above, was seen to be very different; deep surface cracks appeared after relatively short durations of testing, being approximately 0.5mm in length in the direction of sliding

[17,33,40]. The appearance of these cracks was independent of sliding speed (except for during pure rolling) and was therefore considered an intrinsic property of Nylon 66.

Avenzi et al. discussed the fatigue properties of PEEK and PEEK based composites [41]. It was observed that the fatigue mechanisms were different for unfilled PEEK and its composites; micro pitting and deep transversal cracks occurred on unfilled PEEK rollers, whilst delamination and spalling phenomena were found on composite rollers. Additional studies on the rolling contact fatigue of PEEK rolling bearings have shown the importance of self-lubrication ability of this material for determining the component lifetime, which is strongly influenced by adhesion processes [41].

In addition to mechanical fatigue, aging can have a significant effect on the mechanical properties of polymers.

The thermal aging effects of PEEK were discussed by Sinmazcelic and Yilmaz [15]. It was found that following an isothermal aging process, there was a significant decrease in degree of crystallinity but a more organized crystallize structure was achieved. As a result of transcrystalline layer formation, there was a considerable increase in the flexural modulus of materials. Thermal aging affects the impact properties of filled and unfilled PEEK dramatically with the crack initiation force, the energy that was absorbed during crack initiation and the total fracture energy of the samples for both filled and unfilled aged PEEK and its composites dramatically decreased; i.e. as a consequence of thermal aging there was a significant decrease in the toughness of PEEK [15,42].

2.3.4. Impact Wear

The ductility of unlubricated polymer means that their susceptibility to impact loading is low. However, lubrication can significantly affect the impact wear performance of a

surface. Typically the inclusion of a lubricant will act to dampen the loading effects, however, it has been shown that pitting becomes more prevalent in the presence of lubrication and high loads.

Pitting is a phenomenon attributed to repeated loading of the tooth surface to a degree that the contact stress exceeds the fatigue strength of the material. During pitting crack growth is considered to be initiated by surface fatigue, subsequently the large hydrostatic pressures act to force lubricant into cracks formed at the surface; resulting in the eventual removal of material in the form of a pit.

Berer et al. discussed the pitting wear of injection moulded PEEK rolls [43]. It was observed that increased pitting occurred only in lubricated contacts. Further analysis identified surface "pre-cracks" on the surface of the PEEK rolls as a consequence of the injection moulding process. Optimisation of this process improved the fatigue life of the PEEK rolls by a factor of 2-3 times.

Observations of gross pitting has also been observed on highly loaded PEEK gears [11,14,44]. Kono studied PEEK Gears lubricated in heated oil and discovered that pitting wear due to the hydrostatic forces between the meshing gear teeth [44]. This pitting extended over the whole of the tooth flank and was not local to the pitch line and the highest/lowest point of single tooth contact, as in lubricated metal/metal contacts.

In addition, for highly loaded polymer contacts, high temperatures can result in coefficients of friction can be greater than 0.8. These are very much higher than coefficients of friction for oil lubricated steel/steel contacts and are likely to be a contributive factor in causing severe pitting damage.

Reinforcing of polymers significantly affects the impact properties of the materials. Rigid fillers in a ductile polymer decrease the impact strength of the material and increases the crack initiation force of a polymer, but there is a dramatic decrease in the energy absorbed during crack initiation and the total fracture energy of the material [15].

2.3.5. Tribochemical Wear

Lubrication has been shown to reduce abrasive wear and dissipate frictional heat, reducing the shear stress on the surface of the material and minimising the coefficient of friction [45].

However, chemical effects from lubrication and surface degradation may also play a role in interfacial wear as the forces from friction may cause cracking of the polymer chains in the surface layer and creation of molecules of different radicals [28]. For steel vs. polymer contact the oxygen from the oxides on the steel surface could be introduced into a polymer molecule by reaction with a radical. The polymer molecules with oxygen-containing groups could then be chemically adhered onto the metal surface due to their strong polarities, improving the adhesion of material transfer [46]. However, it is expected that the amount of transfer will be significantly less, due to the lubricant preventing asperity contact.

2.4. Selective Laser Sintering of Polymers

The majority of polymers are injection moulded. However, recent developments in additive manufacturing methods have meant that geometry, that was previously very complicated to manufacture, can now be produced automatically through layer deposition techniques.

High temperature selective laser sintering (HT-SLS) is a method of additive layer manufacturing (ALM) used mainly in the aerospace and medical industries [47]. ALM refers broadly to a process by which digital 3D design data is used to build up a component in layers by depositing material[3].

The HT-SLS process begins with the deposition of a thin layer of powder material to a building platform which is then fused together using a high powered laser. The deposited layers are then built up; each layer fused to the previous layer to form the finished part (**Figure 6**).

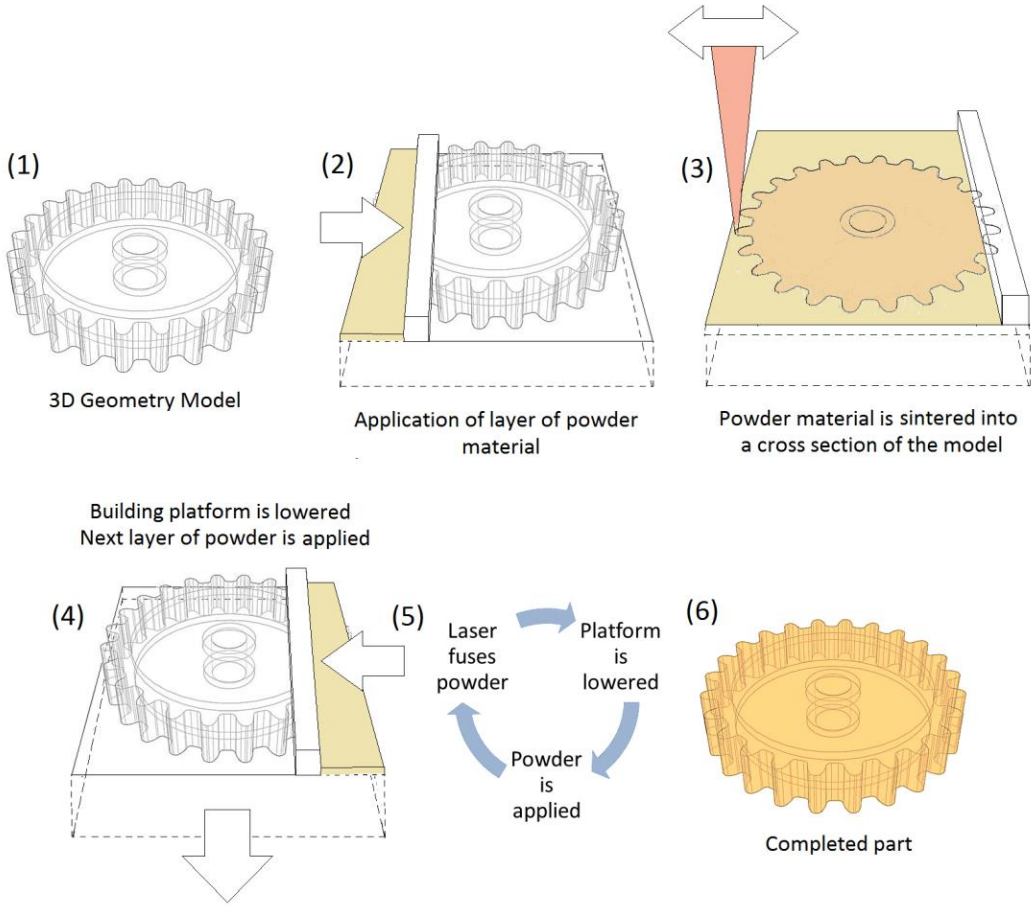

Figure 6: selective laser sintering process

[3] The definition for Additive Manufacturing is taken from the *International Committee F42 for Additive Manufacturing Technologies (ASTM).* http://www.astm.org/

ALM allows for a significant improvement in design flexibility; high complexity bespoke parts can be produced economically, without the need for expensive tooling. Consequently, research into the use of selectively laser sintered materials is increasing.

High performance thermoplastics such as polyamide 12 (PA12) have been used in ALM for many years to produce dense parts with relatively high mechanical strength [48–53]. However, certain material characteristics, such as low melting temperatures and low glass transition temperatures, limit their application. Therefore, there has been an increasing interest in producing high temperature semi-crystalline materials for use in HT-SLS.

Figure 7: EOS P800 HT-SLS system[4]

EOS PEEK HP3 is a material belonging to the group of poly-aryl-ether-ketones (PAEK); this semi-crystalline, thermoplastic material was developed by Electro Optical Systems (EOS GmbH., Munich, Germany) and Victrex (Victrex Plc., Lancashire, UK) for use on the new high-temperature EOSINT P 800 system (**Figure 7**). The EOS P800 high

[4] http://www.eos.info/systems_solutions/plastic/systems_equipment/eosint_p_800

temperature system uses a CO_2 laser that can run at temperatures of 385°C to build three-dimensional geometry in 0.1 mm layers.

This process is capable of laser-sintering high performance polymers such as Poly-ether-ether-ketone (PEEK) and PAEK that otherwise could not be manufactured using conventional laser sintering systems.

Figure 8 shows the reported mechanical properties of selectively laser sintered tensile test specimens. The mechanical performance advantage of laser sintered PEEK over alternative laser sintered polymers can be seen; the modulus of elasticity in tension being 19% higher than POM and 79% higher than PA12 [48].

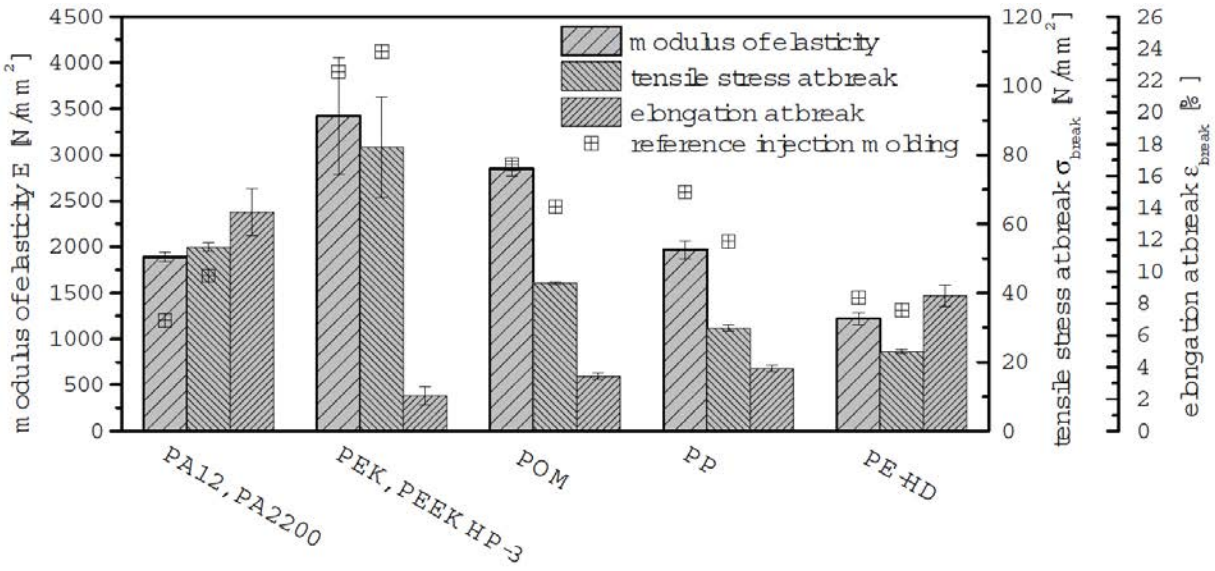

Figure 8: the mechanical properties of various selectively laser sintered polymeric materials [48]

Currently, there is very little information available on the mechanical application of EOS PEEK HP3; PEEK HP3 has been reported to demonstrate "excellent wear resistance[5]",

[5] *EOS website [cited 14th January 2014]*: http://www.eos.info/material-p

however, there is very little documented evidence of this and the majority of the data is based on manufacturer's values, where their significance for a given application is not immediately apparent [54].

Greses and Stoko, and Schmidt *et al.* outlined the SLS process for high performance polymers although there was limited analysis into the material properties [47,55]. Beard *et al.* and Ghita *et al.* have been the only ones to attempt to characterise the mechanical properties of EOS PEEK HP3 components [56–58]. Ghita *et al.* observed that, due to the inherent anisotropy from laser sintering, the manufactured orientation had a significant effect on the mechanical properties of the component.

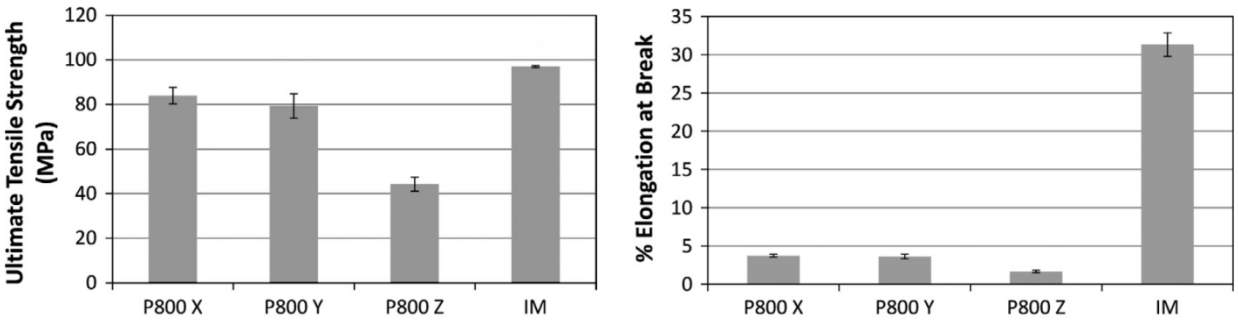

Figure 9: Effect of orientation (X,Y,Z) on the ultimate tensile strength, and the elongation to break for laser sintered EOS PEEK HP3 tensile test specimens versus injection moulded (IM) PEEK [58].

It was shown that, when components were manufactured in the Z direction, there was up to a 45% decrease in tensile strength and a 55% decrease in elongation to break when compared to the X and Y directions (**Figure 9** [58]). In addition, brittle failure was observed in all samples, with the X and Y samples showing crack propagation from the skin of the sample and Z samples fracturing across the layer boundary. This anisotropy is commonly seen in ALM parts, with a decrease of up to 20% in the Z direction previously reported for nylon materials [52].

Due to the anisotropic nature of the samples, and the difficulty in generating a fully homogeneous material with no porosity, the reported elongation to break for laser sintered EOS PEEK HP3 is up to 15 times lower than that of injection moulded PEEK (**Figure 9**) [48,56,58].

In addition, the influence of using 30% used powder versus 70% virgin powder has been shown to reduce the tensile strength of the material by 17% [57].

2.5. Conclusions

The use of polymers in mechanical applications is well established. Motivation for further research into mechanical polymers has been driven by their low cost (when injection moulded), light weight and resilience, coupled with the ability of polymers to operate under dry, un-lubricated, conditions [5]. In addition, in terms of their specific energy consumption, polymerisation of monomeric polymers consumes approximately 60% less oil than that required to produce an equivalent amount of raw steel material [6,7]. These figures are based on 'commodity' plastics; savings are likely to reduce for the production of engineering polymers, but are still likely to be significant [7].

It has been shown that the mechanical properties of polymers are strongly dependent on their environmental circumstances, in particular with temperature; for example, the strength and stiffness of a mechanical polymer will typically fall once the bulk temperature surpasses the glass transition temperature. In addition viscoelastic effects mean that the mechanical behaviour of a polymer will change, when subjected to a mechanical load.

Particular attention was given to the tribology of polymers since wear was regarded as one of the principal forms of failure of mechanical contacts. The significance of

temperature, reinforcement, sliding speeds, and surface roughness on the mechanical response of a polymeric material has been shown to be significant; with the principle wear mechanism varying with operational parameters.

In addition, the potential use of high temperature selective laser sintered polymers in the production of mechanical components has been outlined. It has been shown that although the material is susceptible to fracture during overload, the performance of the laser sintered polymer EOS PEEK HP3 is a significant improvement over previous laser-sintered materials and comparable with high performance injection-moulded materials.

Chapter 3

LITERATURE REVIEW – 'STATE OF THE ART' UNDERSTANDING OF POLYMER GEARING

3.1. Introduction

Polymers and polymer composites are being increasingly applied to automotive and industrial mass balance systems as non-conformal components such as gears, rolling element bearings and cams [3,5]. However, despite being characterised by their mechanical performance the specific response of a polymer to the contact conditions found in machine elements (high contact pressures, temperatures and loads) is complex.

This section of the thesis will look specifically at polymer gear selection for power transmission, and the current understanding of polymer gear wear and failure.

3.2. Polymer Machine Elements

Fundamental machine elements can be categorised based on their degree of conformity. That is, the surfaces show a high degree of geometrical conformity when in contact the load is shared over a relatively large area which doesn't significantly increase with load. However, many machine elements have contacting surfaces that do not conform to each other very well and the full load must be carried by a very small contact area. In general,

the contact area between non-conformal surfaces enlarges considerably with increasing load, but this is still small when compared with the contact areas between conformal surfaces. The load per unit area in non-conformal elements is therefore much higher than in conformal machine elements.

When such components are oil lubricated the consequent high pressures result in a significant increase in lubricant viscosity. In as much as viscosity is a measure of a fluids resistance to flow; this increase greatly enhances the lubricant's ability to support load without being squeezed out of the contact zone.

Table 3 provides a summary of fundamental conformal and non-conformal machine elements.

Table 3: Conformal and non-conformal machine elements

Conformal	Non-conformal
Journal bearings	Gears
Deep groove bearings	Roller element bearings
Chain linkages	Cams
Power screws	
V-belts	
Clutches	
Piston rings	

The characterisation of machine elements based on their conformity allows their fundamental motions to be simulated. **Figure 10** shows the process of characterising non-conformal machine elements based on their roll slide interactions as well as various testing methods used in their simulation.

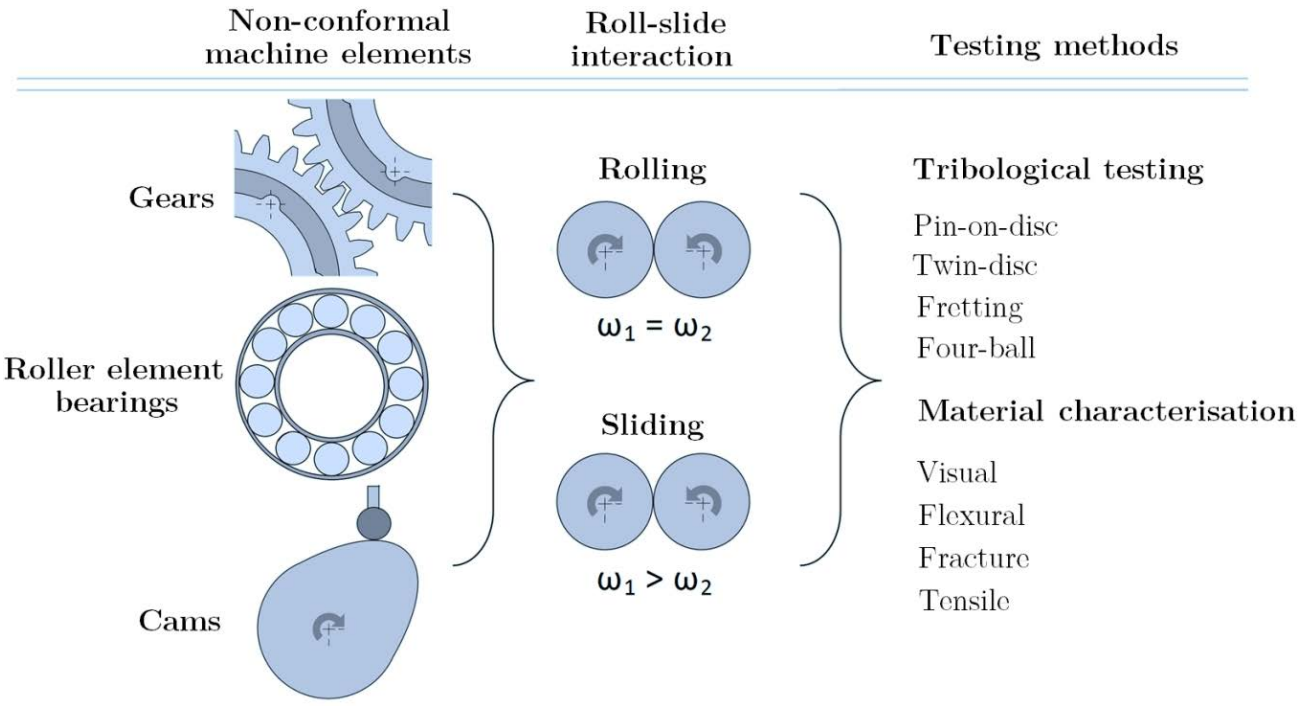

Figure 10: Characterising non-conformal machine elements based on their roll-slide interactions as well as various testing methods used in their simulation

The use of a simplified geometry in the analysis of machine elements means that fundamental material tests can be correlated against numerous applications. For example, twin disc tests can simulate both gears and cams. However, it is important to consider the influence of simplifying geometry on the tribological characteristics of the contact. For example: during fretting contact the wear debris remains circulating in the contact forming a closed tribosystem, whereas, when the wear debris is immediately removed from sliding contact (as in gear contact) it forms an open tribosystem. Both of which significantly alter the tribological characteristics of the material contact.

3.2.1. Specific Requirements of Polymer Gears

When designing polymer machine elements, their specific limitations when used to transmit load must be considered. The application of polymers is significantly different to that of metals; they have much lower modulus values, lower strengths and melting points. In addition, lower thermal conductivity often means that thermal effects are significant. The following sections will consider the requirements of polymer non-conformal machine elements, specifically gears, when transmitting power.

3.2.2. Gear Theory

Gears used in the transmission of motion and power are typically required to produce a smooth, non-fluctuating rotary output. This is achieved when the meshing gears have a constant angular velocity ratio, thus producing conjugate motion [59].

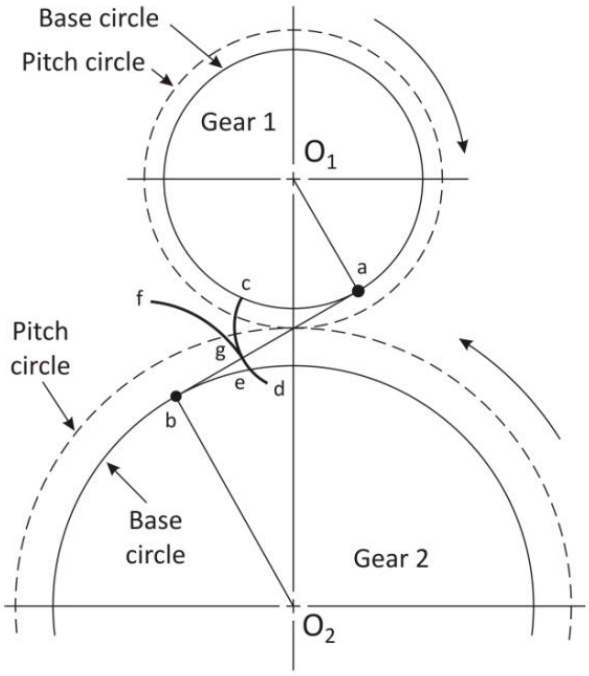

Figure 11: conjugate action [59]

The majority of conjugate gear theory has been established based on an involute gear tooth profile; the "*involute*" of a curve was first considered by Christiaan Huygens in 1673 and first applied to gearing in 1694 by Philipe de la Hire. In an involute profile, the point of contact moves along a line laying tangent to the base circle, but at the point of contact this line is always normal to the involute (**Figure 11**).

The nomenclature associated with spur gears, and which is referred to throughout this thesis, is shown in **Figure 12**.

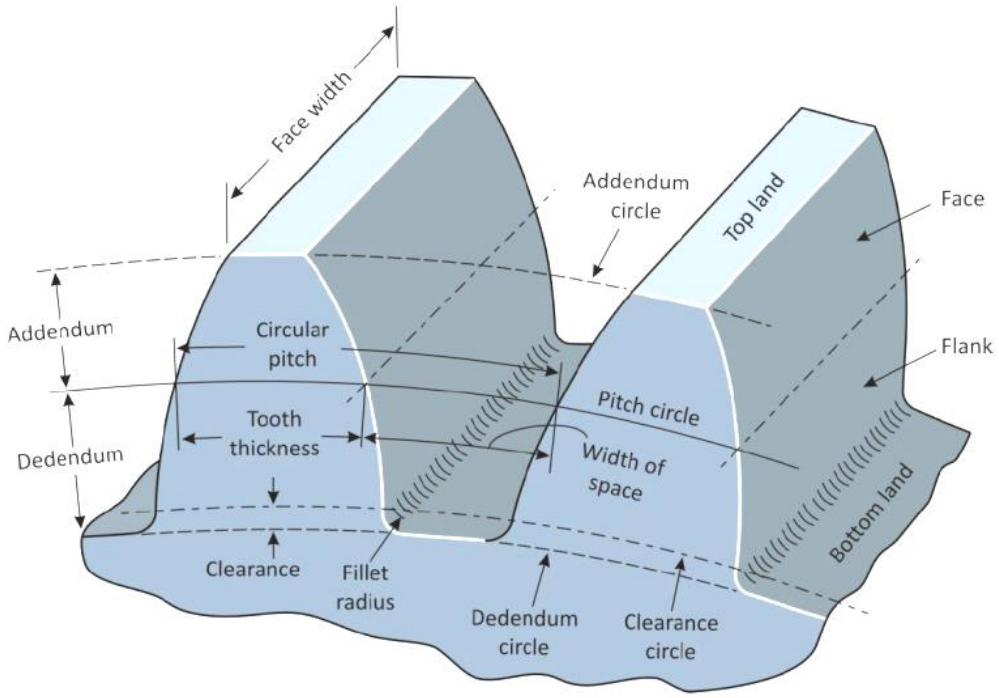

Figure 12: terminology describing the geometry of a spur gear tooth [59]

A fundamental dimension, that determines many of the geometrical features of a gear, is the reference or pitch circle radius. The pitch circle, defined by the pitch circle radius, is the theoretical circle passing through the teeth of a gearwheel, concentric to the gear-wheel, and having a radius that would enable it to be in contact with a similar circle around a mating pinion-wheel.

Therefore, the centre distance, "C", is the distance between parallel axes of the gears and can be defined by Equation 2:

$$C = \frac{d_{p1} + d_{p2}}{2} \qquad \text{Equation 2}$$

The distance along the pitch circle between point on one tooth and the same point on an adjacent tooth, known as the circular pitch, can also be calculated as:

$$P_c = \frac{\pi d_p}{N} \qquad \text{Equation 3}$$

The size of a gear tooth is described by its module "m"; the ratio of pitch circle diameter to the number of teeth (Equation 4).

$$m = \frac{d_p}{N} \qquad \text{Equation 4}$$

The module determines the geometrical value for the addendum and the dedendum; where the addendum and dedendum are the radial distances between the pitch circle and the top land, and the pitch circle and the bottom land respectively. Typically, the addendum is equal to the module and the dedendum equal to 1.25 times the module.

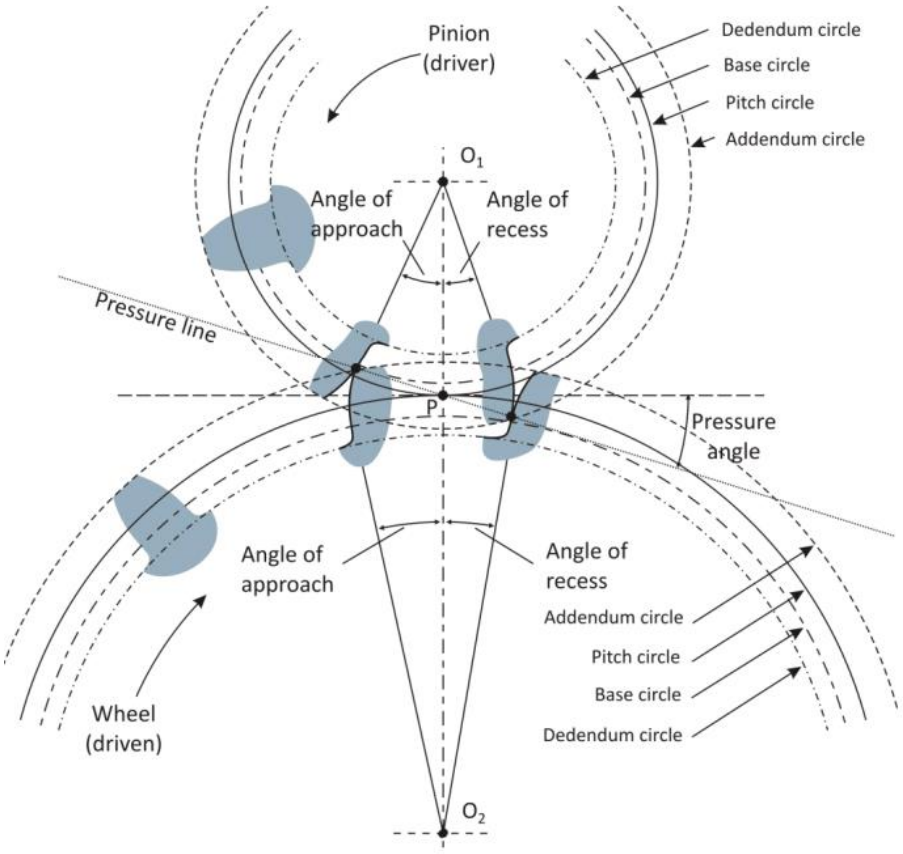

Figure 13: tooth action [59]

Figure 13 illustrates the nomenclature associated with two gears in mesh. When the two gears mesh, there will be a resultant force acting between the gears. The direction this force acts in is known as the pressure line, and the angle this creates with a line that is tangent to the pitch circle at the pitch point is referred to as the pressure angle.

The path of contact "L_{ab}" can therefore be defined as the path travelled between the first and last points of contact and is made up of the path of approach "I_a" and the path of recess "I_r". Similarly the arc of contact, defined as the distance travelled by one tooth whilst in contact with another, is made up of the arc of approach and the arc of recess (**Figure 14**).

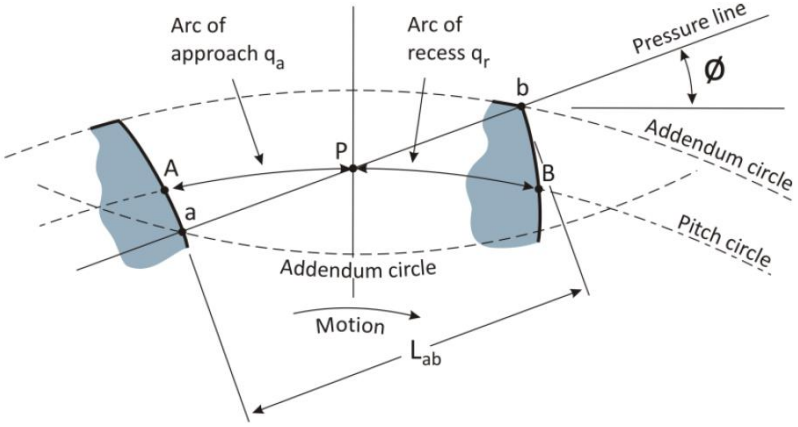

Figure 14: definition of contact ratio [59]

The contact ratio of a pair of meshing gears is the average number of pairs of teeth in action. Mathematically, the contact ration is a function of the ratio of the arc of contact to the circular pitch, p. Expressed in terms of the line of action (Equation 5).

$$\varepsilon = \frac{L_{ab}}{p_c \cdot cos \cdot \varphi} \qquad \text{Equation 5}$$

Finally, as the gear mesh moves along the pressure line, the gear teeth will roll and slide as the gear comes into mesh, passes the pitch point and moves out of mesh. Friction between the meshing teeth creates a power loss proportional to the sliding velocity and loading conditions. The sliding velocity is the velocity of one tooth relative to its mating tooth along the common tangent at the point of contact. It can be shown that over the tooth-tooth contact period the average sliding velocity is:

$$\Delta V = (\omega_1 + \omega_2) \cdot \frac{L_{ab}}{2} \qquad \text{Equation 6}$$

For a geometrically identical pair of meshing gears, it can be shown that the maximum sliding velocity is approximately equal to twice the angular velocity. Theoretically, sliding

velocity will be maximum at the first and last point of contact (when the path of approach/recess is maximum) and will be zero when the tooth mesh is at the pitch point.

3.2.3. Polymer Gear Temperature

In polymers, friction and wear result from the dissipation of mechanical energy which in turn results in deformation (hysteresis) and frictional heating. Sliding temperatures predominantly influence the frictional performance of polymers due to the transitions from glassy into rubbery and from the rubbery into the melting phase. Generally, the sliding properties of polymers are characterised by the "*pv*" relationship (contact pressure x sliding velocity).

In an attempt to increase the transmissible power levels obtainable through polymer gears, problems of surface temperatures arise due to the frictional losses between mating gear teeth [17,60]. High frictional forces generated in some polymeric contacts induce high surface temperatures.

Temperature dominates all aspects of plastic gear performance, and thus limits their operational range [60–62]. It has a detrimental effect on mechanical material properties and has an influence on all of the major plastic gear failure modes. Heat is generated during the meshing of polymer gear teeth through a complex combination of mechanisms. These are:

- Hysteresis loses, generated as a result of viscoelastic deformation and which is mainly converted into heat.
- Frictional heating, caused by the kinematics of the meshing cycle (i.e. the combined rolling and sliding).
- Heat conducted through drive shafts of the gears.

- Ambient radiation.

In most applications in which polymer gears are used, ambient radiation and conduction through the drive shafts represents a negligible contribution to overall heat generation and can be all but eliminated through careful design of application.

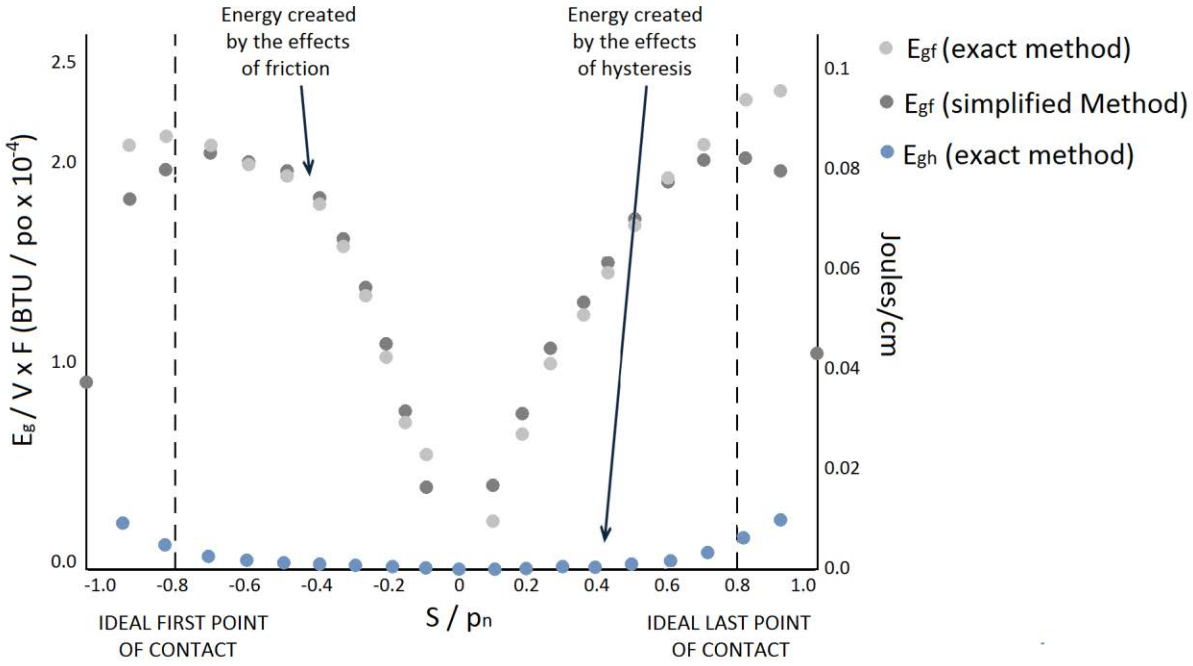

Figure 15: A comparison of the calculated energy created from friction and hysteresis for a pair of meshing polyamide gears [Note: Gears modelled with 20 teeth, transmitting 53 Nmm with a storage modulus of 2.07 GPa, a loss modulus od 0.05 and a co-efficient of friction of 0.1 [63]]

Of the remaining two factors, frictional heating has been shown to be by far the most dominant mechanisms of heat generation. Koffi *et al.* first modelled the components of heat generation per unit facewidth for a polyamide 66 gear [63]. **Figure 15** shows the results of the model for both frictional and hysteretic heating. It predicts that heat generated hysteresis will be much lower compared to that generated from friction. This is

shown to be the case except for pure rolling (i.e. at the pitch point of the gears, where sliding velocities are zero) and during tooth contact outside the line of action where tooth deformation is increased [64]. Both Hooke *et al.* and Kukureka *et al.* confirm that this is the case for polyamide roll/slide twin disc tests [17,18,65].

Based on the above, for the experiments described in this thesis, the frictional heating is assumed to be much greater than the other mechanisms of heat generation in the test gears. Hence with the loading, rotational speed and ambient laboratory conditions held constant, differences in measured temperatures are attributed to a change in the friction sliding friction between the meshing tooth flanks.

There have been many attempts to reduce temperatures in polymer gears by reducing surface friction, with varying degrees of success. These include the use of PTFE filled polymer composites [66]; this reduced temperature and wear although the high filler content required was shown to degrade the matrix, tooth geometry modification to reduce the specific line loads carried by individual teeth and the introduction of cooling holes throughout the gear body [61,67]. If temperature is not controlled, then failure often occurs in the form of gross wear.

3.2.4. Polymer Gear Wear

The majority of polymer gear failures and failure mechanisms have been attributed to wear [13,17–19].

It has been shown that the ability of a polymer to resist wear is not solely dependent on the E/H ratio. This is emphasised when one considers the fundamental motions involved in some machine elements. In dry-running polymer applications, wear has consistently been shown to be the most prevalent mode of failure and has been widely reported

[39,66,68,69]. It is also one of the most difficult forms of failure to predict. The rate at which wear occurs in a given polymer gear set is dependent on many different factors which include:

- Operational factors – sliding velocity, contact pressure and ambient temperature
- Material factors – surface energy; similar materials meshes, dissimilar materials, fillers and the addition of internal lubricants
- Gear geometry – pressure angle, module and facewidth

Rao *et al.* [66] showed that controlling the friction generated at the meshing point had a positive effect on the wear resistance of polymer gears. All authors suggest that reducing flash temperatures reduces gear wear.

Most of the published work on the tribology of non-conformal polymer pairs relates to the performance of gears. The typical surface topography demonstrated by a polymer gear tooth flank is shown in **Figure 16**. The raised pitch line is clearly visible across the entire flank indicating that this is the driven gear of the test pair. Above this point wear patterns may be observed where the roll/slide is in the same direction. Below the pitch-line roll/slide are in opposition and show typical scalloped wear damage. In addition to the expected patterns, a zone of premature contact is also visible at the tooth tip.

The importance and effects of the combined roll/slide are thus underlined. Cropper [14] found that some polymers were far more susceptible to the transition between the phases of approach and recess, such that significant differences in wear resistance between driver and driven were observed.

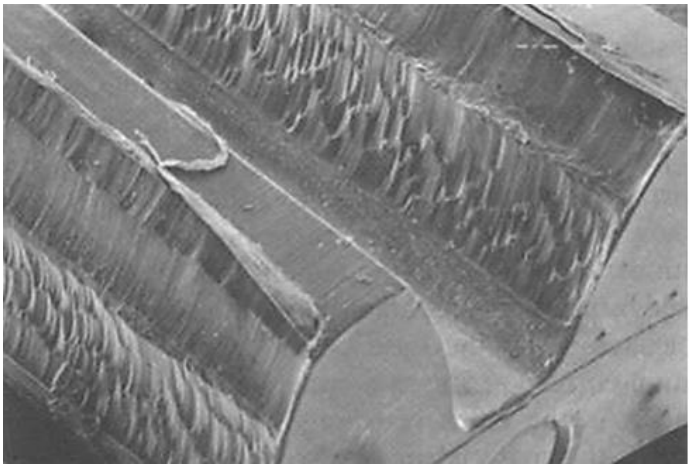

Figure 16: Severe wear damage to a polymer gear and effects of roll slide motion [68]

Despite the difficulties faced in predicting wear rates for different materials, the demonstration of wear in polymer gears displays similar characteristics despite the vast variation in materials.

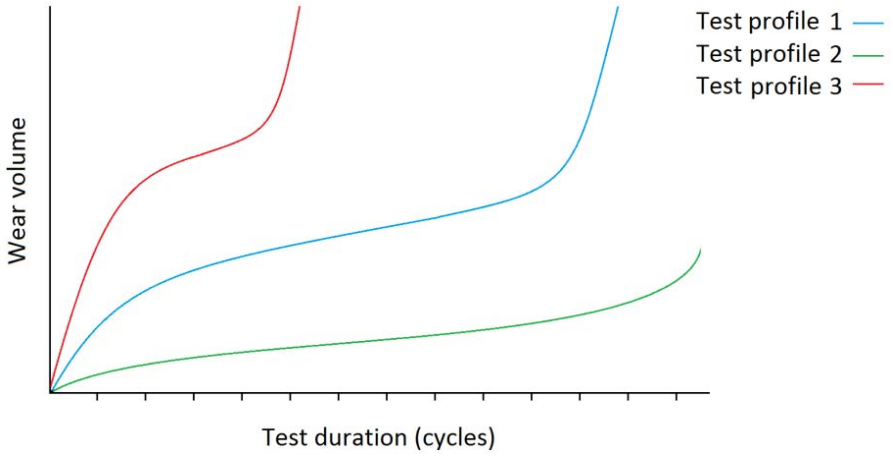

Figure 17: Typical wear, usually independent of material [5]

The most common wear record is that shown by profile 1, where three distinct regions may be observed (**Figure 17**); the gear first experiences a '*running-in*' period where the tooth profile adjusts to an optimum geometry (this is usually the period where manufacturing errors are removed). There is secondly a period of steady-state wear

followed by a final period of rapid wear and failure. The second data set is similar to the first with the running-in period removed; this response is indicative of an accurate gear set designed for a specific application. Finally, data set three shows a sudden onset of rapid wear, most likely to be associated with the surface melting of the active tooth flanks as the flash temperature approaches the material melting point. Hooke *et al.* [17] defined this operational limit as the transition torque and indicated that it was a weak function of operational speed and a much stronger function of applied load.

3.2.5. Polymer Gear Failure

Unlike their metallic counterparts, deflection and temperature play a significant role in the response of a polymeric material to a mechanical application. The influence of temperature, lubrication, load and sliding speed on the tribological performance of a polymeric material has been discussed. However, the failure response of polymer gears can also be significantly different to that for steel gears.

Polymer gears share many failure modes with metal gears such as bending fatigue. **Figure 18** shows a PEEK gear demonstrating bending fatigue in the root of both the active and non-active gear flanks as well as rim failure. It can also be seen that the tooth has been permanently deformed following load removal [14].

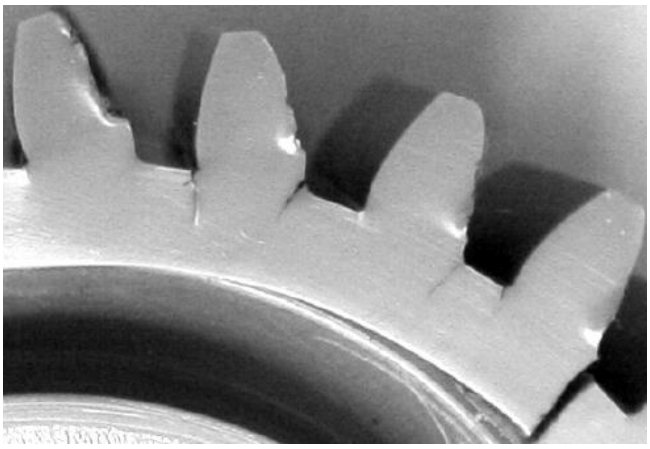

Figure 18: Root and gear wall failure [44]

However, some failure modes only occur in polymer gears. Hatchman and Strickle [70] observed four main groups of failure; root bending fatigue, pitch-line fracture, excessive wear and pitting damage. In addition, the failure mechanisms observed were all significantly affected by temperature.

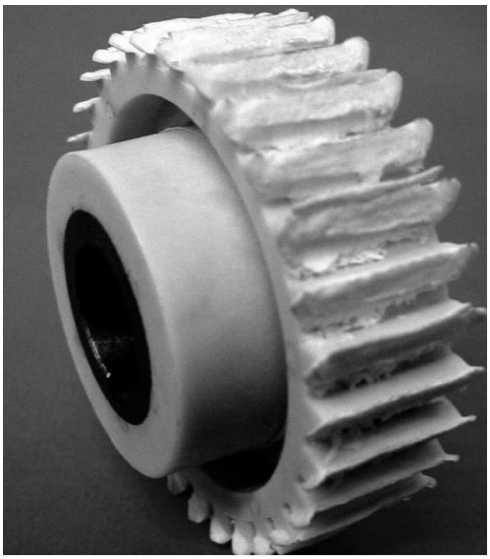

Figure 19: Nylon 6/6 composite gear (30% Glass fibre and 15% PTFE) that has thermally failed resulting in gross wear [14]

Figure 19 shows a thermally overloaded PA 6/6 composite gear containing 30% glass fibre and 15% PTFE by volume, dry run at 15Nm and 1500rpm. Thermal failure can occur as the conjugate motion of a polymer is lost due to excessive deflection, or as the surface of the polymer is subjected to flash temperatures exceeding the melting point of the material. Both are the result of the plastic flow of the material caused by overloading.

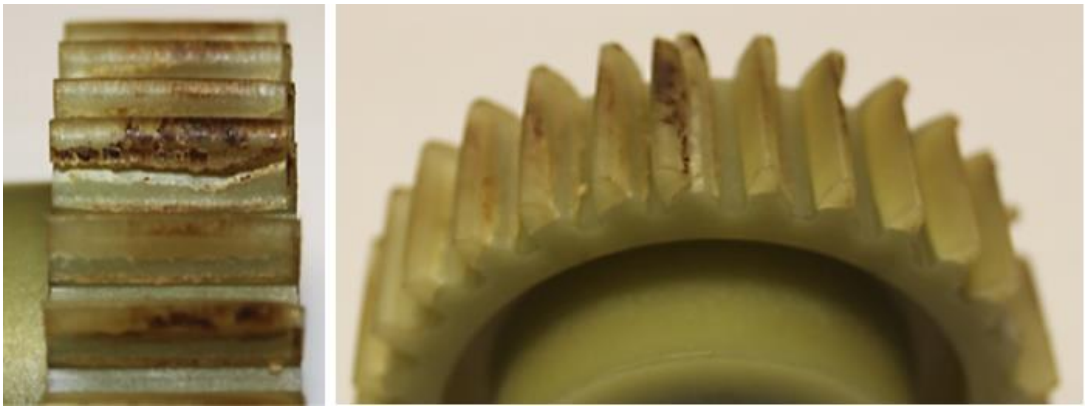

Figure 20: Pitch line fracture in glass fibre reinforced Nylon 6/6

Another form of failure only seen in polymers is pitch-line-fracture (PLF) (**Figure 20**). PLF is a form of failure predominantly associated with un-lubricated polyamide and polyamide composites. However, its occurrence has been observed in both dry and lubricated polyetheretherketone (PEEK) gears [44].

In unreinforced nylon gears the initial PLF occurs on the driver gear, below the pitch line, following a direction approximately normal to the contact force and at the centre of the face width, where the bulk temperatures are highest [62,71]. The mechanisms of failure are not fully understood with several authors suggesting that the failure is a result of a complex combination of factors [5,18,68,72,73].

The introduction of lubrication, by definition, will reduce the coefficient of friction and subsequently the flash temperatures during the meshing cycle. However, fatigue

experiments conducted with PEEK and PA6/6 gears, run lubricated at high temperatures, have resulted in gross pitting (**Figure 21**)

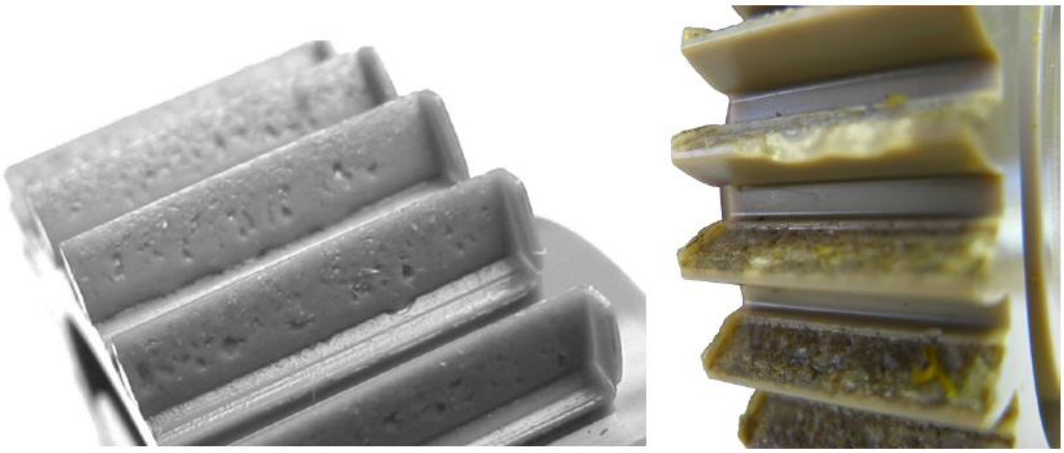

Figure 21: Severe pitting when run in lubricant under high loads, a) PEEK gear, b) PA 6/6 gear [14]

3.3. Polymer Gear Material Selection

Much of the literature on polymers gears relates to nylon and POM, which reflects the fact that these materials are used in over 85% of plastic gearing applications [14]. However, polymer gear design has predominantly been centred on motion and control in applications such as those found in office equipment, automatic telling machines, domestic appliances and small electric motors; where the transmissible loads and running speeds were low.

More recently, preliminary investigations into the use of high temperature polymers in automotive mass balance and pump gear applications to reduce system inertia, power consumption and noise levels have re-emphasised their potential benefits for power transmission applications [3,4].

When selecting a polymer for mechanical applications (specifically gearing), the flexural stress, stiffness and shear strength to resist tooth deflection, and tooth root failures should all be considered. Depending on lubrication conditions, consideration may also be given to compressive stress and frictional properties. And economic considerations must also be made.

Kurokawa *et al.* compared the performance of unreinforced PEEK, a CFR PEEK composite, and POM, run against a steel pinion in dry and partially lubricated conditions [74]. They reported that the CFR composite carried twice the load conveyed by the POM gears. The same authors conducted a comparative study with PEEK and other advanced engineering polymers such as PAI (polyamideimide) and PPS (polyphenylenesulphide) with results indicating that PEEK was the best performing [75].

Experiments conducted under dry running conditions show that PEEK is superior to most other engineering polymers. However, it is questionable whether this outweighs the disadvantage in terms of the higher costs incurred when it is specified.

Rösler (2005) demonstrated that under lubricated conditions at high temperatures, PEEK gears maintain their mechanical properties and fatigue life, relative to other polymers, such that high loads can be carried. This suggests that PEEK gears, if designed correctly, could be specified in moderate power transmission applications.

Initially the resilience of polymers was considered to be greatly desirable for mechanical applications; it meant that during motion both noise and contact forces were reduced, however, recent research on polymer gear noise has shown that friction also plays a very important role in noise generation and wear [29]. In addition, the resilience of a material can significantly alter the path of contact of a meshing gear pair, promoting premature

and extended contact [64]. Hence, efforts have been made to reduce the resilience of polymers by fibre reinforcement.

However, the inclusion of reinforcing fillers can alter the wear mechanism. Typically, the exposure of a reinforcing element results in abrasive wear as the filler contacts the softer base matrix. Hooke *et al.* investigated the effect of glass fibre reinforcement on the wear properties of polyamide discs and gears [17]. It was found that the reinforcement was dispersed within the matrix and once an initial layer was removed, they observed the most prolific form of wear was abrasion.

The specification of a polymer for a specific mechanical application is complex. Walton and Shi compared several institutional and commercial rating standards for polymer gears. They observed large discrepancies between them, concluding that the combined influence of application factors such as temperature, geometry, wear and friction means that the only way of confidently specifying a polymer for a mechanical application is to physically test them [8].

Therefore, to investigate the applicability of a polymer for a specific mechanical application, consideration of the gear system kinematics and the influence of these on material properties must be made.

Material testing been shown to provide an indication of a materials performance for an application, however, at present, the use of mechanical simulation tests to replicate the operating conditions of polymeric gears are limited to twin-disc studies investigating the roll/slide interaction near the pitch point.

To conclude, the selection of a polymer for a mechanical application is complex; the physical and mechanical properties of the material result in the kinematic response of

compliant polymer gear materials not conforming to current gear selection standards. Therefore, the only way of confidently specifying a polymer for a specific mechanical application is to physically test them.

Chapter 4

TEST METHODOLOGY

4.1. Introduction

Due to the large discrepancy between the commercial and institutional rating standards for polymer gears, the only way to confidently specify gears made of polymeric materials is to physically test them [72].

This section outlines the test methodologies used throughout this thesis; methods of measuring and quantifying the physical and mechanical properties of polymers are outlined. In addition, the use of tribological testing methods in the simulation of polymer gear contact is discussed, and the operation of both the tribological and gear test rigs summarised.

4.2. Physical Properties of Polymers

The physical properties of a material provide an indication of the process capabilities and also an initial suggestion of the surface and bulk material characteristics.

4.2.1. Surface Microscopy

Throughout this project, scanning electron microscopy (SEM) was used as well as optical microscopy. For the SEM imaging, there was a requirement for the specimens to be electrically conductive, thus it was necessary to sputter coat the polymer surfaces. This deposited an ultra-thin layer of gold onto the surface allowing the polymer surface to be imaged.

Scanning electron microscopy was carried out using a Jeol 6060 SEM fitted with an Oxford instruments Inca 300 energy-dispersive X-ray spectroscopy (EDS) system.

4.2.2. Topographical Methods

Topographical measurement was used to understand how the surface condition of a sample varied with operation; providing wear scar volumes and surface roughness characteristics through three-dimensional surface profiling.

3D measurements of the surface were made using an Alicona infinite focus measurement system[6] (Alicona Imaging GmbH., Austria) and a KLA Tencor MicroXAM2 optical interferometer (KLA-Tencor., California, USA).

4.2.3. Mercury Porosimetry

Mercury porosimetry was used for sub-surface characterisation. By measuring the differential intrusion of mercury into a porous structure under controlled pressure, sample

[6] The optical interferometer used in this research was obtained, through Birmingham Science City: *Innovative Uses for Advanced Materials in the Modern World (West Midlands Centre for Advanced Materials Project 2), with support from Advantage West Midlands (AWM) and part funded by the European Regional Development Fund (ERDF).*

properties such as pore size distributions, total pore volume, median pore diameter, and sample densities (bulk and skeletal) could be determined. In this study, a Micrometrics AutoPore IV was used allowing theoretical pore diameters from 6 nm to 360 μm to be detected. Mercury intrusion into the sample was analysed using the Washburn equation (**Equation 7**) in order to determine the pore diameter distribution, assuming cylindrical pore geometry [76]:

$$D = -\frac{4 \cdot \gamma}{P} \cdot cos\theta \qquad \textbf{Equation 7}$$

where D is pore diameter, P is the applied pressure, γ is the surface tension of mercury at 20 °C, which was assumed to be 0.485 N/m, and θ is the contact angle between the Mercury and the solid, which was assumed to be 130 degrees [76].

4.2.4. Crystallinity

To determine whether the surface of the test samples underwent any thermal ageing/ enthalpic relaxation during testing, the crystallinity of the samples were investigated using Differential Scanning Calorimetry (DSC).

DSC was used to measure variation in relative heat flow of the material with temperature. The Perkin Elmer DSC 7 unit used in this thesis consisted of a sample and a reference cell, both of which have separate heaters and platinum resistance temperature sensors. The heaters are coupled so that the differential power needed to maintain the two cells at the same temperature, can be measured [77,78].

The DSC was calibrated using the melting points of high purity Zinc (Tm = 419.53°C) and Indium (Tm = 156.63 °C). From this corrections for thermal lag were made by extrapolating for a zero heating rate.

To assess the crystallinity of the test samples material was removed from the test surface. This was then weighed and held in Aluminium pans; an empty pan was used as a reference for the relative heat flow of the container with temperature.

Thus it was possible to obtain the percentage crystallinity for the samples using **Equation 8**, where ΔH is the enthalpy.

$$\% \, Crystallinity = \frac{\Delta H_{measured}}{\Delta H_{fusion}} \qquad \textbf{Equation 8}$$

4.3. Mechanical Testing of Polymers

This section reports on the standard testing methods used in the determination of the mechanical properties of the polymers used in this research. However, it should be noted that the mechanical tests performed are based on standards for traditional methods of polymer production as, currently; no standard for the mechanical testing of SLS polymer materials exists. Therefore, as roughness was a result of the manufacturing process, samples were tested '*as produced*', i.e. neither polished nor machined to fit surface roughness tolerances described in the ISO standards.

4.3.1. Flexural Properties

Flexural properties define a materials response to bending. **BS EN ISO 178:2010** suggests a three-point-bending method for determining the flexural strength and flexural modulus of rigid and semi-rigid plastics.

The test required a specimen of rectangular cross section, resting on two supports, to be deflected by means of a loading edge acting on the specimen midway between the supports (**Figure 22**). The test specimen was deflected in this way at a constant rate

until rupture occurred at the outer surface of the specimen or until a maximum strain of 5% was reached, whichever occurred first. During this procedure, the force applied to the specimen and the resulting deflections were measured.

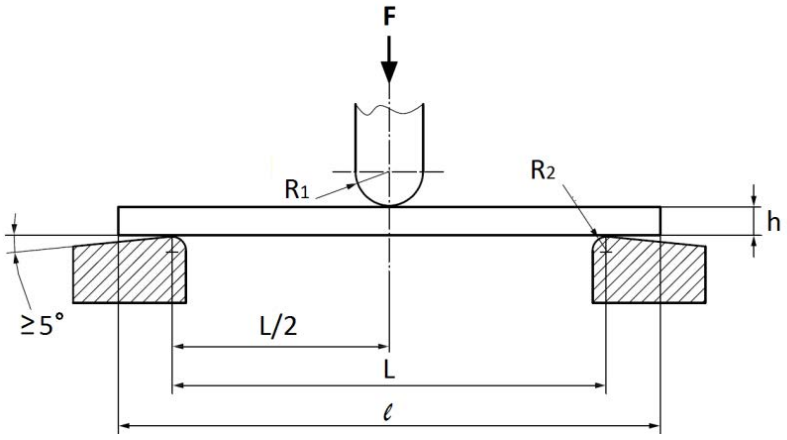

Figure 22: 3 point bending test layout

The specimen dimensions, according to **BS EN ISO 178:2010** were:

- Length, *l*: 80 ± 2mm
- Width, *b*: 10.0 ± 0.2mm
- Thickness, *h*: 4.0 ± 0.2mm

It was recommended that at least five test specimens were tested at a strain rate of approximately 1%/min. Each specimen was located so that the load was applied through the centre point of the sample, it was supported so that:

$$L = (16 \pm 1)\bar{h} \qquad \textbf{Equation 9}$$

For determining the flexural modulus of the material, it was necessary to select an appropriate test speed, defined in **Equation 10** where (v), is the speed of the loading edge relative to the specimen supports, and r is the flexural strain rate (%/min).

$$v = \frac{r \cdot L^2}{600 \cdot h} \qquad \textbf{Equation 10}$$

It was then possible to calculate the flexural stress (**Equation 11**) and the flexural strain (**Equation 12**), where s is the deflection in millimetres:

$$\sigma_f = \frac{3 \cdot F \cdot L}{2 \cdot b \cdot h^2} \qquad \textbf{Equation 11}$$

$$\varepsilon_f = \frac{600 \cdot s \cdot h}{L^2}\% \qquad \textbf{Equation 12}$$

Thus the associated flexural modulus can be calculated (**Equation 13**):

$$E_f = \frac{\sigma_{f2} - \sigma_{f1}}{\epsilon_{f2} - \varepsilon_{f1}} \qquad \textbf{Equation 13}$$

Alternative standards for determining the flexural properties of polymers are **ASTM D790-10**, **ASTM D6272-10** and **BS EN ISO 14125:2011**. These standards cover both three and four point bending; however, for four point bending tests it is difficult to determine failure as the load distribution is not defined.

4.3.2. Tensile Properties

EN ISO 527:2012 provides the general principles for determining the tensile properties of plastics and plastics composites.

The test specimen is extended along its major longitudinal axis at a constant speed until the specimen fractures. It was recommended that five tensile tests were run following **ISO 527-2/1A/1**; this corresponded to an extension rate of 1mm/min and a strain rate of approximately 1%/min assuming uniform deformation. The load sustained by the specimen (**Figure 23**) was then measured against the material elongation.

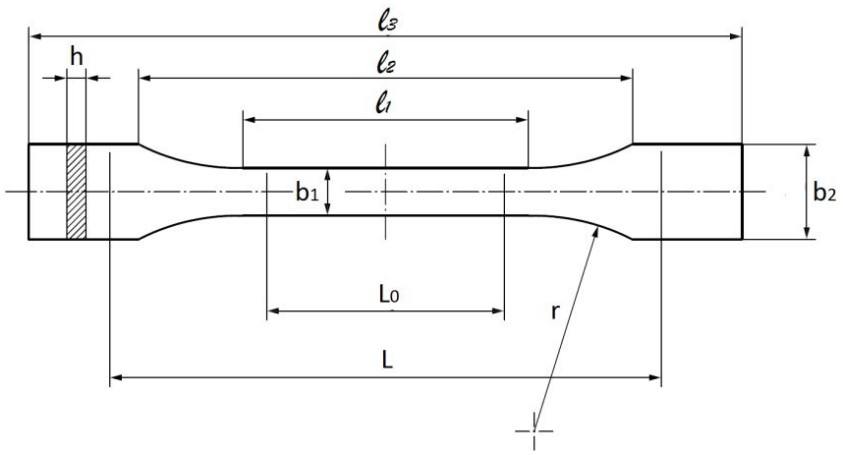

Figure 23: Type 1A and 1B tensile test specimen (**EN ISO 527-2:2012**)

The specimen dimensions, according to **EN ISO 527-2:2012** for injection-moulded multipurpose test specimens and for compression-moulded specimens were:

- Overall length, l_3: 170mm
- Length of narrow parallel-sided portion, l_1: 80 ± 2mm
- Radius, r: 24 ± 1mm
- Distance between broad parallel-sided portions, l_2: 109.3 ± 3.2 mm
- Width at ends, b_2: 20.0 ± 0.2mm
- Width at narrow portion, b_1: 10.0 ± 0.2mm
- Preferred thickness, h: 4.0 ± 0.2 mm
- Gauge length (preferred), L_0: 75.0 ± 0.5 mm
- Initial distance between grips, L: 115 ± 1 mm

It should be noted that at 4mm thickness, the specimen type is identical to the multipurpose type A test specimen according to **ISO 3167** and type A1 of **ISO 20753**.

From the tested samples, the stress and strain values could be determined using **Equation 14** and **Equation 15** respectively:

$$\sigma = \frac{F}{A_0} \qquad \textbf{Equation 14}$$

$$\varepsilon = \frac{\Delta L_0}{L_0} \qquad \textbf{Equation 15}$$

where, F is the measured force, A_0 is the initial cross-sectional area and L_0 is the gauge length of the specimen.

Thus the tensile modulus could be calculated by:

$$E_T = \frac{\sigma_2 - \sigma_1}{\varepsilon_2 - \varepsilon_1} \qquad \textbf{Equation 16}$$

where σ_1 and σ_2 are the measured strain values at 0.05% and 0.25% respectively. Poisons ration was determined using **Equation 17**:

$$\nu = \frac{\Delta \varepsilon_n}{\varepsilon_l} \qquad \textbf{Equation 17}$$

where ε_n is the strain decrease in the selected transverse direction and ε_l is the longitudinal strain increase expressed as a dimensionless ratio or percentage.

Alternative standards for determining the tensile properties of polymers are **ASTM D638**, **ASTM D3039**.

4.3.3. Fracture Properties

A fracture is defined as the separation of an object into two or more pieces under the action of stress. A materials resistance to this action is described as its fracture toughness. A method for determining this property for a polymer is defined in **BS ISO 13586:2000**. The test specimen is shown in **Figure 24**, with an integral notch. The sharp edge at the tip of the notch was produced, post production, using a razor blade as specified in **BS**

ISO 13586:2000. The length of the crack thus created should be more than four times the original notch tip radius. Additionally, the crack length a should preferably be in the range given by $0.45 \leq a/w \leq 0.55$.

Figure 24 also shows the test layout. It should be noted that the test equipment conforms to **BS EN ISO 178:2010** for the determination of the flexural properties of a polymer under three point bending.

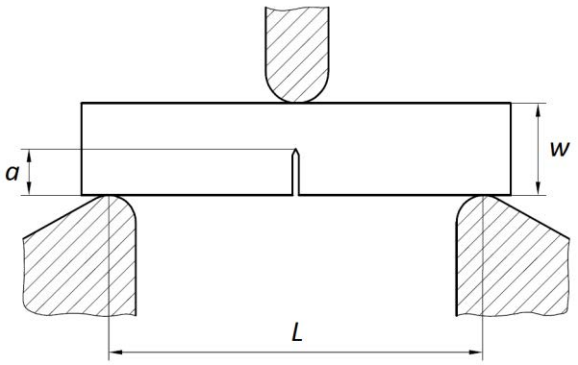

Figure 24: Fracture toughness test specimen

The specimen dimensions according to **BS ISO 13586 (2000)** were:

- Width, w: arbitrary
- Length, l: $\geq 4.2w$
- Crack length, a: $0.45w \leq a \leq 0.55w$
- Thickness, h: $w/4 < h < w/2$
- Span between rollers, L: $4w \pm 0.1w$

The critical stress intensity factor (K_{IC}) is related to the critical energy release rate (G_{IC}) by the equation:

$$G_{IC} = \frac{{K_{IC}}^2}{2} \qquad \textbf{Equation 18}$$

where E is the modulus of elasticity under plain strain conditions:

$$E = \frac{E_t}{1 - \nu^2} \qquad \textbf{Equation 19}$$

E_t is the tensile modulus (**ISO 527-1**) and ν is poison's ratio.

4.3.4. Compressive Properties

BS EN ISO 604 (2003) describes a test method for determining the compressive strength and compressive modulus of a polymer.

The test specimens for this methodology should be a right prism, cylinder or tube satisfying the following inequality (**Equation 20**):

$$\varepsilon_c{}^* \leq 0.4\frac{x^2}{l^2} \qquad \textbf{Equation 20}$$

where, $\varepsilon_c{}^*$ is the maximum nominal compressive strain occurring during the test; l is the length of the specimen measured parallel to the axis of the compressive force; and x is the diameter of the cylinder, the outer diameter of the tube or the thickness (the shortest side of the cross section of the prism, depending on the shape of the test specimen).

In the measurement of compressive modulus and strength, two different geometries and operating conditions were chosen:

To determine the compressive modulus, five 'type A' (right prism) compressive specimens (Length, l: 50 ± 2 mm, width, b: 10 ± 0.2 mm, thickness, h: 4 ± 0.2 mm) were tested according to **ISO 604/A/1**, corresponding to a compression rate of 1mm/min.

For compressive strength, five 'type B' (right prism) compressive specimens (Length, l: 10 ± 0.2 mm, width, b: 10 ± 0.2 mm, thickness, h: 4 ± 0.2 mm) were tested according to **ISO 604/B/5**, corresponding to a compression rate of 5mm/min.

The test specimens were compressed along their major axis at a constant speed whilst the load sustained by the specimen was measured.

The compressive modulus was calculated using a similar method to that for the tensile modulus defined in **section 4.3.2**.

4.4. Thermal Analysis

Dynamic Mechanical Thermal Analysis (DMTA) was used to characterise the viscoelastic or time-dependent behaviour of the polymer materials.

By applying a sinusoidal load to the sample, the time-dependence of the resultant strain was measured with respect to the applied stress. This allowed the in-phase storage modulus (*E'*) and the out-of-phase loss modulus (*E"*) to be measured. The ratio *E"/E'* defined the loss tangent ($tan\,\delta$).

In this study DMTA tests were performed using a Rheometric Scientific DMTA MK III (TA instruments., New Castle, USA). The experiments were performed in a dual-cantilever arrangement in three-point-bending for a range of frequencies. The samples were heated from 100 to 250 °C at a heating rate of 0.5 °C/min and the displacement was kept constant at 20 µm to ensure measurements were limited to the linear viscoelastic region.

4.5. Tribological and Application-related Analysis

4.5.1. Theory of Polymer Gear Contact

Physical testing methods are the most reliable method for determining the mechanical properties of a polymer for a specific application. However, the response of a specific

polymer to changes in load, speed and geometry can significantly affect the performance of a polymer gear.

To develop appropriate test conditions, the dynamic effects specific to polymer gear contact need to be understood, and their effect on tribological conditions outlined.

4.5.1.1. Gear Kinematics

In polymeric gears, the compliance of the material means that the path of contact extends at the start and end of mesh beyond the theoretical path for a perfectly stiff gear mesh (**Figure 25**) [3–5]. When the path of contact is extended, the load distribution between meshing teeth and the sliding velocity are also altered.

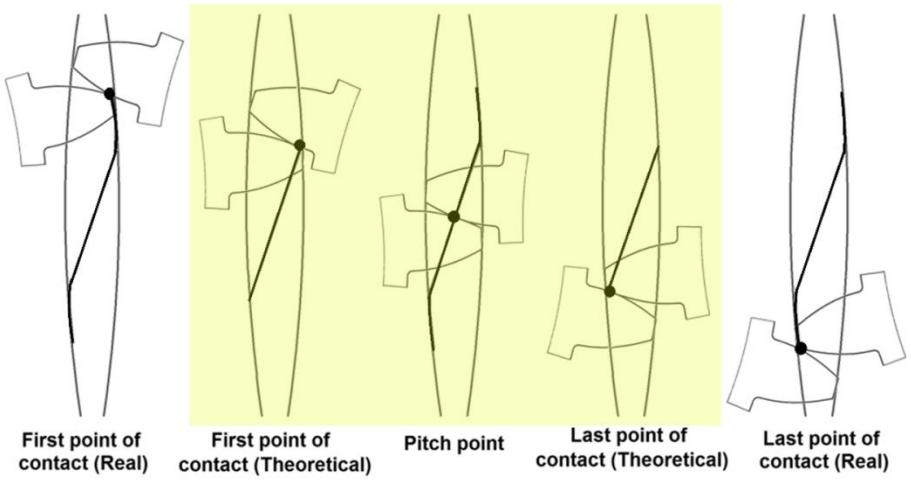

Figure 25: The real and theoretical paths of contact for a pair of meshing polymer gear teeth [19]

The Birmingham standard gear geometry has a theoretical contact ratio of 1.653, this means that during the mesh there are stages where only a single tooth is transmitting the torque. However, in high compliance polymer gears Karimpour *et al.* showed that the path of contact is extended, and that the load is shared, increasing the true contact ratio [64].

Figure 26 shows how the load sharing ratio varies with roll angle for a high compliance polymer gear based on the University of Birmingham test geometry [64].

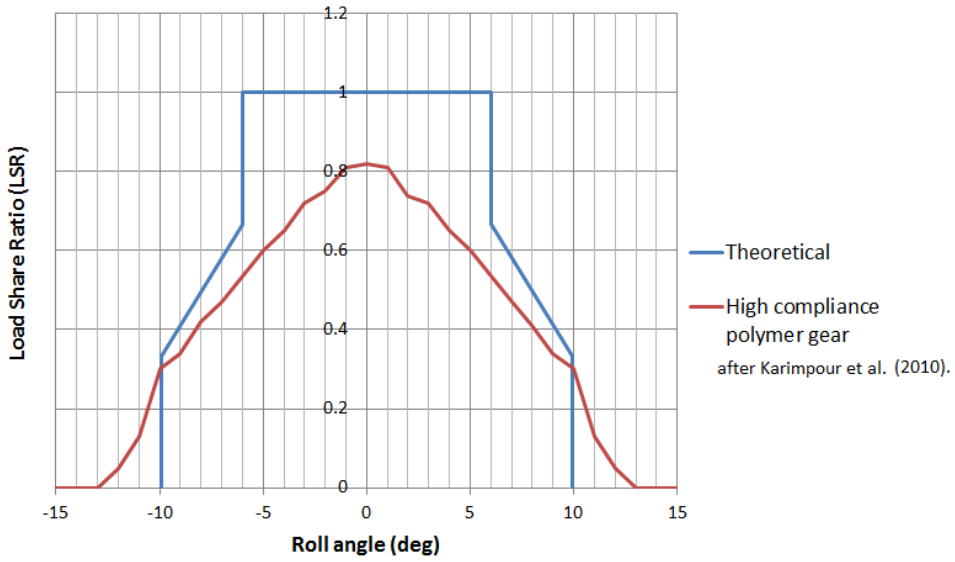

Figure 26: Load share ratio based on a perfectly stiff gear tooth, and incorporating deflection associated with polymer gears

From **Figure 26** it can be seen that for a perfectly stiff gear, single tooth contact theoretically occurs over 12 degrees of tooth contact, this corresponds to a path of contact of 5.9mm. However, in reality, the profile becomes more parabolic, as tooth damping effects in polymer gears reduce the step from single to multiple tooth contact. In addition, the compliance (deflection 'lag' of successive mating teeth) means that the path of contact is extended, and that the load is shared, increasing the true contact ratio in the Birmingham standard geometry gear to above 2 in some cases [64].

By increasing the path of contact, the dynamics of a gear mesh will change.

The slip ratio of a pair of meshing gears refers to the ratio of the sliding velocity at the point of contact, to the rolling velocity. For two discs, rotating at V_1 and V_2 respectively, the slip ratio can be described by **Equation 21**.

$$slip\ ratio\ (\%) = 2 \cdot \frac{V_2 - V_1}{V_1 + V_2} \qquad \textbf{Equation 21}$$

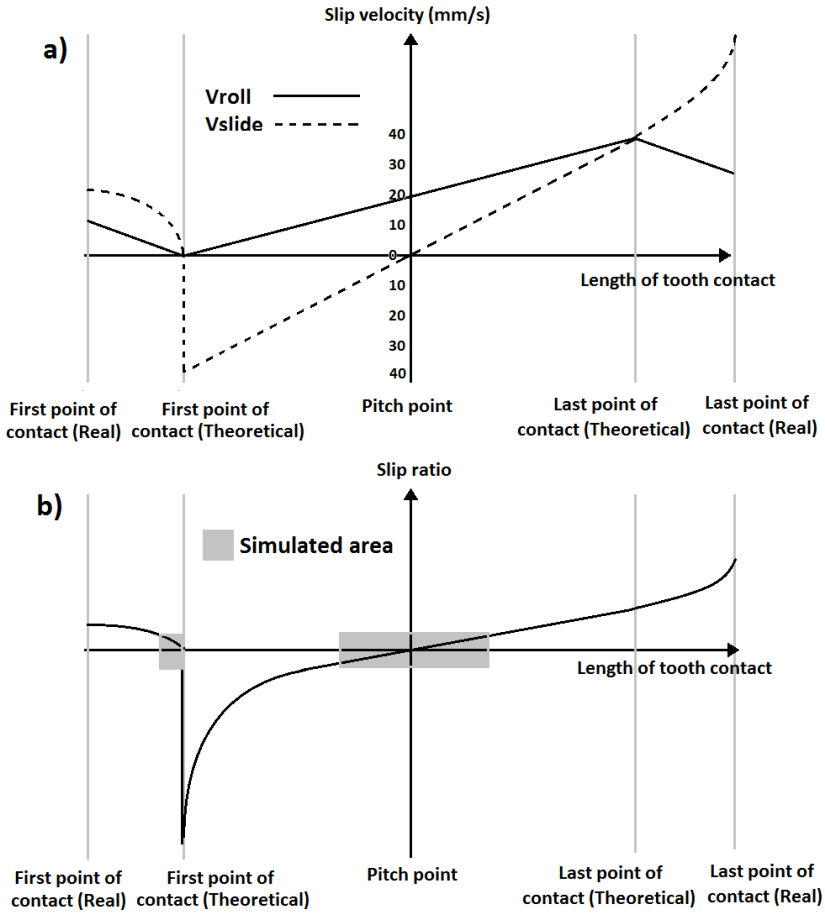

Figure 27: a) Shows the sliding velocity (Vslide), rolling velocity (Vroll), and **b)** the slip ratio for a polymer gear contact: Grey areas representing simulated areas when using twin disc testing [13]

Figure 27 shows the theoretical slip-ratios for a pair of meshing gear teeth without deflection and the influence of the extension in the path of contact. It was observed that twin disc testing can model different meshing positions on a simulated gear tooth depending on the extent to which deflection affects the system. In addition, from **Figure 27** it can be seen that slip ratios of up to 30% obtainable using twin disc tests, will

simulate both the region surrounding the pitch-point and the theoretical first point of contact when large deflections occur.

4.5.2. Twin Disc Test Rig

To simplify gear contact, a simple twin-disc test rig was used for un-lubricated, rolling-sliding tests and is shown schematically in **Figure 28**. Two cylindrical test discs were mounted on spindles contained in a friction block and a pivoted loading block. An electric motor was used to drive the input shaft using two toothed drive belts and a pair of speed changing gears the discs could be driven at a controlled speed, and by alteration of the gear ratio, the relative slip ratio between the contacting discs could be adjusted.

During operation, loads are applied to the system by a weight attached to the upper, pivoted loading block to provide a normal force between the two discs. The lower block is mounted on vertical leaf springs and strain gauges are used to determine the sliding frictional force by noting the tangential force on the lower disc. Wear of the samples is measured by detecting the displacement of the upper block using a linear variable differential transformer (LVDT) to record the displacement of the disc centres.

Twin disc testing is typically used, when simulating gears, to investigate the performance of a polymer around the pitch-point where the slip-ratio is close to 0; i.e. the contact is based on low sliding and high rolling velocities.

However, the kinematic model in **Figure 27** shows that when large deflections occur, the path of contact is extended; thus allowing tooth conditions to also be modelled for the extremities of the contact.

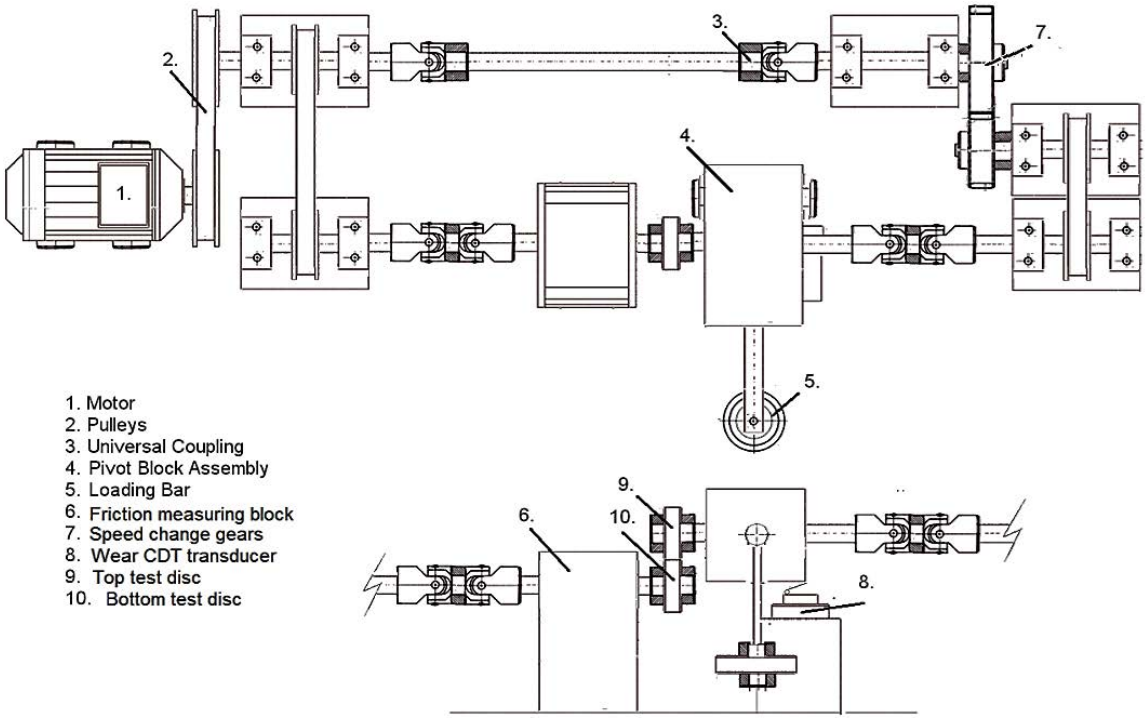

Figure 28: Schematic of the twin-disc test rig

Figure 29 shows the test geometry. The test discs were machined from an extruded bar, and all specimens were polished to a surface roughness of approximately 5 μm whilst maintaining the cylindricity of the discs.

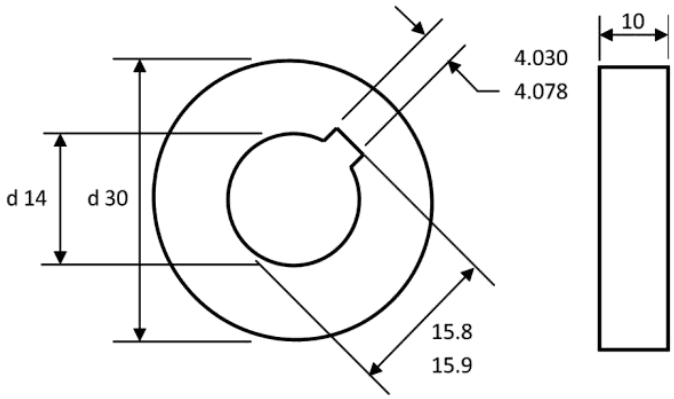

Figure 29: Twin disc test geometry

The test discs were placed on the shafts in the twin-disc test rig and tests were run for a range of loads and slip ratios. During testing the friction, wear and temperature data for the system was recorded.

Table 4 shows the twin disc test conditions investigated in this thesis:

Table 4: Twin disc test conditions (unlubricated, PEEK 450G vs. PEEK 450G)

Load	Max. Contact Pressure*	Slip ratio		
		3.92%	14.29%	28.57%
400N	56MPa	✓	✓	✓
300N	48.5MPa	-	✓	✓
200N	39.6MPa	-	-	✓
100N	28MPa	-	-	✓

Note: PEEK 450G – General grade injection moulded PEEK,

4.5.3. HFRR Test Methodology and Principles

A high frequency reciprocating rig (HFRR) was used to investigate the fretting properties of polymer materials.

The HFRR is an electro-mechanical tribometer that typically employs a (weighted) ball on a (stationary) disc configuration under fretting and boundary lubrication, to produce a wear scar. **Figure 30** shows a schematic of the test rig.

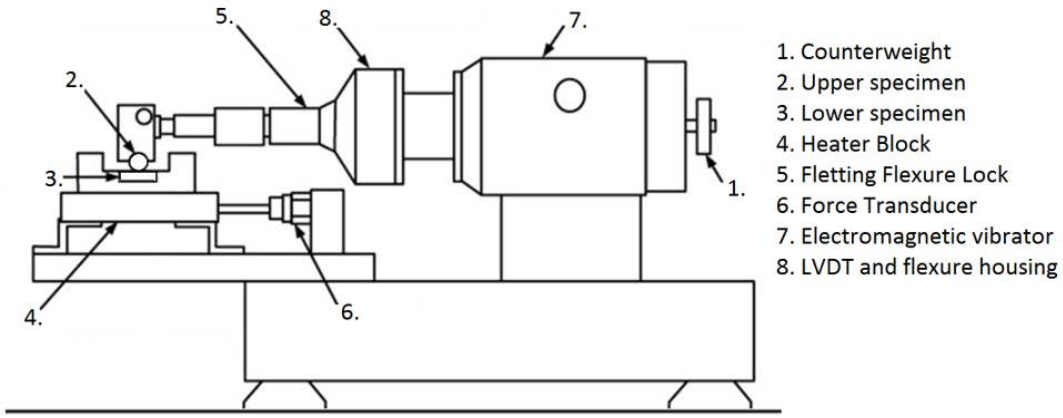

Figure 30: HFRR test rig [80]

The 6mm **ANSI E-52100** steel balls (point 2 in **Figure 30**) were specified to grade 28 (**ANSI B3.12**), with a Rockwell hardness "C" scale (HRC) number of 58-66 (**ISO 6508**), and a surface finish of less than 0.05 µm R_a.

To test the tribological properties of PEEK, test samples were machined from 10mm diameter extruded bar into 3mm length discs. To remove any residual surface damage and to provide uniform surface characteristics in the material, the test discs were individually polished to remove any thermally affected area. This produced a surface roughness of 0.1µm. Polishing was shown by Shen *et al.* to greatly reduce the uncertainty in the surface properties of nylon 66 and its composites when performing nanoindentation experiments. It was concluded that the polishing effect could be ignored for homogeneous polymer systems as the effect of strain hardening was negligible [81].

The experiments were run under defined loads and stroke lengths to produce damage to the contact surfaces, from which the tribological and surface characteristics could be established.

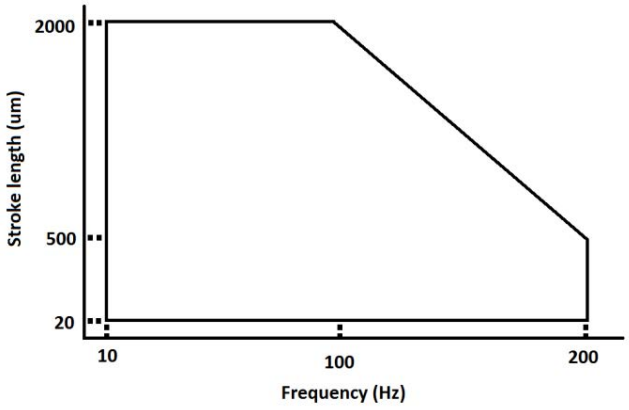

Figure 31: HFRR working envelope

Measurable parameters included: temperature, friction, lubrication film thickness (in conductive samples), and wear (based on the measurement of a wear scar). Surface analysis on both specimens could be observed after testing. The limitations in the working envelope of the HFRR are shown for frequency and stroke length in **Figure 31**.

4.5.3.1. Contact Calculations

The application of fretting tests to the simulation of high performance gears has traditionally been centred on the physical testing of material, and not the direct simulation of the operating conditions of a gear.

To model a gear tooth using a fretting type test, it is necessary to establish appropriate values for contact pressure, fretting frequency and stroke length.

Hertz theory of elastic contact states that, when two curved bodies are brought into contact they initially contact along a line or at a single point. With the smallest application of load, elastic deformation occurs and contact is made over a finite area. A method for determining the size of this region was first described by Hertz in 1881 [82]. It was assumed that:

- The size of the contact area is small compared with the size of the curved bodies
- Both contacting surfaces are smooth and frictionless
- The gap, 'h' between the un-deformed surfaces may be approximated by an expression of the form $h = Ax^2+By^2$ (e.g. the contact between spheres, cylinders and ellipsoids)
- The deformation is elastic and can be calculated by treating each body as an elastic half space*

*An elastic half space is the term given to a flat surface on an infinite elastic solid

Through the use of Hertz's theory, the contact area and contact pressure could be estimated for a load 'F'.

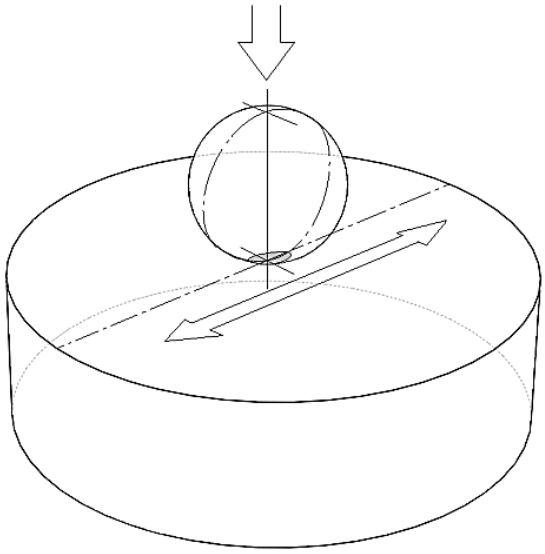

Figure 32: Ball loaded onto a flat surface

Figure 32 shows the ball on flat contact associated with the HFRR. To calculate the contact area and thus the contact pressure, the effective radius 'R' and the reduced modulus 'E^*' were defined as:

contact modulus: $$\frac{1}{E^*} = \frac{1-{v_1}^2}{E_1} + \frac{1-{v_2}^2}{E_2}$$ **Equation 22**

effective curvature: $$\frac{1}{R} = \frac{1}{R_1} + \frac{1}{R_2}$$ **Equation 23**

The region of contact will be spherical with a semi width of contact given by:

$$a = \sqrt[3]{\frac{3 \cdot F \cdot R}{4 \cdot E^*}}$$ **Equation 24**

The peak contact pressure could then be calculated for the contact.

$$P_0 = \frac{3 \cdot F}{2 \cdot \pi \cdot a^2}$$ **Equation 25**

In order to correlate the HFRR test results with polymeric gears, it was necessary to establish appropriate test parameters.

Meshing gear teeth are subjected to bending and contact stresses. For spur gears contacting at the pitch point, the contact stress can be determined through Hertz theory by analysis of two equivalent cylinders in line contact. Under these conditions, the radius of curvature, *'ρ'* at the pitch point can be determined from the gear base circle diameter, *'d_B'* and the working pressure angle, *'ψ'*.

$$\rho = \frac{R_B \cdot \tan\varphi}{2}$$ **Equation 26**

The contact load per unit width, *'F'* acting normal to the contact, was determined from the nominal torque, *'T'* transmitted by the gears, of facewidth, *'w'*.

$$F=\frac{2\cdot T}{d_P\cdot\omega\cdot\cos\alpha} \qquad \textbf{Equation 27}$$

It is important to note that the contact load calculated above is based upon a perfectly stiff gear tooth.

As previously discussed, in high compliance polymer gears the path of contact is extended, and that the load is shared, increasing the true contact ratio. Thus the contact load per unit facewidth becomes:

$$F=\frac{2\cdot T}{d_P\cdot\omega\cdot\cos\alpha}\cdot LSR \qquad \textbf{Equation 28}$$

where the load share ratio (LSR) is determined by the degree of deflection of the material at a specific point.

Through Hertz theory, the effective curvature and the contact modulus of a gear set can be calculated in a similar method to the HFRR sample. Thus, the semi-width of contact was calculated as:

$$a=\sqrt{\frac{4\cdot F\cdot R}{\pi\cdot E^*}} \qquad \textbf{Equation 29}$$

Therefore, the maximum contact pressure could be determined as:

$$P_0=\frac{4\cdot F}{2\cdot\pi\cdot a} \qquad \textbf{Equation 30}$$

As expressions for the contact pressure have been established, the maximum sliding velocity and the length of the path of contact had to also be calculated so that appropriate stroke lengths and operating frequencies could be selected.

To find the maximum velocity of sliding on a gear tooth, it was necessary to find the path of approach and recess, shown in **Figure 33** for a perfectly stiff gear:

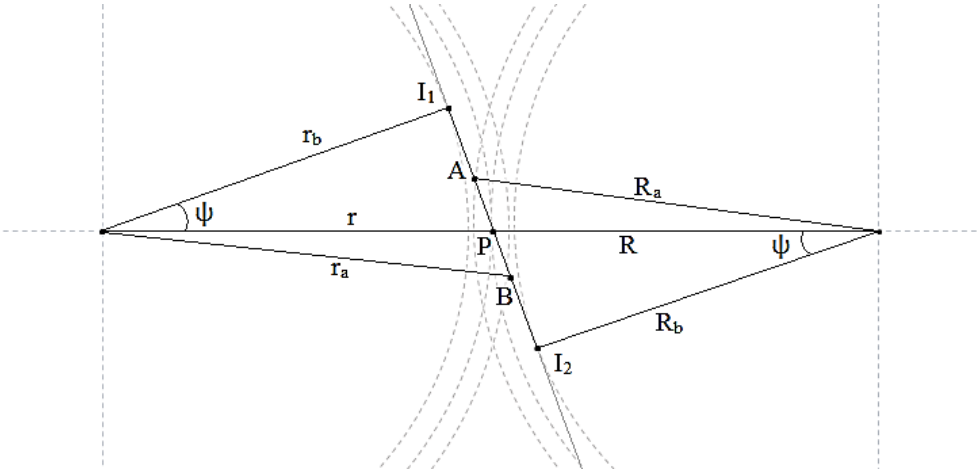

Figure 33: Path of contact of gears, showing the path of approach (A-P), and the path of recess (P-B).

From **Figure 33**, an equation describing the path of approach and recess could be derived:

$$AP = AI_2 - PI_2 = \sqrt{\left({R_a}^2 - {R_b}^2\right)} - Rsin\varphi = \qquad \textbf{Equation 31}$$

$$\sqrt{\left({R_a}^2 - R^2cos^2\varphi\right)} - Rsin\varphi$$

Therefore the path of contact:

$$PC = AP + PB = 2 \cdot AP \qquad \textbf{Equation 32}$$

The maximum sliding velocity ($\hat{C}$) is calculated by:

$$C = (\omega + \Omega) \cdot PC \qquad \textbf{Equation 33}$$

Where the maximum values for the path of contact (PC) occur at the first point of contact and the last point of contact, assuming perfectly stiff gears. Therefore:

$$\hat{C} = (\omega + \Omega) \cdot \left(\frac{PC}{2}\right) \qquad \textbf{Equation 34}$$

Thus, comparison to the maximum sliding speeds for the HFRR could be made, assuming the HFRR operated under simple harmonic motion (SHM) (**Equation 35**).

$$V_{max} = 2 \cdot \pi \cdot f \cdot \frac{l}{2} \qquad \textbf{Equation 35}$$

Where *'V_{max}'* is the maximum sliding velocity, *'f'* is the frequency and *'l'* is the stroke length.

Table 5 shows the equivalent path of contact, maximum contact pressure and maximum sliding velocity that models the central portion of the gear tooth for which there is single tooth contact, assuming perfectly stiff gear teeth for a 7Nm load applied during steel vs. PEEK gear tests at 1000rpm.

Table 5: selected gear test conditions for HFRR testing based on 7Nm steel vs. PEEK gear test @ 1000rpm

Path of contact	5.904 mm
Maximum contact pressure	60.20 MPa
Maximum velocity	618.27 mm/s

Table 6 shows the HFRR load and frequency needed to replicate the contact pressure and the maximum sliding speed over the stroke length.

Table 6: Matching HFRR operating parameters

Stroke length	2.019 mm
Load	0.606 N
Reciprocating frequency	97.47 Hz

However, there are several limiting assumptions that need to be considered when developing a test programme for the HFRR when simulating gears:

- The simulated gear tooth is modelled based on a cyclic single tooth engagement; the main limitation of this is that the cooling effect in the gears during the non-active part of the gear rotation is not simulated.
- The maximum value of sliding speed for a gear is calculated at the extremities of contact; which for perfectly stiff teeth correlates to a contact pressure approaching zero. However, the contact pressure is assumed to be constant across the stroke length in HFRR testing.
- As the sample wears, the contact pressure will change. In addition, bulging effects due to loading were not considered.
- Due to the nature of closed tribosystem testing, if the wear debris is contained within the contact zone the tribological properties of the contact will change.

Although there are limitations in the stroke length on the HFRR, made worse when the effect of regions of extended and premature contact are incorporated into the simulation, the 2mm stroke length is representative of the tooth flank for the Birmingham standard gear geometry. In addition, the HFRR frequencies mirror the maximum sliding velocities in gear tooth contact, again emphasising the strength of this form of testing.

Table 7 shows the HFRR test conditions used in this thesis:

Table 7: HFRR test conditions (PEEK 450G vs. Steel, and EOS PEEK HP3 vs. Steel)

		Loads (Max. contact pressure)			
Frequencies (Max sliding speed)	**Material combination**	**100g** (65.7MPa)	**300g** (94.8MPa)	**500g** (112.3MPa)	**1kg** (141.5MPa)
25Hz (157mm/s)	PEEK 450G vs Steel	UL	UL	UL, UL®	UL, L
	EOS PEEK HP3 vs Steel	-	UL	UL	UL, L
50Hz (314mm/s)	PEEK 450G vs Steel	UL	UL, UL®, L, L®	UL	-
	EOS PEEK HP3 vs Steel	-	UL, UL®, L, L®	UL, L	-
100Hz (628mm/s)	PEEK 450G vs Steel	-	UL, UL®	-	-
	EOS PEEK HP3 vs Steel	UL	-	-	-

Note: UL – Unlubricated, L – Lubricated., ® - Repeated test

PEEK 450G – General grade injection moulded PEEK,

EOS PEEK HP3 – Selectively laser sintered PEEK

4.5.4. Gear Testing

In this project a polymer specific gear test rig was used; this section will briefly describes its main operating principles and specification. However, a more comprehensive analysis of the calibration and commissioning processes is presented by [83].

4.5.4.1. Birmingham Standard Gear Geometry

The gears use in all of the tests described in this thesis conformed to the Birmingham standard gear geometry to conform with previous results. The basic rack that forms the

Birmingham standard gear geometry meets with the now obsolete **ISO 53 (1974)** standard and is shown in **Figure 34**.

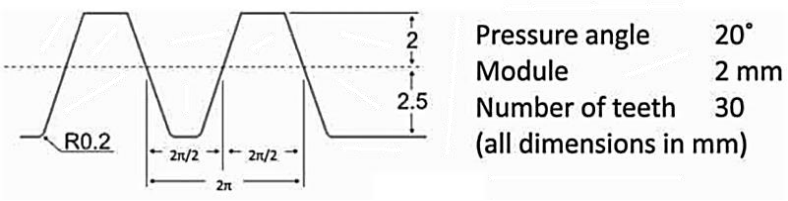

Figure 34: Basic rack geometry [14]

Figure 35 shows the full Birmingham standard gear geometry. It should be noted that the gears, when injection moulded, are coupled to the shaft of the Mark II test rig using an over moulded course knurled metal hub and keyway to prevent failures at the coupling.

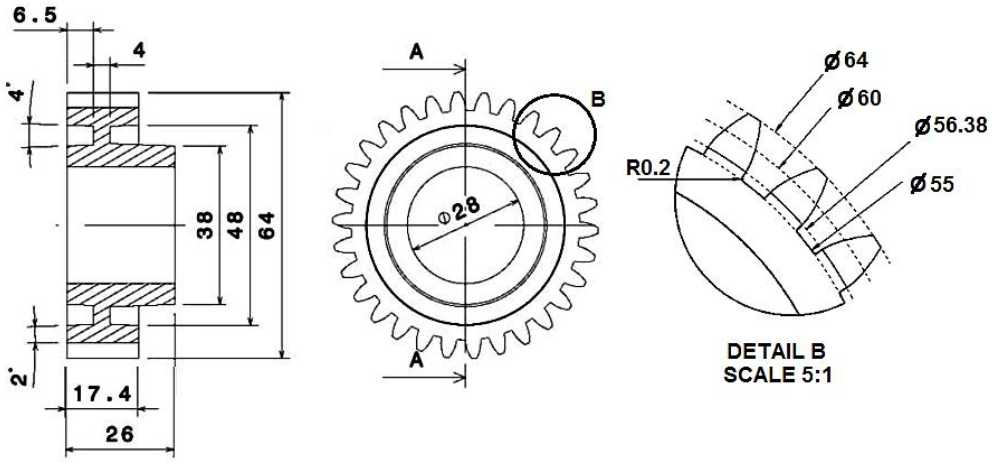

Figure 35: Birmingham standard 20 degree pressure angle gear

4.5.4.2. Mark II Gear Test Rig

The University of Birmingham Mark II test rig, shown in **Figure 36** was designed specifically for the testing of non-metallic gears. It operates based on power recirculation

principles and was designed and built by White to improve the dynamic behaviour shown by the loading mechanism of previous rigs, thought by Cropper to induce load error fluctuations of ±5% [14].

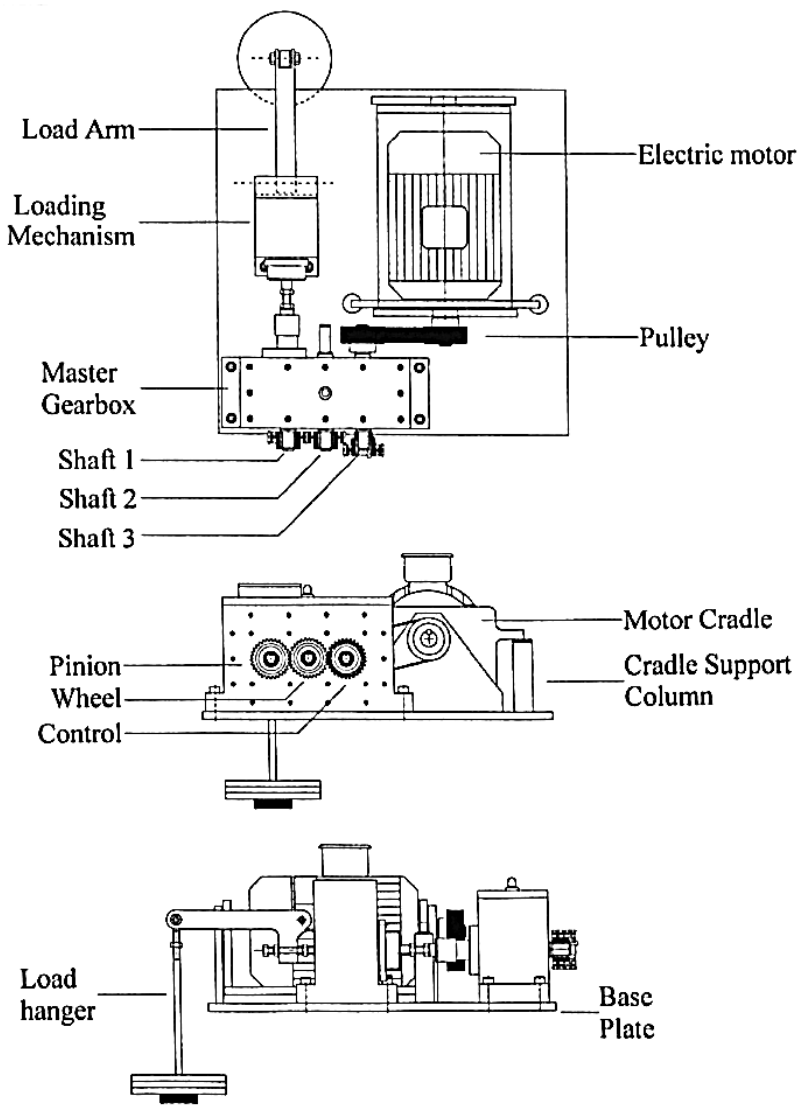

Figure 36: Mark II test rig, developed by White [83]

The test gears were loaded using suspended weights on a load arm, which induced an axial force that was transmitted through the housing assembly to a master gearbox. This configuration provided a mechanical advantage of 4:1 in the induced axial force, i.e.

$$F = 4 \cdot m \cdot g \qquad \textbf{Equation 36}$$

Within the master gearbox, the load was transmitted to the load shaft (via a piston and load collar) and a helical gear (the load gear) without axial location i.e. free to slide along the shaft. The load gear was forced into mesh with a mating helical gear, meaning that the load shaft rotated relative to shaft 2 and that the axial force induced a rotational moment or torque in all of the gears (including the polymer test gears). The induced torque as a function of axial force and gear geometry is given by:

$$T_r = \frac{F \cdot D_p}{\tan \beta} \qquad \textbf{Equation 37}$$

Thus:

$$T_r = \frac{4 \cdot m \cdot g \cdot D_p}{\tan \beta} \qquad \textbf{Equation 38}$$

This assumes negligible system frictional losses. Cropper conducted an extensive calibration of the rig, and quantified its performance, in the light of such inefficiencies, as follows:

- 1% error in speed control
- Less than 5% error in axial load

Wear of the test gears was measured by weight loss. To do this the meshing gears would be stopped periodically, their relative positions noted, removed and after weighing they would be replaced as close as possible to the original positions. This was done to minimise the loss of a transfer film whilst weighing and to minimise the disruption to the meshing action of the individual teeth. There are clearly disadvantages to using this method. Alternative, indirect methods of measuring wear, such as by measuring the displacement of the loading arm, have been shown to be inaccurate on previous rigs [17]. However, surface replication techniques using CharmFlex®Putty (Denkist, Inc., South Korea) were

used in this thesis, as suggested by Kono [44]. This meant that the gears did not need to be removed from the test rig during measurement and that the measurement time was significantly reduced.

The test parameters investigated in this thesis are summarised in **Table 8**.

Table 8: Gear Test Conditions

Test No.	Test	Lubricated	Load, Speed
1	Steel vs. EOS PEEK HP3	✓	8.2Nm, 1500rpm
2	Steel vs. EOS PEEK HP3	✓	12.2Nm, 1000rpm
3	Steel vs. EOS PEEK HP3	✓	8.2Nm, 1000rpm
4	Steel vs. EOS PEEK HP3	✗	8.2Nm, 1000rpm
5	Steel vs. EOS PEEK HP3	✗	8.2Nm, 500rpm
6	PEEK 450G vs. EOS PEEK HP3	✗	8.2Nm, 1000rpm
7	EOS PEEK HP3 vs. EOS PEEK HP3	✗	8.2Nm, 1000rpm
8	EOS PEEK HP3 vs. EOS PEEK HP3	✓	8.2Nm, 1000rpm

4.6. Summary

This section of the thesis outlined the test methodologies used in measuring and quantifying the physical, thermal and mechanical properties of injection moulded and laser sintered PEEK. In addition, the use of tribological testing methods to simulate polymer gear contact were presented; it was shown that the simulation methods described provide a representative simulation of the contact conditions found in polymer gears.

In this thesis, HFRR testing was used to investigate the tribological performance of both laser sintered and injection moulded PEEK, whilst twin disc testing was used to verify the performance of the baseline injection moulded material to high severity loading conditions, typical for highly loaded polymer gears.

However the limitations in the obtainable simulated conditions mean that direct testing of injection moulded and laser sintered PEEK gears, to verify and complement the tribological testing, were also outlined.

Chapter 5

TRIBOLOGICAL SIMULATION OF PEEK GEARS

5.1. Introduction

The selection of a polymer for a specific mechanical application is complicated. The combined influence of application factors such as temperature, geometry, wear and friction means that the only way of confidently specifying a polymer for a mechanical application is to physically test them with parameters matching, as closely as possible, the actual application.

This chapter examines the influence of contact stress, sliding-speed and temperature on the tribological properties of injection moulded poly-ether-ether-ketone (PEEK) when simulating polymer gear contact.

The frictional properties of PEEK will be assessed using two experimental arrangements, simulating the complexities of gear motion and loading mechanisms. The first will be a fretting based test using the HFRR. The applicability of this form of testing to the simulation of polymer gear contact is established. Following this, twin-disc testing of PEEK is used to give an indication of the performance of PEEK in an open tribosystem operating above the glass transition temperature.

The simplification of polymer gear contact, through the use of fretting and twin disc tests, allows the materials response to the conditions found at the gear tooth interface to be separated from dynamic issues, such as deflection. Thus gear tooth optimisation can be made to replicate those conditions for which the material responds best.

5.2. Materials

In polymers, friction and wear result from the dissipation of mechanical energy which in turn results in deformation (hysteresis) and frictional heating [63]. Thus, the development of high performance polymer gears has mainly been centred on developing a material capable of coping with the high interfacial temperatures.

In this investigation, the engineering thermoplastic polyetheretherketone (PEEK) was selected based on its current usage in high performance polymeric machine elements.

PEEK 450G is an unreinforced grade of polyetheretherketone; a linear homopolymer developed by Victrex®. The linear aromatic PEEK family consists of repeated monomers of ether and ketone and is chemically expressed as $[O\text{-}C_6H_4\text{-}O\text{-}C_6H_4\text{-}CO\text{-}C_6H_4]_n$ ([-oxy-1,4-phenylene-oxy-1,4-phenylene-carbonyl-1,4-phenylene-]) [9]. This is a general-purpose grade, which has the highest elongation at break and also the lowest general mechanical properties (tensile strength, flexural strength and flexural modulus) at a given temperature. However, unfilled PEEK also has the best impact properties of the PEEK range.

5.3. HFRR Test Conditions

As described in the methodology section of this thesis (**Chapter 4**), there are limitations in the obtainable operating conditions on the HFRR: The stroke length is limited to 20µm

and 2mm; the load is applied using supplied weights from 0.1 to 1kg; and the oscillation frequencies range from 10 to 200 hertz. Therefore, selection of appropriate test conditions has to fall within these boundaries, whilst, the load and speed values have to be comparable with gear condition defined above so that correlations can be made.

The path of contact for the mesh of two Birmingham standard gear geometry gears, assuming that there is no deflection, has been shown to take place over 9.76mm. This correlates to a movement on the gear flank of 3.34mm (2.02mm for theoretical single tooth contact). To replicate these gear test parameters, appropriate HFRR parameters were selected.

The test parameters in **Table 9** were established based on the calculations in **section 4.5.3.1**, and by limitations of the test rig. To allow preferential wear of the EOS PEEK HP3 sample, a high stiffness steel ball was used and measurements of friction were made over a four hour period.

Table 9: HFRR test parameters

	Loads (Max. contact pressure)			
Frequencies (Max sliding speed)	**100g** (65.7MPa)	**300g** (94.8MPa)	**500g** (112.3MPa)	**1kg** (141.5MPa)
25Hz (157mm/s)	UL	UL	UL, UL®	UL, L
50Hz (314mm/s)	UL	UL, UL®, L, L®	UL	-
100Hz (628mm/s)	-	UL, UL®	-	-

Note: UL – Unlubricated, L – Lubricated., ® - Repeated test

The test parameters shown in **Table 9** provided values of:

- Frequencies correlating to maximum sliding speeds at the theoretical end of single tooth contact for a gear rotating at approximately 250, 500 and 1000rpm (254, 508 and 1016rpm), and approximately 150, 300 and 600rpm (154, 307 and 614rpm) for maximum sliding speed at end of theoretical tooth contact.
- HFRR Loads correlating with gear loads of approximately 10, 20, 29 and 45Nm.
- Stroke lengths that correlate with the theoretical path of contact for single tooth contact using the Birmingham standard gear geometry (2mm). This incorporated the reversal of sliding motion occurring at the pitch point.
- Contact pressures for a steel ball running against injection moulded PEEK.
- Lubricated and unlubricated running conditions.

The HFRR operating parameters have been selected to simulate polymeric gear contact conditions as closely as possible. The selection of load was made using fundamental Hertzian contact pressure mechanics assuming no deformation, and the oscillation frequency was chosen to provide the equivalent sliding velocities associated with the modelled area on the gear tooth.

5.4. Frictional Properties of PEEK

Figure 37 shows the unlubricated HFRR results. These are based on average results and have been smoothed based on a 200 point moving average for ease of reading. It can be seen that following an initial period of bedding in, the coefficient of friction approaches

steady state. However, the frictional measurements showed significant amounts of noise in the high frequency, low load tests.

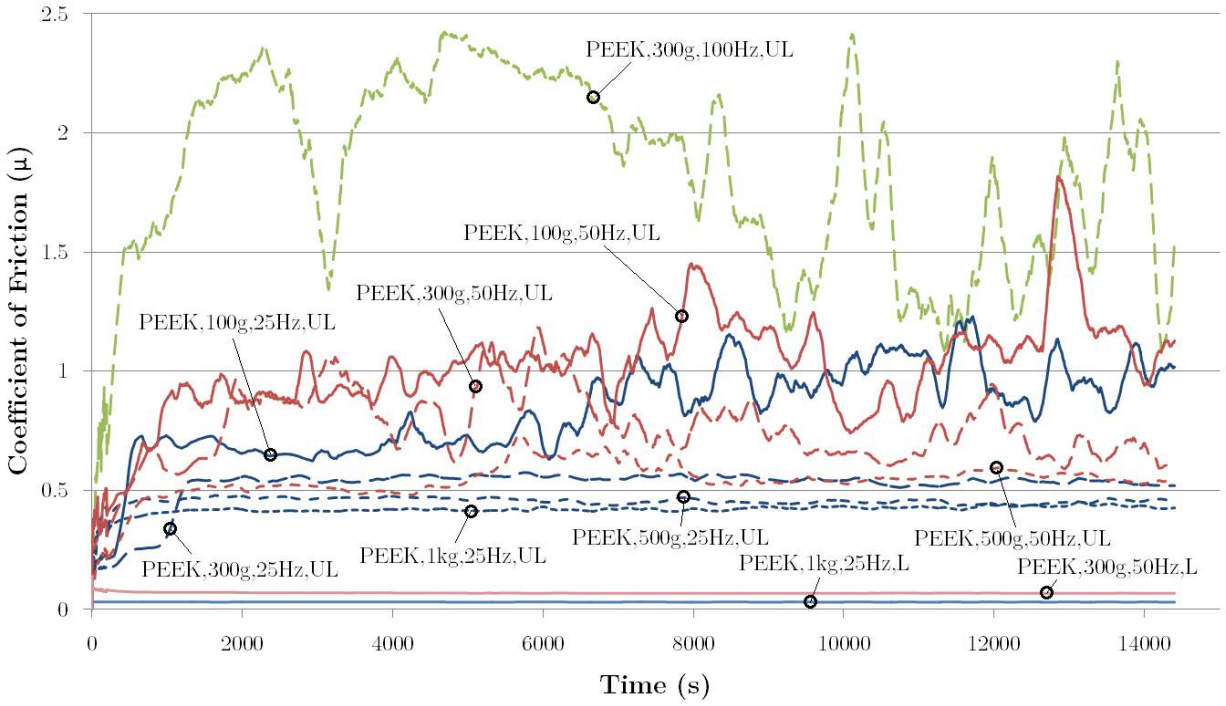

Figure 37: Coefficient of friction vs. time for HFRR testing of a steel ball vs. PEEK

To understand the friction response shown, correlations with load and speed were made.

Figure 38 shows the influence of load on the frictional response for a testing frequency of 25Hz. It can be seen that by increasing the load, the coefficient of friction reduced. This is typical of polymer gears as the efficiency has been shown to increase with load [84]. Similarly, **Figure 39** shows the influence of frequency on the friction response for a testing load of 300g. A reduction in both the coefficient of friction and the perceived noise in the frequency signal could be seen with reducing frequency.

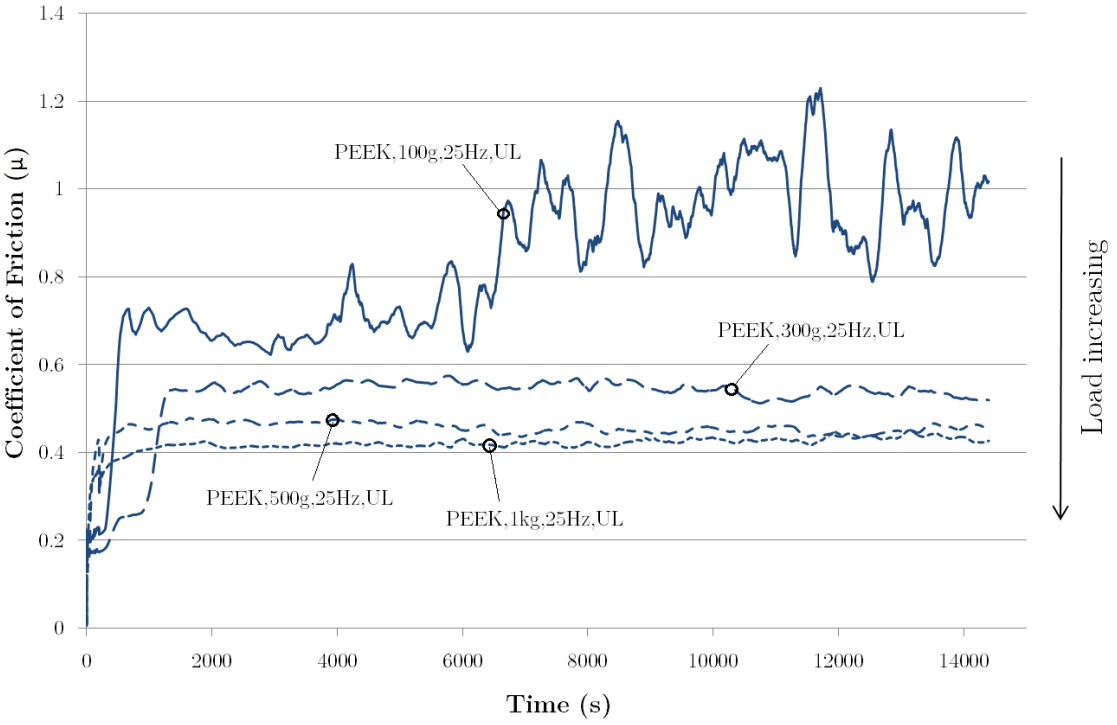

Figure 38: Influence of load on friction shown for an input frequency of 25Hz

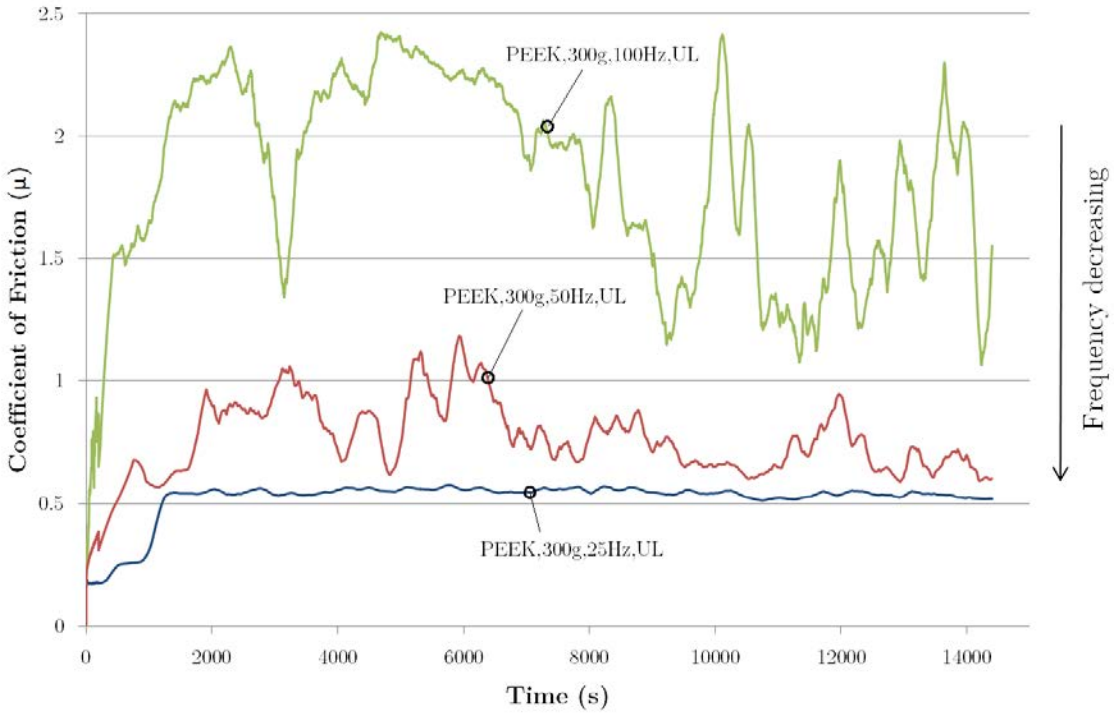

Figure 39: Influence of frequency on friction shown for an input load of 300g

However, in the high frequency tests there was increased noise in the signal; it was not possible to determine whether this increase was the result of elevated temperatures and increased adhesion, or due to vibrations in the system caused by oscillations of the loading mechanism.

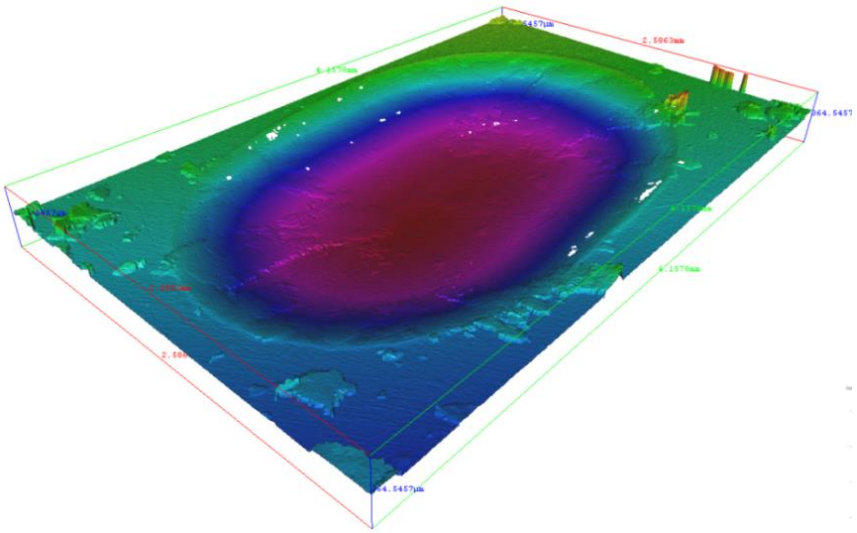

Figure 40: Wear scar topographical and area measurement (100Hz, 300g)

Topographical measurements were made to see if correlations could be made between the wear area and the frictional response (**Figure 40**).

Table 10: Average measured wear area vs. load and frequency (unlubricated steel vs. PEEK)

	Loads (Max. contact pressure)			
Frequencies (Max sliding speed)	**100g** (65.7MPa)	**300g** (94.8MPa)	**500g** (112.3MPa)	**1kg** (141.5MPa)
25Hz (157mm/s)	1.41 mm^2	1.60 mm^2	1.73 mm^2	1.91 mm^2
50Hz (314mm/s)	4.72 mm^2	5.15 mm^2	5.23 mm^2	-
100Hz (628mm/s)	-	6.91mm^2	-	-

It could be seen that the effects of frequency on the measured wear scar were more significant than that of load (**Table 10**).

Observations of the worn surface were used to provide additional insight into the tribological performance of the material.

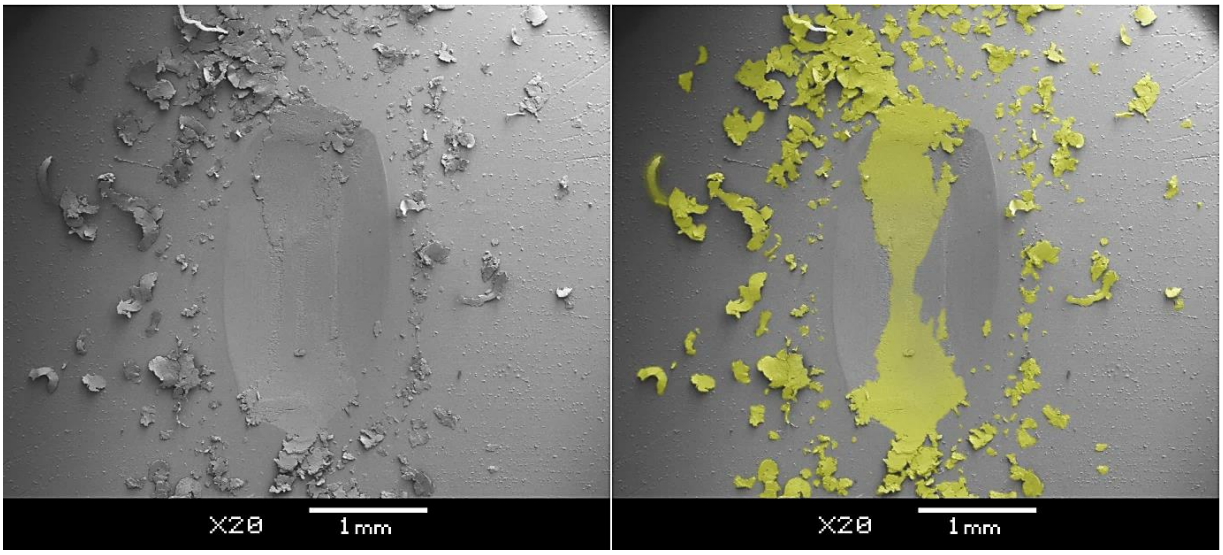

Figure 41: Wear scar showing the debris that is both expelled from, and contained within the contact zone (500g, 50Hz)

It could be seen that significant amounts of debris was produced in the high speed, high load tests (**Figure 41**). However, despite large amounts of debris being expelled from the surface (**Figure 42**), a significant amount was contained within the system. The influence of this *'third body'* on the tribological properties of the contact was significant; reducing interfacial wear of the bulk material whilst increasing cohesive wear and surface fatigue as debris was forced into the contact zone (**Figure 42**).

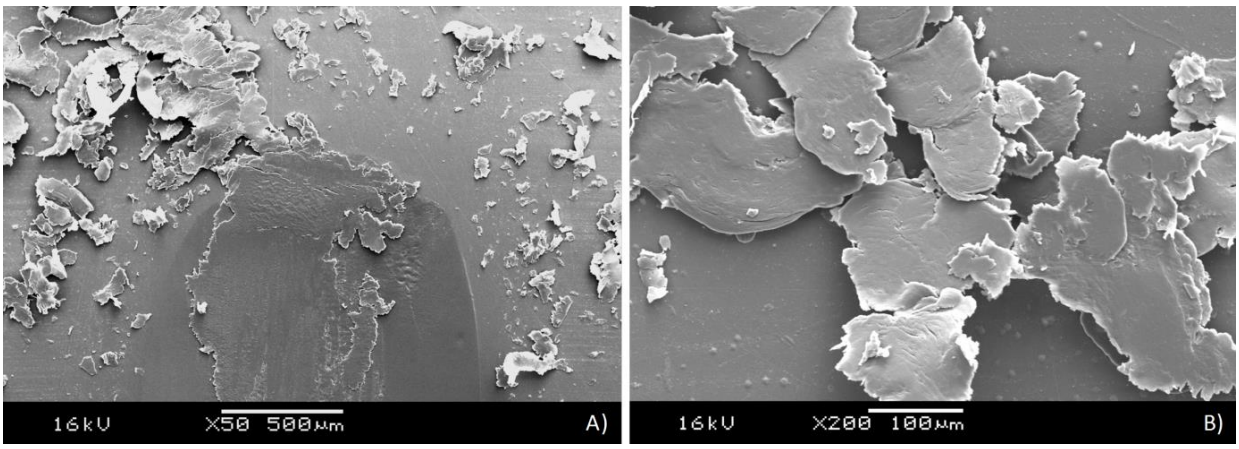

Figure 42: A) material build up at ends of contact, B) smeared debris expelled from surface

Figure 43 shows the surface of the material. Underneath the smeared debris in the centre of the wear track, adhesion can be seen. It is probable that this is the result of stick-slip; evident from the '*fish scaling'* seen on the surface of the material. It was observed that following the rupture of the cohesive junctions in the bulk of the polymer, adhesion between the bulk of the material and the counterface was significant. This is likely to have stabilised the coefficient of friction and reduced the wear of the surface. However, the increased temperatures and the influence of fatigue resulted in the accumulation of material transfer until the formation of a viable transfer layer was no longer possible; increasing the debris produced and consequently the amount of smeared material that was seen in the contact.

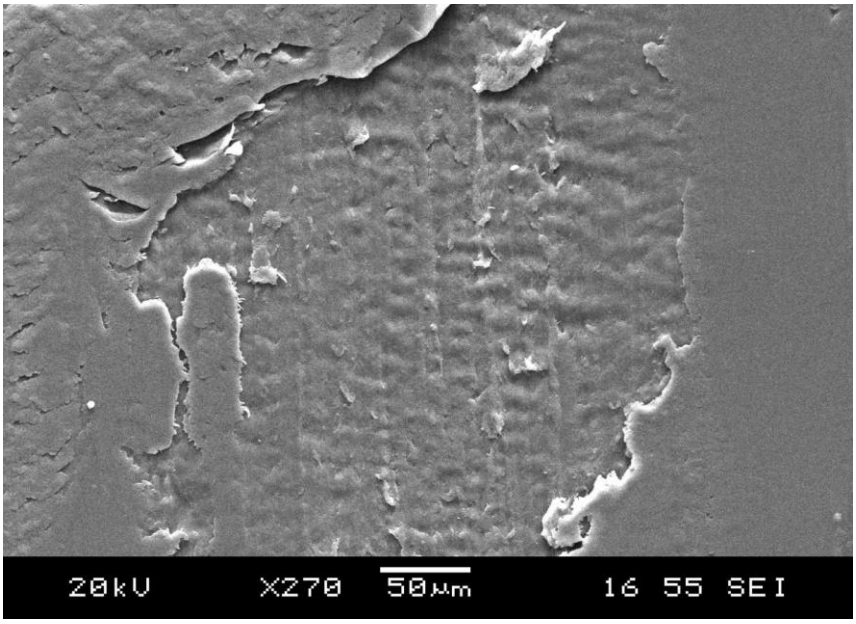

Figure 43: wear under smeared surface

Due to the viscoelastic nature of polymers, some of the strain energy applied in loading is dissipated in the form of heat. Thus, when the product of stress and frequency is too great, the failure mode is thermal rather than by fatigue. However, surface fatigue could be seen at the extremities of contact where the sliding velocity reduced (**Figure 44**). This correlates with the conclusions of Hooke *et al.* who observed similar surface fatigue in both twin-disc testing and gear testing as the sliding velocities reduced [17].

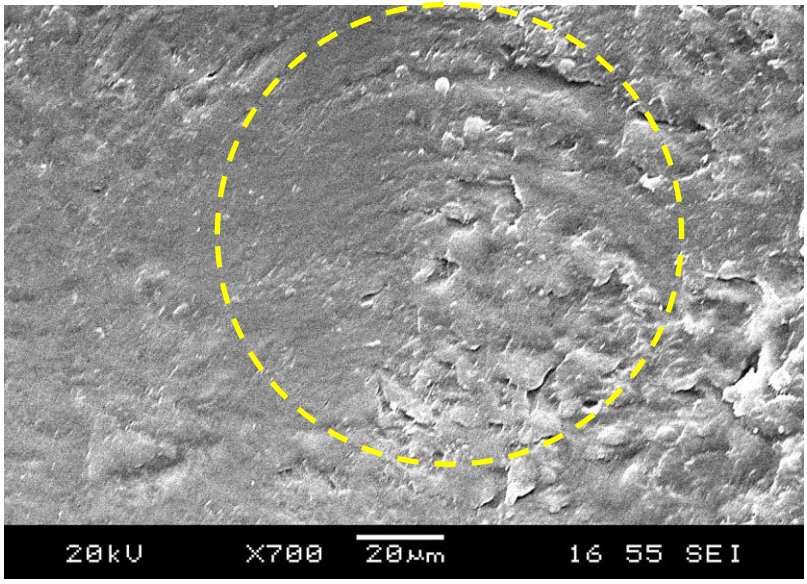

Figure 44: Surface fatigue at extremities of contact (Vs = 0)

Looking closer at the worn surfaces, wear damage was dominated by surface fatigue, adhesion and the subsequent ploughing of the counterface through the material. It was also concluded that the high coefficient of friction seen was a result of the temperature induced in the closed tribo-system, significantly affecting the occurrence of adhesion. However, the tribological performance of PEEK when subjected to high loads and speeds was shown to demonstrate similar failure mechanisms to those observed in polymer gear contact [14,44].

5.5. Twin Disc Testing of PEEK

To investigate the response of the baseline injection moulded material to high severity loading conditions, typical for highly loaded polymer gears, twin disc testing was used.

As previously discussed, this form of open tribosystem provides a simplified method of analysing and understanding the dynamic response of high performance polymeric gears in and around the pitch point and the first point of contact.

Tests were conducted without external lubrication over a range of loads and slip ratios using a twin-disc test rig to investigate the influence of temperature on the tribological properties of injection moulded PEEK running against itself (**Table 11)**. During the tests, the friction, wear and temperature data for the system were collected.

Table 11: Test conditions for PEEK vs PEEK twin disc tests

Load	Max. Contact Pressure*	Slip ratio		
		3.92%	14.29%	28.57%
400N	56MPa	✓	✓	✓
300N	48.5MPa	-	✓	✓
200N	39.6MPa	-	-	✓
100N	28MPa	-	-	✓

**approximate Hertzian contact pressures*

The loads selected were equivalent to a calculated gear torques of 3.4, 6.7, 10.1 and 13.4Nm.

5.5.1. Wear Mechanisms and Topographical Analysis

As shown in **Figure 45,** all tests displayed three distinct regions of wear which could be correlated with both the temperature and friction profiles. This is a common observation in both twin-disc and gear tests and represents: a 'running-in' period, a period of steady-state running, and a period of increased wear signifying the end of the test specimen's lifecycle.

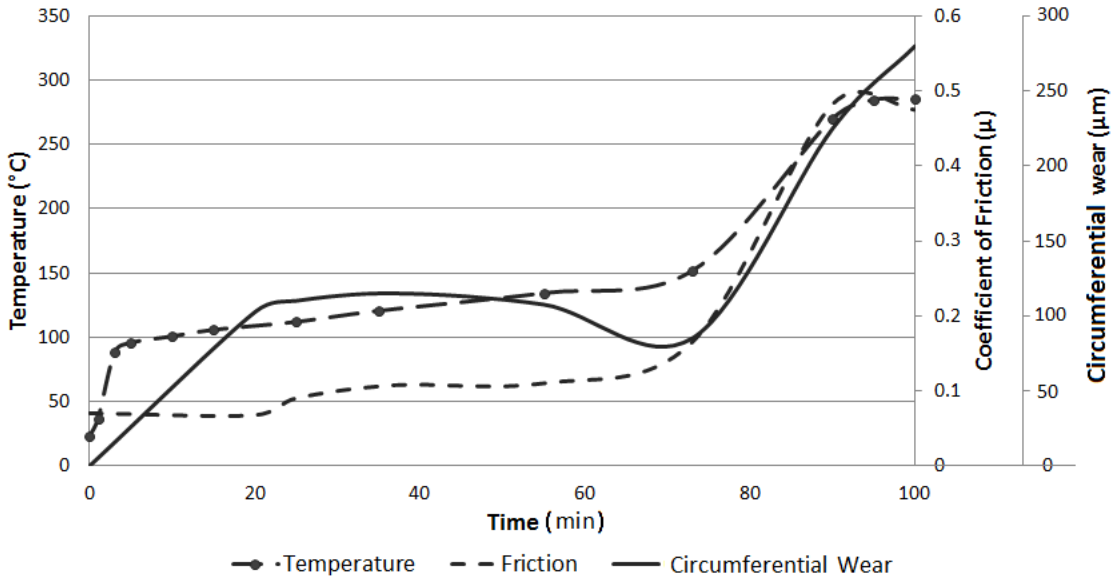

Figure 45: Temperature, friction and wear results for 14% slip ratio and 400N test

SEM images of the worn disc surfaces are shown in **Figure 46**. The images show a 14% slip-ratio test which induced dramatically-increased temperatures and coefficients of friction. This test eventually resulted in localised damage on the disc surface producing significant amounts of wear.

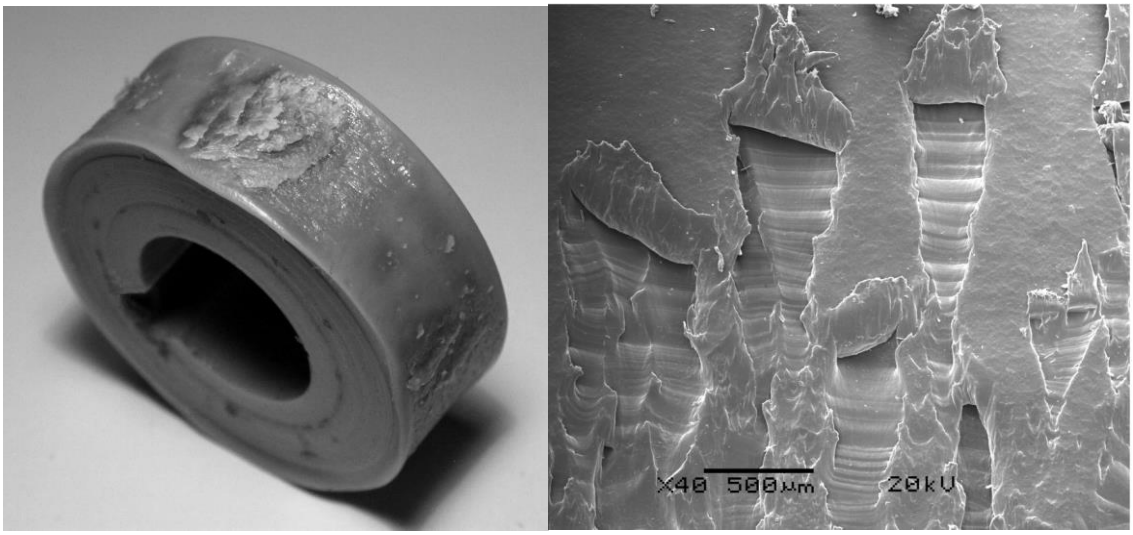

Figure 46: Surface damage in 14% Slip ratio and 400N tests

From **Figure 46** it can be seen that the disc material softened in the high severity tests (The severity of the test was calculated as the average thermal output from the contact integrated over time, allowing the wear rates to be quantified based on the operating conditions.). This was a result of the discs being thermally overloaded, and also because of yielding (permanent deformation). In addition, localised damage could be seen on the surface of the disc. It is thought that this was a consequence of the high temperatures generated at the point of contact forcing the expulsion of wear debris. A proportion of this debris is subsequently trapped in the mesh, damaging the surface of the disc. Following cyclic fatigue and adhesion, this failure could then be seen on the surface of the disc.

It is important to understand the influence of crystallinity on the wear mechanisms observed. The simulated position of each twin-disc test on a gear tooth correlates with a specific contact condition. If the severity at this point exceeds that required for in-service crystallisation or a change in crystallinity to occur, optimising methods to change the loading and temperature at this point may be required to improve the efficiency of the geared system.

Figure 47 shows the relative test severity correlated with the average wear rate. The severity of the test was calculated as the average thermal output from the contact integrated over time, allowing the wear rates to be quantified based on the operating conditions. It was found that the high slip-ratio, high load tests were the most severe and thus produced the greatest wear rate and temperature increase. The low slip-ratio, low load tests produced the lowest wear rate and temperature increase, and were thus considered to be the least severe.

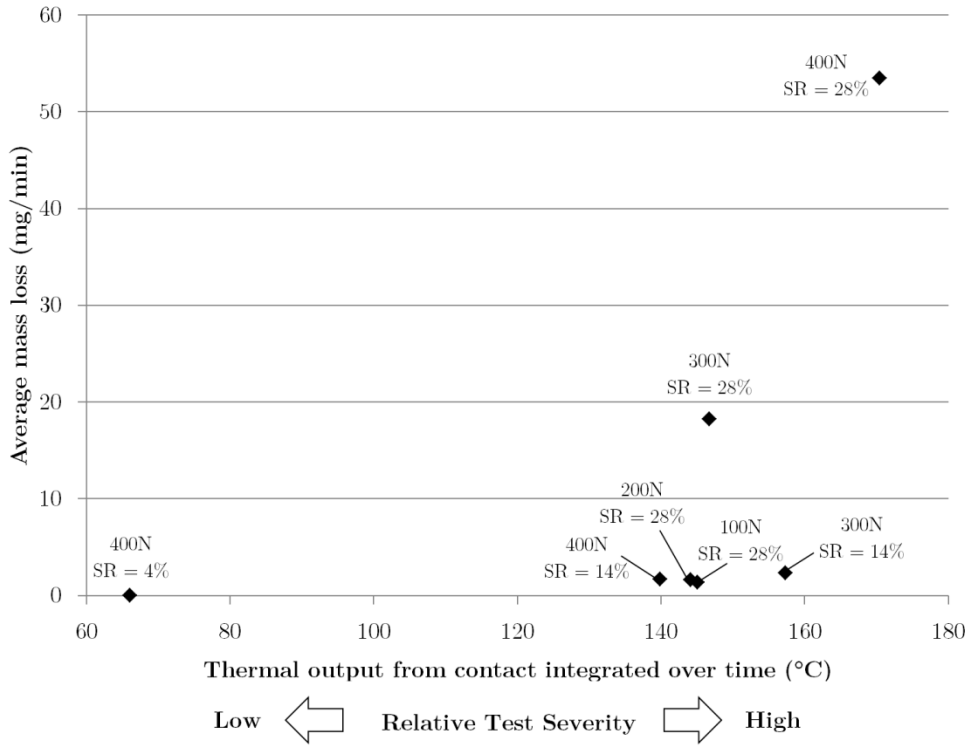

Figure 47: Average wear rate vs test severity for twin disc tests

The high severity tests showed localised damage on the surface (as shown in **Figure 46**). However, several different wear mechanisms were observed in the tests.

In the later stages of the high-severity tests as the material began to soften, the discs began to expel wear debris as material was transferred between the surfaces of the discs. This is associated with interfacial wear, where the energy from the sliding component of friction due to contact is dissipated in a thin region adjacent to the surface.

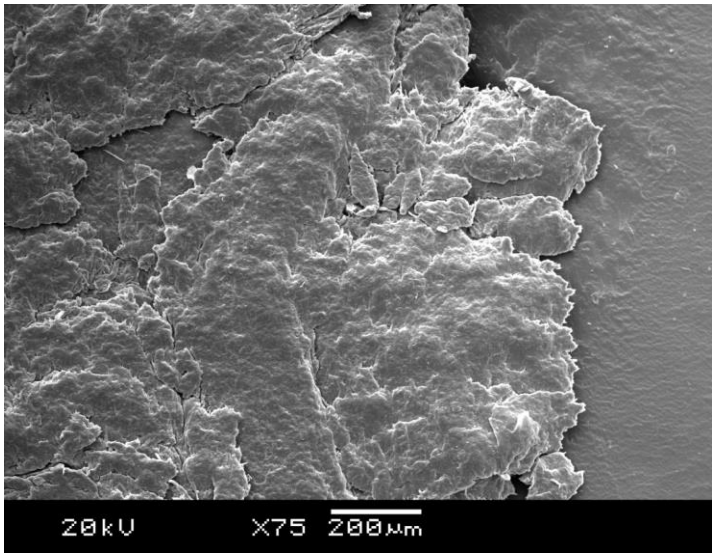

Figure 48: Wear debris on the disc surface

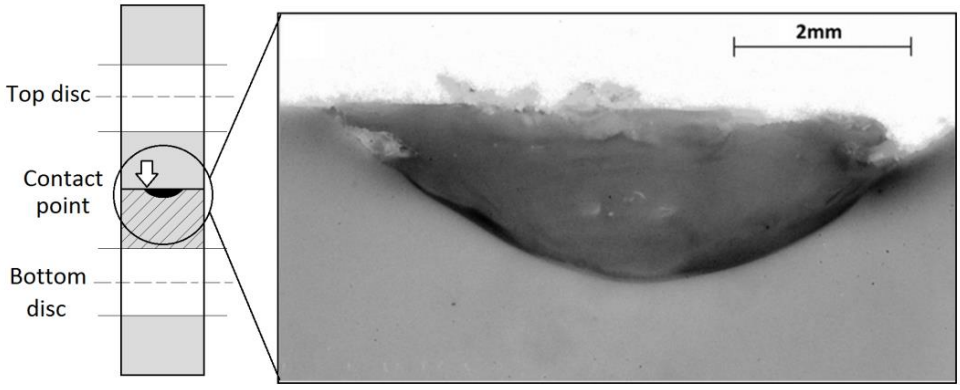

Figure 49: The cohesive region in the centre of the sectioned and polished disc associated with the highest temperatures

Once the discs began to expel wear debris, the temperature became less steady. Wear debris was forced into the surface of the material by the contact pressure (**Figure 48**). It can be seen from the polished sample in **Figure 49** that there is a definite change in the material around the centre of the sectioned disc. This area is associated with the highest temperatures during running and is symptomatic of cohesive wear [5].

Overall, when operating under severe loading conditions PEEK shows considerably less wear than other reported materials (for a 28% slip ratio and a 300N load, the wear was approximately 10^{-4} μm/cycle); for slip ratios above 11% Acetal discs were reported to have a wear rate of 10^{-4} μm/cycle [39], whilst Nylon 6-6, for a slip ratio of 28% and a load of 200N showed wear rates exceeding 10^{-2} μm /cycle [17]. Although the wear rates in some of the more severe tests were high, there was very little visible wear at lower temperatures. Even above the glass transition temperature the material maintained its mechanical strength until approximately 250°C, when the surface began to soften.

5.5.2. Measured Temperature and Friction

The predicted temperature generated at the interface between two contacting discs can be modelled as the sum of the prevailing temperatures at that point (**Equation 39**).

$$T_{interface} = \delta T_{flash} + T_{bulk} \qquad \textbf{Equation 39}$$

where T_{flash} is the instantaneous temperature due to frictional heating, and T_{bulk} is the measured bulk temperature of the two bodies, combining ambient temperature and physical heating effects.

Assuming that a system is based on steady-state sliding where parameters such as heat intensity, sliding speed, and normal pressure are regarded as constant, the flash temperature can be approximated using Blok's equation [85] (**Equation 40**).

$$\delta T_{flash} = \frac{1.11 \cdot \mu \cdot F \cdot \left[V_1^{\frac{1}{2}} - V_2^{\frac{1}{2}}\right]}{\mathrm{b}\sqrt{2 \cdot k \cdot \rho \cdot c \cdot a}} \qquad \textbf{Equation 40}$$

where the semi-width of contact between the two contacting surfaces, a, can be calculated from **Equation 24**.

In **Equation 40**, μ is the coefficient of friction, F is the normal load, V_1 and V_2 are the rolling velocities of the disc surfaces, k is the thermal conductivity, ρ is the density of the material and C is the specific heat capacity.

Therefore, the predicted contact temperature can be estimated through use of **Equation 39** and the measured bulk temperature.

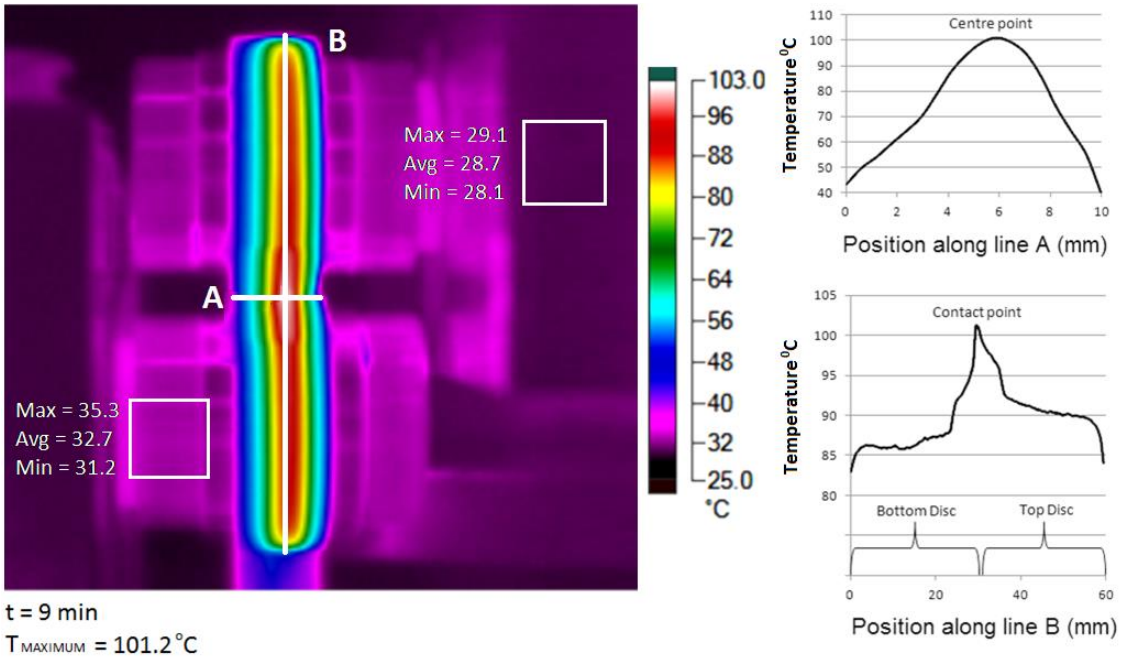

Figure 50: Infrared temperature profile for 28% SR, 200N test at 9 minutes, and temperature plots showing measured temperature variation during disc rotation

Figure 50 shows the temperature profile for the 28% slip-ratio, 200N test. It can be seen that the maximum temperature (101.2°C) is generated at the meshing point of the two discs. The temperature variation across the disc (line B) represents a flash temperature increase at the point of contact and the proportion of heat dissipated from the discs during rotation. It can also be seen that the upper disc is running hotter than the lower disc; this is due to the top disc rotating at a higher speed thereby having less time to cool down between rotations. The variation in temperature from the centre to the outer edge

of the disc (line A) is due to a combination of convection, conduction and radiation from the disc to the surrounding area [19].

The infrared temperature profiles shown in **Figure 51**, illustrate how the temperature of the contacting discs, run at 14% slip-ratio and 400N load, progressed over time. The test samples began to expel large amounts of wear debris after 80 minutes. This can be related to the temperatures exceeding the Relative Thermal Index (RTI) of PEEK for mechanical use with impact (180°C) [86].

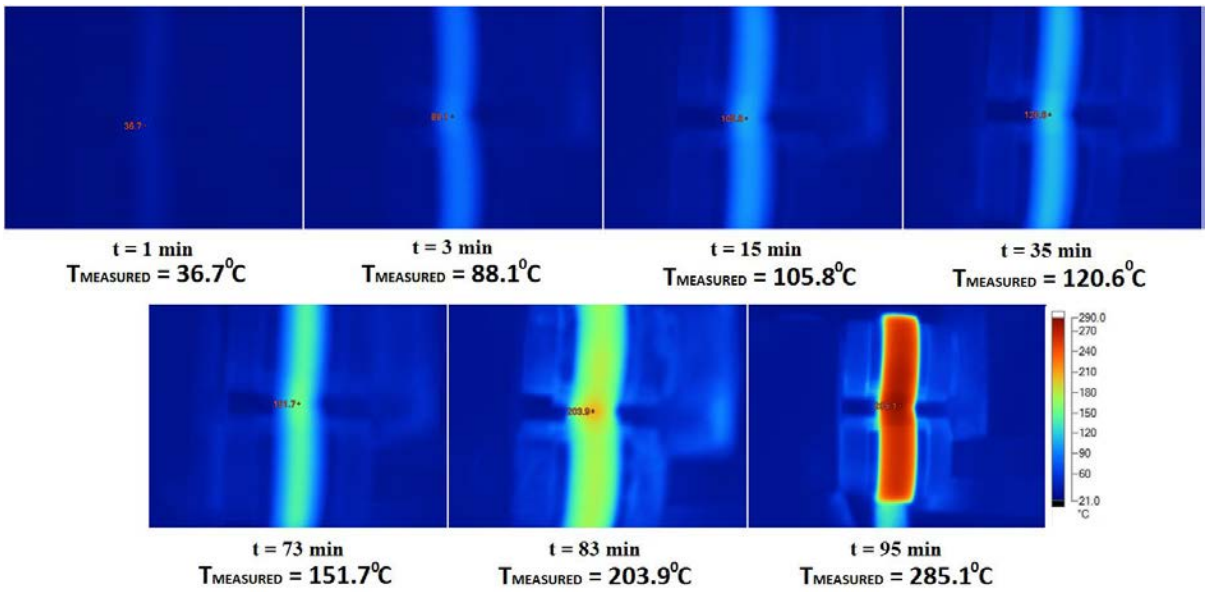

Figure 51: Infrared temperature plots for 14% SR, 400N test

Through use of **Equation 39** the maximum flash temperature for the test combinations can be found. **Table 12** summarises these results. It is important to note that the expulsion of wear debris from the interfacial region between the discs reduced the bulk and flash temperatures, and so there was not a strong correlation between this flash temperature and test severity. However, it is possible to see that as slip-ratio and load increased, so too did the flash temperature.

Table 12: Showing the estimated interfacial temperature (T_i) and associated flash temperature rise (T_f) for the test conditions

Load (N)	Max. Contact Pressure	Slip ratio		
		3.92%	**14.29%**	**28.57%**
400	56MPa	Tf = 2°C, Ti = 104°C	Tf = 14°C, Ti = 299°C	Tf = 26°C, Ti = 296°C
300	48.5MPa		Tf = 13°C, Ti = 298°C	Tf = 21°C, Ti = 302°C
200	39.6MPa			Tf = 15°C, Ti = 303°C
100	28MPa			Tf = 9°C, Ti = 295°C

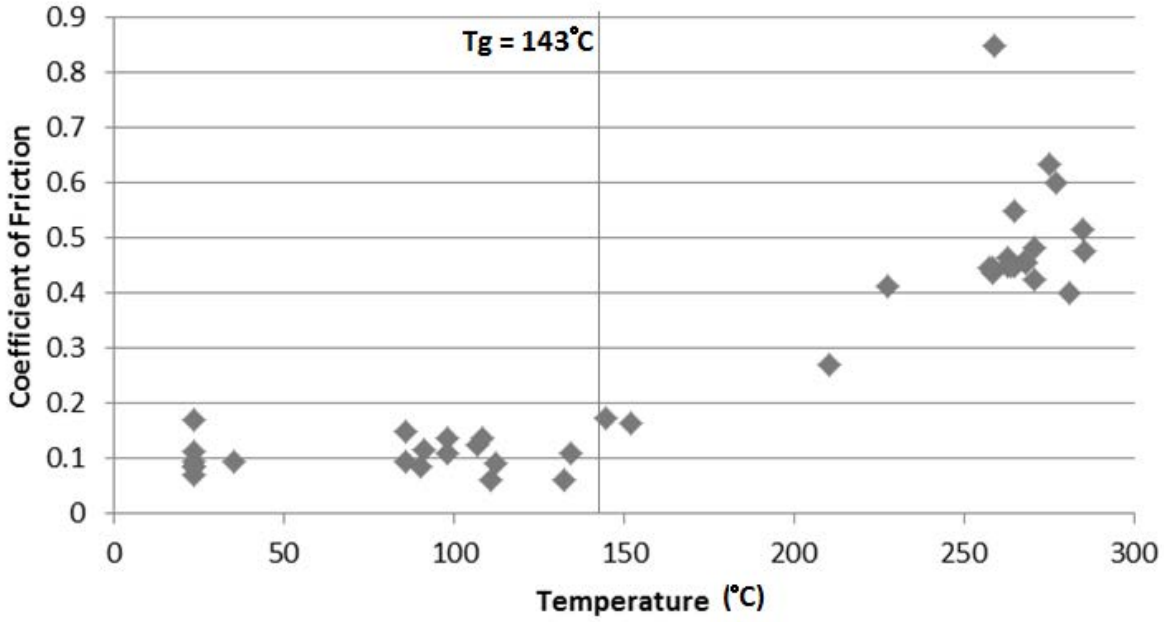

Figure 52: Measured temperature vs. coefficient of friction for all test conditions

Figure 52 shows the temperature plots for all twin-disc test conditions and the relationship between measured friction and temperature. It can be seen that frictional heating is one of the main contributing factors to the heat generated by the discs. In addition, a rapid increase in the coefficient of friction can be seen as the temperature goes

beyond the glass transition temperature of the material. This transition temperature, and its effect on friction and wear, has been seen in polymer twin discs and fretting tests [17,87].

After an initial period of testing, the material was observed to discolour, possibly due to thermal degradation, becoming predominantly darker as temperatures increased. This phenomenon was also observed by Rae *et al.* who described a discoloration in PEEK as temperatures exceeded 200°C [88]. Following the discolouration of the test samples, the observed wear rate substantially increased.

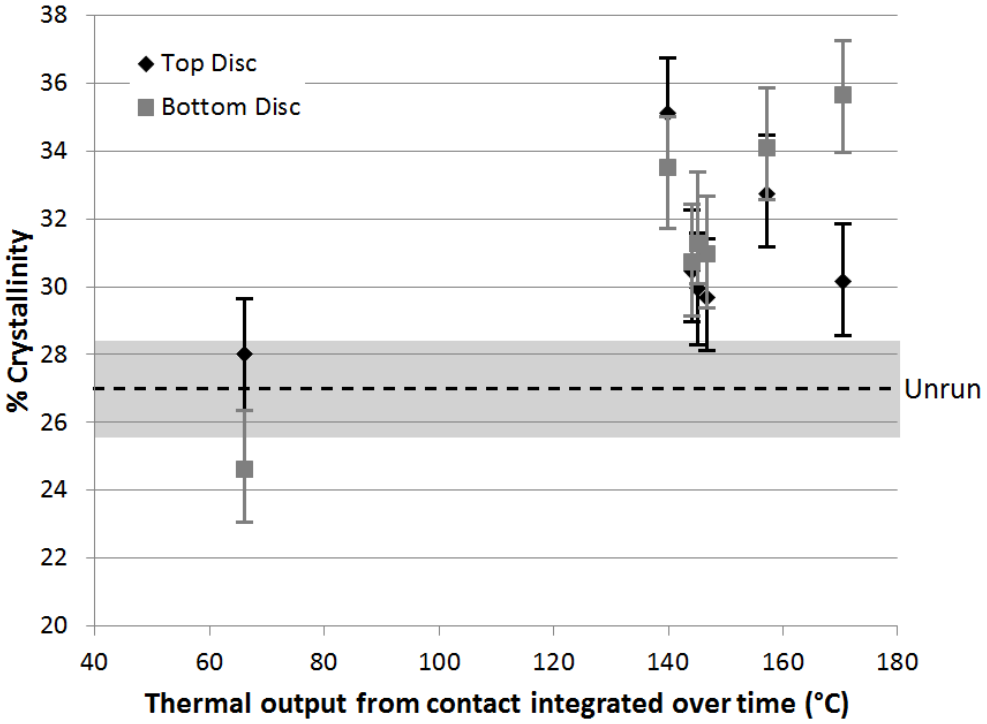

Figure 53: Crystallinity of PEEK discs verses test severity following testing

Operation near or above the glass transition temperature of PEEK (143°C) and below the principle crystalline melt transition (335°C), will induce enthalpic relaxation. Crystallinity measurements were taken following the tests to see if there is any evidence of this (**Figure 53**). It was found that crystallinity values of 30-35% were present in all tests

that exceeded the glass transition temperature of the material. These values are 3-8% higher than those measured on untested samples, suggesting that enthalpic relaxation had occurred. This is supported by the conclusions of Ostberg and Seferis who described the effects of annealing above the glass transition temperature on the crystallinity of PEEK [89]. Additionally, the influence of molecule orientation as a result of the high shearing friction forces present in this series of testing can lead to additional enthalpic relaxation during operation [90].

However, due to increased wear rate at the end of testing, much of the surface material was removed as debris. Thus, the crystallinity measurements are only able to provide limited information related to this stage of testing.

5.6. Conclusions

The simplification of polymer gear contact, through the use of fretting and twin disc tests, allows the materials response to the conditions found at the gear tooth interface to be separated from dynamic issues, such as deflection. Thus gear tooth optimisation can be made to replicate those conditions for which the material responds best.

It has been shown that fretting wear was dominated by surface fatigue, adhesion and the subsequent ploughing of the counterface through the material. It was also observed that the high coefficient of friction seen was a result of high temperatures induced in the closed tribosystem, significantly affecting the occurrence of adhesion.

It was observed that simulated gear tests on PEEK demonstrated similar failure mechanisms to those observed in polymer gear contact, such as, fatigue at low sliding velocities and fretting at higher speeds.

However, the severity of the test conditions was difficult to control; pressure profiles were based on tooth loading for gears and a constant load for HFRR tests. Therefore, to enable appropriate maximum loads and sliding speeds to be modelled, the maximum tested PV values (pressure x velocity) were up to 60% higher than the maximum values for a perfectly stiff gear.

The wear mechanisms of PEEK running against itself in non-conformal, unlubricated, rolling-sliding contact have been investigated over a range of loads and slip-ratios to determine the effect of temperature and roll/slide interactions on the tribological properties of PEEK.

Overall, the possibility of using PEEK in low slip ratio conditions, for both low and high loads, has been demonstrated, with high temperature operation being possible despite an increase of wear. It has been shown that wear, friction and temperature increase as the slip ratio and the load are increased. However, the wear rates are significantly lower than for other polymers tested using the twin-disc configuration. Failure mechanisms observed on the contact surfaces included surface melting and contact fatigue failures, particularly in the more severe high slip-ratio, high load conditions.

The reduction of load and slip-ratios has been shown to help reduce the generated temperature, and its associated effects around the pitch-point and the region of premature contact. Thus, the possibility of optimising polymeric gear tooth geometry to reduce the slip-ratio away from the pitch point will potentially increase the service life and reduce the occurrence of those wear mechanisms shown in the high slip-ratio tests.

The use of simplified geometry has provided an indication of a materials performance for a specific gear application, with similar wear responses being shown and appropriate sliding speeds and loads being achievable. Therefore the use of these results in conjunction with

the design process, can aid in the development of more effective, highly loaded, polymeric gear systems. However, the kinematics of a polymeric gear is complex and to fully understand a material response to the loading conditions found direct gear testing is recommended.

Chapter 6

THE TRIBOLOGICAL AND MECHANICAL PROPERTIES OF LASER SINTERED EOS PEEK HP3

6.1. Introduction

As previously discussed, there is very little information available on the properties of laser sintered EOS PEEK HP3. The majority of the data is based on manufacturer's values, where their significance for a given application is not immediately apparent.

In this section, the results of physical, mechanical and tribological testing of laser sintered EOS PEEK HP3 are presented and compared against the baseline tests on injection moulded PEEK discussed in **chapter 5**. The significance of these results is outlined along with specific properties that should be considered in the application of the material to machine elements.

6.2. Methods

Test samples were manufactured by Paramount Industries (Paramount Industries Inc., Langhorne, USA), using an EOSINT P800 (EOS Electro Optical Systems 2011a) high

temperature laser sintering system. EOS PEEK HP3 powder, specifically designed for the EOSINT P800 system, was used to produce the parts.

Sample geometries were produced in the x-y plane and were based on the corresponding ISO standard. This allowed the mechanical properties of the samples to be evaluated against existing data for high performance polymers. However, it should be noted that the mechanical tests performed were based on standards for polymers processed by injection moulding as, currently; no standard for the mechanical testing of SLS materials exists. Therefore, as roughness was a result of the manufacturing process, samples were tested '*as manufactured*', i.e. neither polished nor machined to fit roughness tolerances suggested in the ISO standards.

6.3. Physical Property Characterisation

Figure 54 shows the surface of the EOS PEEK HP3 laser sintered material. It can be seen that the component roughness was determined by the partially sintered powder on the surface of the material.

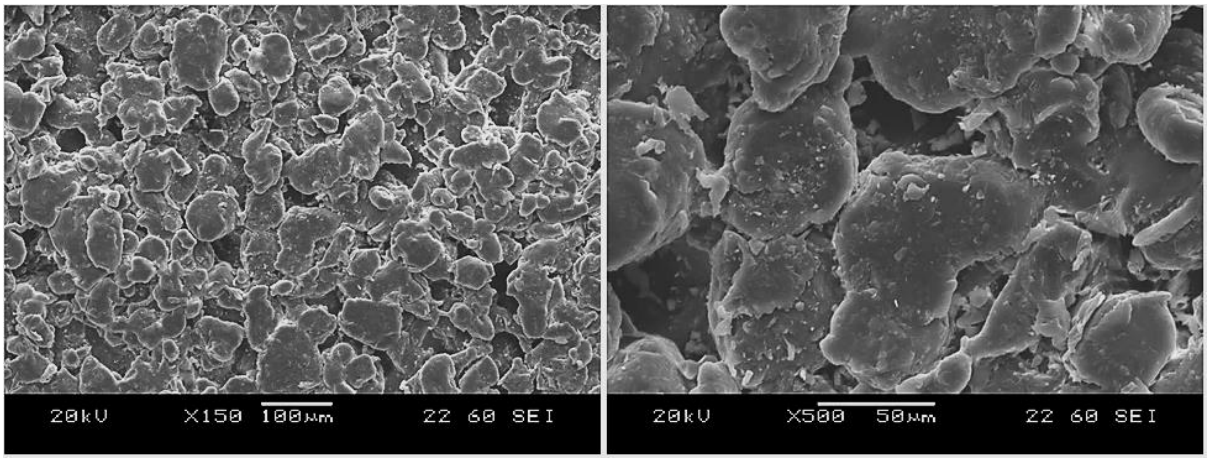

Figure 54: SEM micrographs of the surface of EOS PEEK HP3 (as produced)

Laser sintering is known to give a porous surface due to the partial sintering effect of powder around the contour of the geometry [56], however, this can be minimised through careful parameter selection [55]. Surface porosity can significantly affect the lubricant retention of the surface and consequently the friction and wear mechanisms observed. However, nano-scale porosity is still apparent in the structure and to study sub-surface porosity mercury porosimetry is used.

Table 13 summarises the results of the porosity testing:

Table 13: Porosity results for EOS PEEK HP3 samples

Total Intrusion Volume	0.035	mL/g
Average Pore Diameter	24.4	nm
Bulk Density at 0.51 psia	1.25	g/mL
Apparent (skeletal) Density	1.31	g/mL
Porosity	4.36	%

It can be seen that the samples tested were 4.36% porous, and that the average pore diameter was 24.4 nm.

Figure 55 shows the dispersion of values of pore diameter for the EOS samples. It can be seen that the material porosity consists of sub-100 nm pores, which are mainly 10 nm or smaller. The dotted line represents the minimum measurable pore diameter, and is a limitation of the testing equipment.

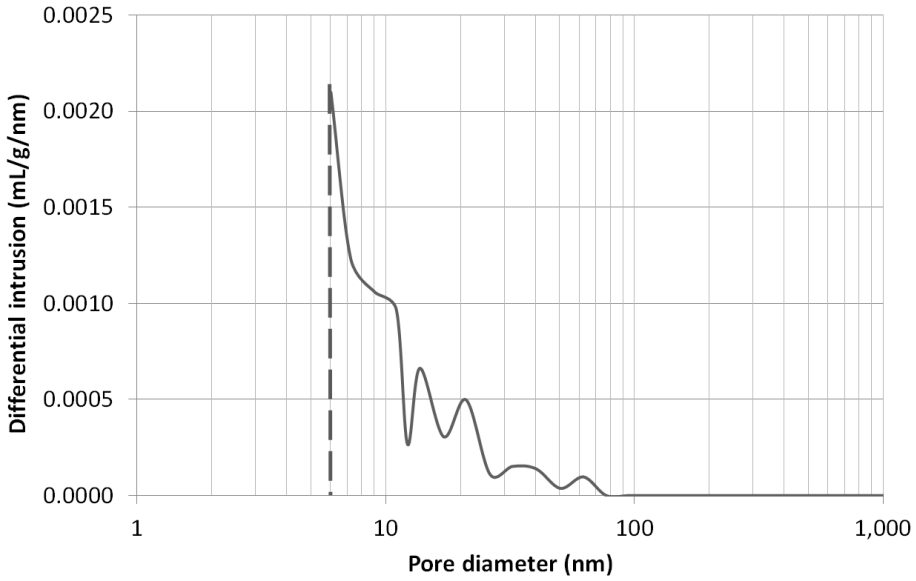

Figure 55: Differential intrusion vs. Pore diameter for EOS PEEK HP3

Another method used in the measurement of porosity is microtomography (µCT). Beard et al. used µCT techniques to analyse the sub-surface properties of EOS PEEK HP3. They concluded that the parts were fully dense throughout [56]. However, the subjective nature of analysing µCT images, especially when attempting to see nano-scale porosity, limits its applicability to only measuring large-scale pores as small-scale porosity cannot be seen.

Hooreweder et al. compared the material performance of laser sintered and injection moulded polyamide and found that injection-moulded and selective-laser-sintered samples had similar fatigue properties despite the presence of pores in the sintered samples. They attributed this to the high molecular mobility, resulting from the high local cyclic stresses near the pores or initial cracks, increasing the inner material temperature and thus delaying fracture [51].

The roughness characteristics of the laser sintered surface were dependent on the orientation of the component produced. As manufactured, the vertical surface roughness

was generally higher than the horizontal. **Table 14** quantifies the two 3D roughness profiles shown in **Figure 56.**

Table 14: Measured Roughness of EOS PEEK HP3 parts

Property	X-Y Plane	Z Plane
Sa (Average asperity height)	16.37 µm	23.87 µm
Sq (Root-Mean-Square height)	19.86 µm	29.75 µm
Ssk (Skewness)	-0.32	-0.44
Sku (Kurtosis)	2.40	3.15

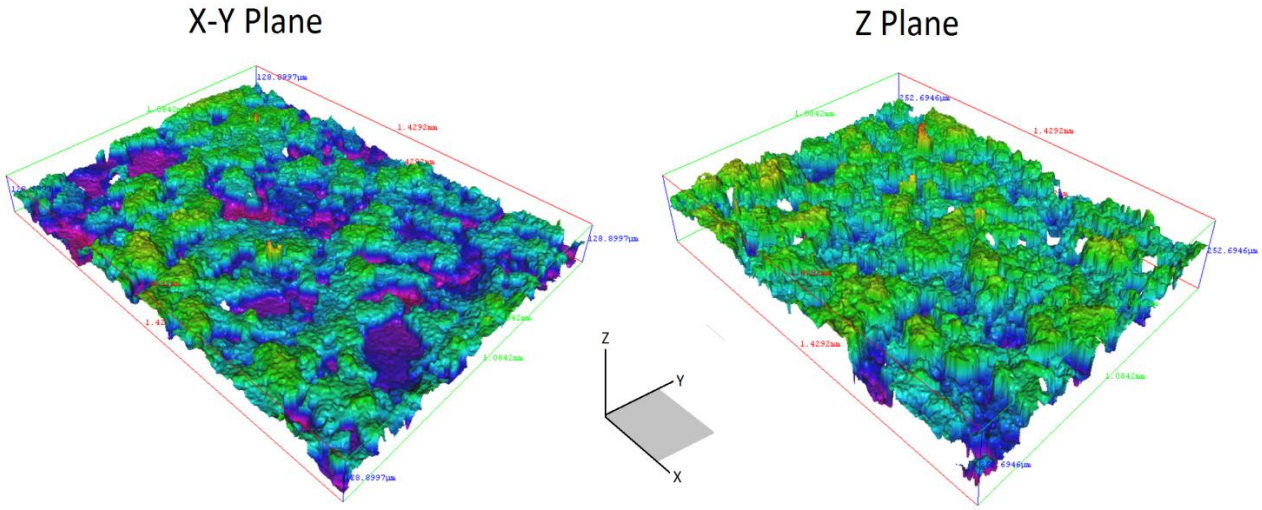

Figure 56: Surface roughness profile for EOS PEEK HP3

As expected, the roughness of the surface on the z-axis is significantly more than on the x-y axis. However, it is interesting to note the differences in skewness and kurtosis. Both surfaces have negative skewness, due to the partially-sintered outer surface of the material. However, the x-y axis kurtosis shows rounded asperities whereas the z-axis shows sharper asperities. This is a consequence of the manufacturing process and is likely to have a significant impact on the mechanical properties of the surfaces. Thus, due to

the high roughness, and the impact this may have on wear mechanisms and debris production, some industrial applications may require polishing following manufacture to maintain uniform wear over the entire surface.

6.4. Mechanical Property Characterisation

As discussed in **section 2.4**, selective laser sintered materials demonstrate anisotropic behaviour, therefore the materials response will differ in compression to tension.

However, in this thesis, the samples were all tested "as produced"; there was no investigation into the effect of material anisotropy. Therefore conclusions, based on the specific response of laser sintered EOS PEEK HP3 to the methods of mechanical testing used in this thesis, are considered only for the manufactured orientation.

From tensile testing, the EOS PEEK HP3 samples were found to have a tensile modulus of 2.76 ± 0.15 GPa, a tensile strength of 88.7 ± 1.5 MPa, and an elongation to break 4.2 ± 0.2 %. The tensile specimens showed very little plastic deformation, with a sudden fracture occurring; typical of brittle materials. **Figure 57** shows the fracture surfaces of the tensile test specimen.

The tensile samples each had a central fracture (**Figure 57a**) and surrounding secondary fractures (**Figure 57b**); This is supported by observations of the failed surfaces; it can be seen that the central fracture was progressive and showed a small amount of plasticity in failure, however, the secondary failures are typical brittle failures, showing very smooth failure planes with no identifiable necking of the sample.

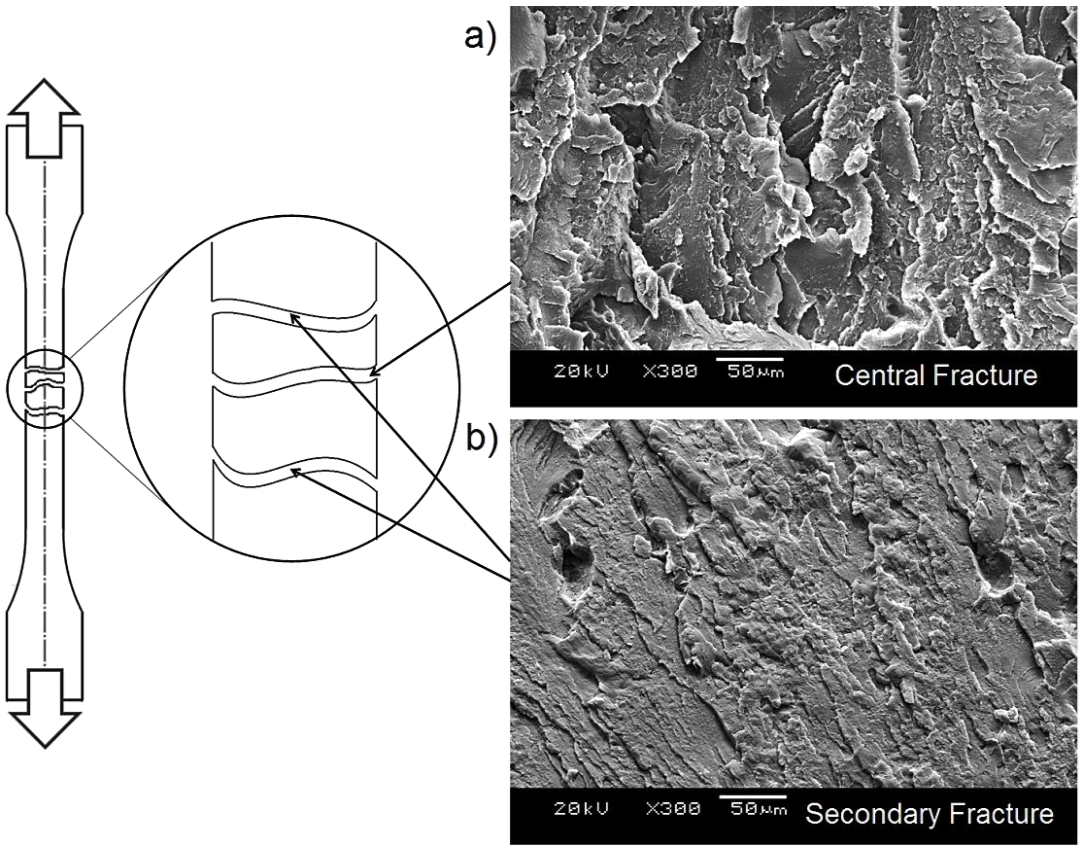

Figure 57: Fracture surfaces from tensile testing; a) central fracture, b) secondary fracture

Flexural testing showed a similar fracture response to that in tensile testing. The initial fracture surface was similar in appearance, although, there were no secondary fractures resulting from the initial failure. **Figure 58** shows the fractured surface. Two regions can be identified from the surface; an initial region of progressive failure, and a region of fast fracture. The layers of sintered material (approximately 120 µm) can be clearly seen in **Figure 58a**.

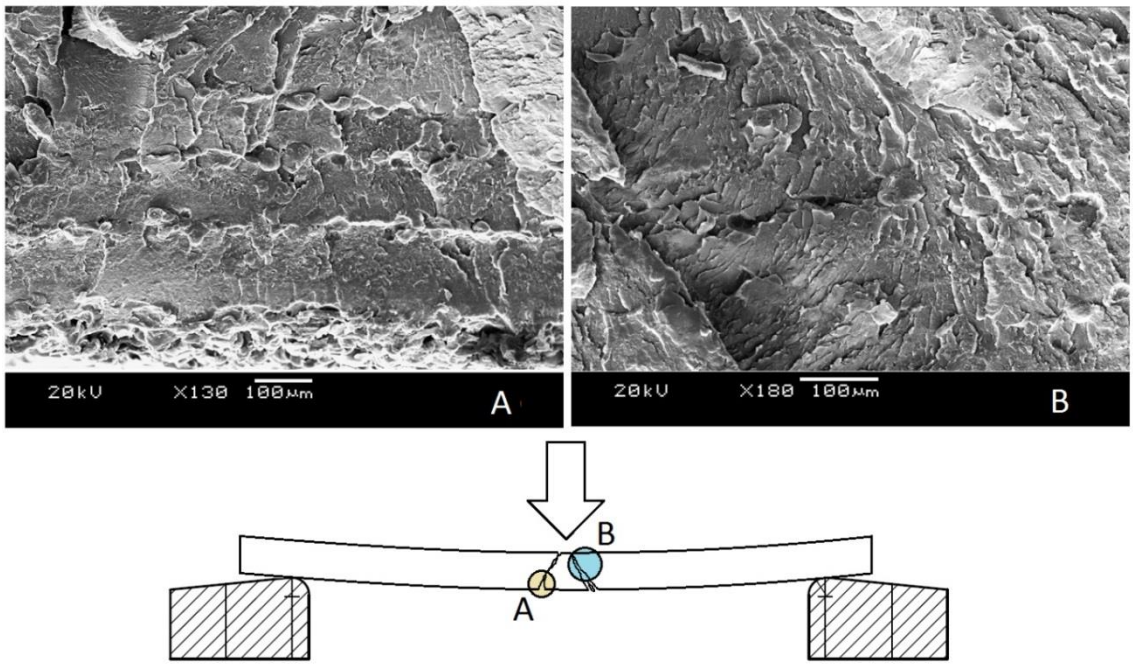

Figure 58: flexural failure; a) progressive fracture of layers b) fast fracture

Fracture toughness (K_{IC}) was calculated according to BS ISO 13586:2000 as 1.40 ± 0.2 MPa/m2. This is comparatively low when compared with that for injection moulded PEEK (5.4 - 7.5 MPa/m^2) [86]. **Figure 59** shows the fracture surface.

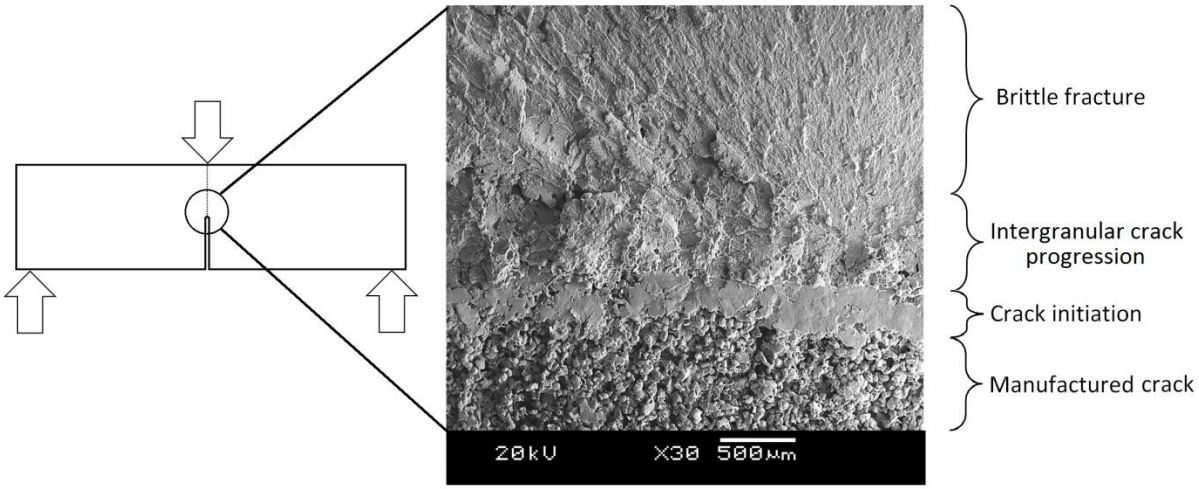

Figure 59: Fractured surface showing regions of failure (Note: crack propagation is from bottom to top)

Compressive testing was done in two stages; the compressive modulus was determined to be 610 ± 15 MPa and the compressive strength to be 184 ± 15 MPa. It was observed that the anisotropy of the sample had a significant effect on the failure characteristics; the compressive strength samples showed severe delamination following a period of deformation (**Figure 60**).

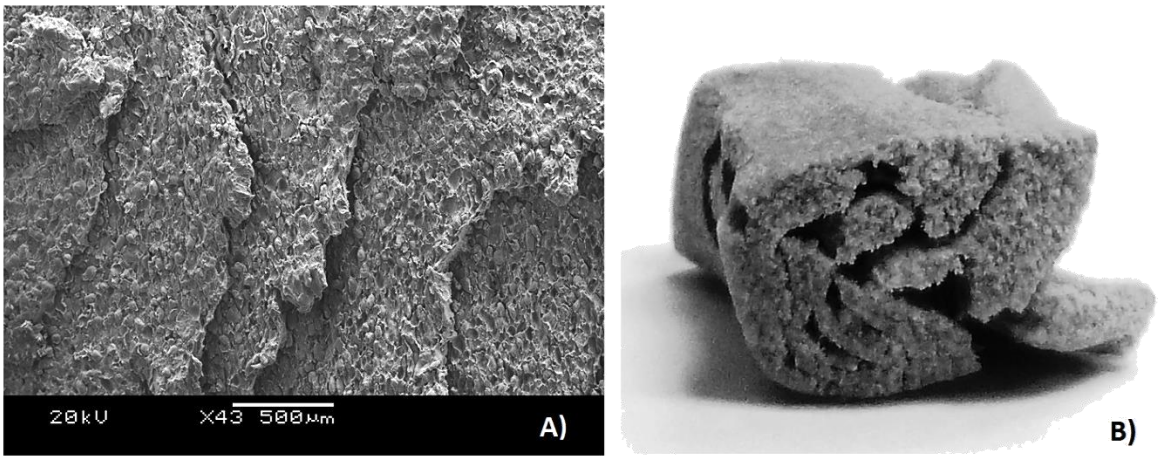

Figure 60: Compressive EOS PEEK HP3 sample delamination showing, a) the fractured surface and b) the compressive strength sample following test.

From the observed fracture surface, the delamination in the compressive samples appeared to occur in two stages: firstly, void nucleation and coalescence at the boundary between the sintered layers resulted in crack propagation in the sample; following this, progressive delamination between the layers occurred as the stress induced between these layers was increased; finally, a period of fast fracture occurred where the surfaces were ruptured.

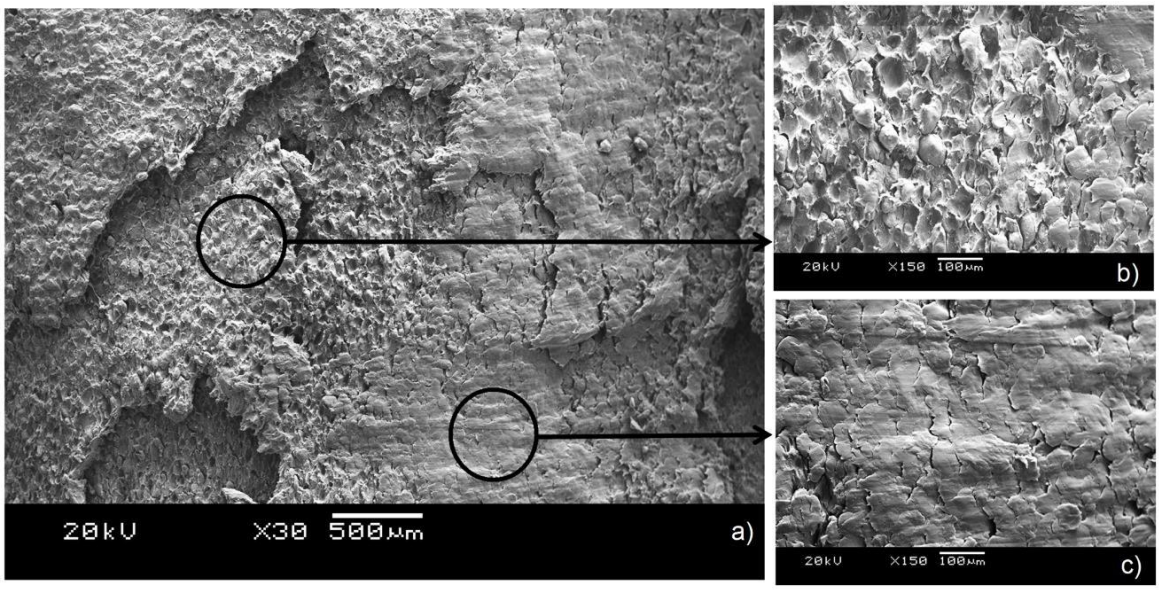

Figure 61: Compressive failure surfaces showing a) regions of failure, b) partially sintered material, c) worn path due to failure.

Figure 61a shows two regions of failure in the compressive samples. The failed surface, shown in **Figure 61b** is created as the sample is compressed. Following delamination, the surfaces are free to move and the loaded surfaces within the sample move against the failed surface forming the topography seen in **Figure 61c**.

The failure surface in the compressive strength samples (**Figure 61b**) shows a significant amount of partially-sintered material. Particles can be clearly identified and are approximately 60µm in diameter; correlating with the reported particle size for EOS PEEK HP3 powder [54]. This is an issue as the inter-granular strength at the interface between the layers is not sufficient to hold together the material under high loads; as shown by the failure surface. Thus, it is necessary to refine the material processing parameters to allow for a fully-sintered material to be produced. This should increase the fracture toughness and also the mechanical strength of the material.

The mechanical performance of EOS PEEK HP3 is dependent on the mechanism of loading. The response of the material is predominantly brittle, with failure surfaces showing delamination, sharp fracture planes and surface tearing. Partially-sintered material is still identifiable in the finished material and can be seen to significantly affect the mode of failure.

6.5. Thermal Property Characterisation

The dependence of polymers on load has been discussed in the previous section, however, the combined effect of temperature and strain rate play a significant role in the selection of a material for mechanical applications.

As a polymer is heated, it will pass through a glass transition temperature. However, since the glass transition is a second order, kinetically limited transition; that is, Tg is both time and temperature dependent; it is strongly influenced by the frequency (strain rate) of testing. Thus the use of Tg in characterising the performance of a mechanical polymer for specific applications is vital.

As the sample passes through Tg, the rate of energy absorption goes through a maximum; resulting in peaks in the loss modulus (E") and tan δ curves. The glass transition can be characterised based on the three DMTA events. For a frequency of 1Hz, the Tg values are 170.2 °C (storage modulus, E' onset), 178.6 °C (E" peak) and 186.8 °C (tan δ peak), as shown in **Figure 62**.

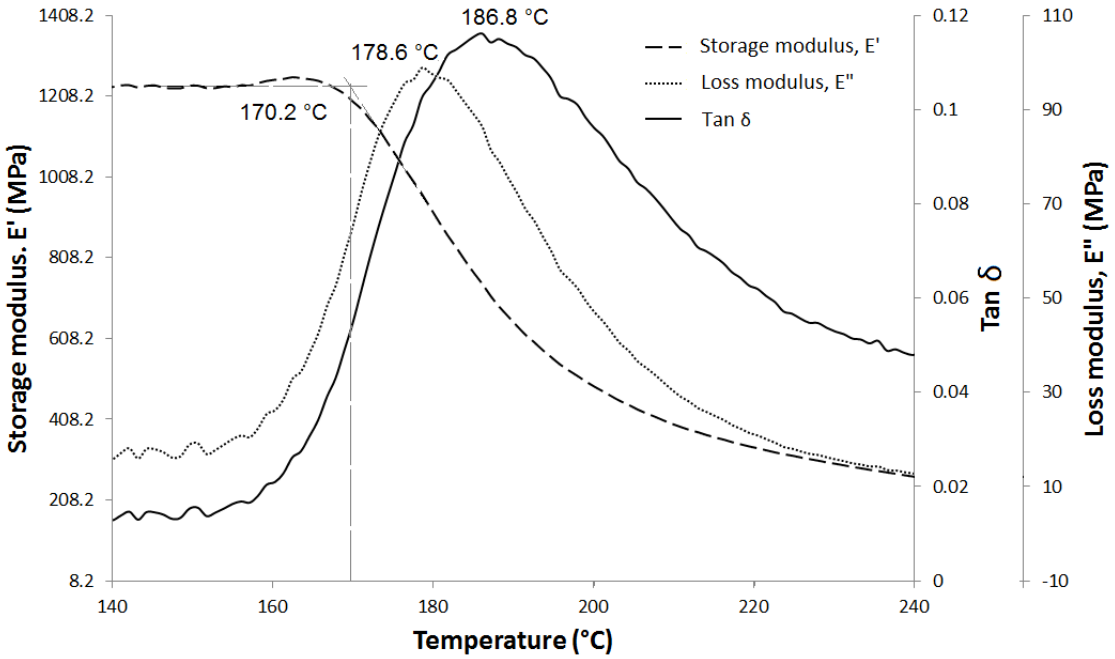

Figure 62: Glass transition temperature of EOS PEEK HP3 as determined by DMTA using three methods, for 1Hz.

The E' (storage modulus) onset defines the temperature at which the material strength will begin to decrease, such that the material may no longer be able to bear a load without significant deformation. The peak in the loss modulus (E") represents the temperature at which the material undergoes the maximum change in polymer mobility, which corresponds to Tg, and the loss tangent (tan δ) peak describes the damping characteristics of a material.

Figure 63 shows the progression of storage modulus and tan δ with frequency. It can be seen that as the frequency increases, there is a slight decrease in the intensity of the tan δ, a broadening of the tan delta peak, and a decrease of the slope of the storage modulus curve in the region of the transition.

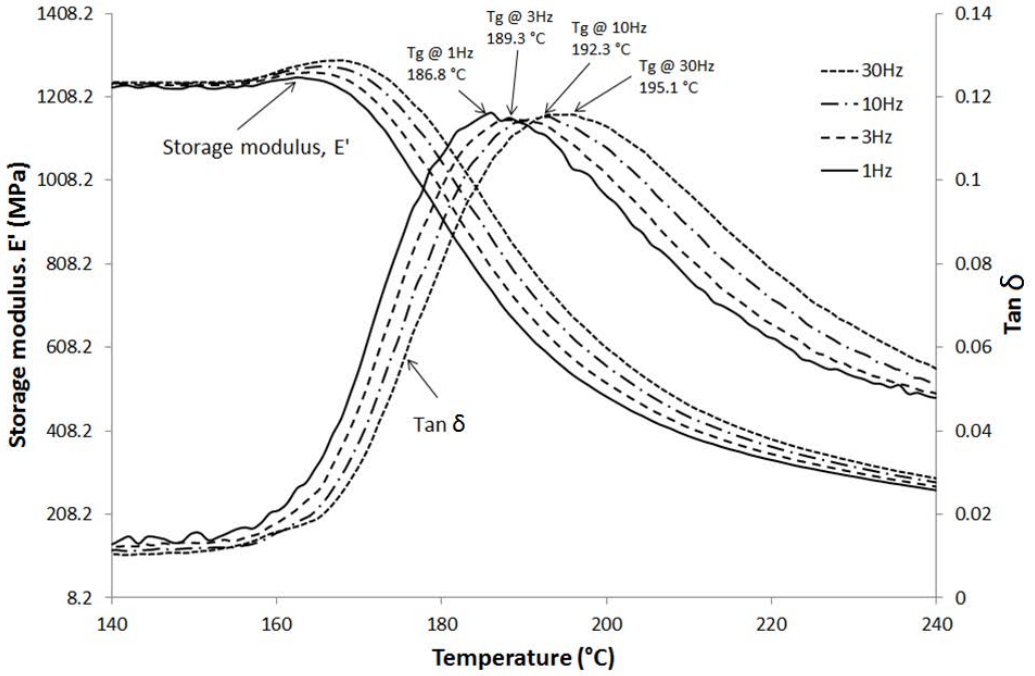

Figure 63: DMTA output, showing the progression of storage modulus and tan δ with frequency for EOS PEEK HP3.

Table 15 shows the Tg determined using the three different methods from the DTMA analysis. These values demonstrate the applicability of the material for high temperature mechanical application. The dynamic glass transition temperatures are a significant improvement on the values typically associated with laser sintered polymers (4).

Table 15: Tg of EOS PEEK HP3 based on oscillation frequency; DMTA methods

	Frequency			
Method	**1 Hz**	**3 Hz**	**10 Hz**	**30 Hz**
tan δ	186.8 °C	189.3 °C	192.3 °C	195.1 °C
E" peak	178.6 °C	181.5 °C	183.4 °C	185.3 °C
E' onset	170.2 °C	172.3 °C	173.8 °C	177.1 °C

The physical and mechanical properties of semi-crystalline polymers are highly dependent on their degree of crystallinity.

To characterise the crystallinity of EOS PEEK HP3 DSC was used. Assuming the enthalpy of fusion of the pure crystalline phase of PEEK to be 130J/g [78], it was found that the EOS PEEK HP3 had a crystallinity of 35.4%. This is comparable with typical values for high performance injection moulded polymers, making it much stronger, stiffer and denser than previous laser sintered plastics.

From the DSC analysis, for a heating rate of 10 °C/min, the glass transition and melt temperature were found to be 160.3 °C and 398.1 °C respectively. These values are both significantly higher than those typically associated with laser sintered polymers [91].

The thermal characteristics of EOS PEEK HP3 are far superior to previous laser sintered polymers outlining its suitability for use in high temperature mechanical applications.

6.6. Material Property Comparison

The use of high temperature semi-crystalline materials in SLS has significant benefits in terms of component development and manufacture.

Table 16 shows a comparison of the material properties of EOS PEEK HP3 versus the reported properties for injection moulded PEEK 450G and selectively laser sintered PA 2201/PA12.

- PEEK 450G is the general grade injection moulded PEEK developed by Victrex [86]. It is widely regarded as one of the highest performance mechanical polymers.

- PA 2201/PA12 is an unreinforced, laser sintered polyamide developed by EOS for the EOSINT P [92]. This material is typically applied to fully functional parts; parts that are manufactured as fully operational components; for high mechanical and thermal load.

Table 16: Mechanical Properties summary [50,52,54,86,88,92,93]

Material	EOS PEEK HP3	PEEK 450G	PA2201/PA12 (SLS)
Tensile Modulus (EN ISO 527)	2.76 ± 0.15 GPa	3.7 GPa	1.70 ± 0.15 GPa
Tensile Strength (EN ISO 527)	88.7 ± 1.5 MPa	100 MPa	45 ± 3 MPa
Elongation at Break (EN ISO 527)	4.2 ± 0.2 %	34 %	20 ± 5 %
Compressive Strength	184 ± 15 MPa	125 MPa	53 ± 15 MPa
Flexural Modulus (EN ISO 178)	3.26 ± 0.7 GPa	4.1 GPa	1.24 ± 0.13 GPa
Glass Transition Temperature (DSC)	174.5 °C	143 °C	52 °C
Fracture Toughness, K_{IC}	1.40 ± 0.2 MPa/m^2	5.4 - 7.5 MPa/m^2	-
Glass Transition Temperature (DMTA, tan δ)			
@1Hz	186.8 °C	165.8 °C	48 °C
@3Hz	189.3 °C	-	-
@10Hz	192.3 °C	-	-
@30Hz	195.1 °C	-	-
Density: Bulk (DIN 53466)	0.43 ± 0.01 g/cc	1.30 g/cc	0.44 ± 0.01 g/cc
Density: Laser sintered part (DIN EN ISO 1183)	1.307 ± 0.01 g/cc	N/A	0.930 ± 0.01 g/cc
Porosity (BS ISO 15901)	4.359 %	N/A	7 %
Melting point (DSC)	372 °C	343 °C	172-180 °C
Crystallinity (DSC)	35.4 %	30 %	-

Temperature has thus far limited the application of laser sintered materials such as PA 2201/PA12. However, it can be seen that EOS PEEK HP3 has a melting point 200 °C higher than PA 2201/PA12, and a glass transition temperature 400 % higher (defined by the peak in the tan δ curve at 1Hz). In addition, it can be seen that the tensile and flexural properties of PEEK 450G and EOS PEEK HP3 are significantly higher than those reported for PA 2201/PA12. The low elongation to break of EOS PEEK HP3 shows that the material is more brittle than PEEK 450G and PA 2201/PA12; this is to be expected as the porosity in the bulk and on the surface of the material will encourage fracture.

Overall, there are small discrepancies between the measured parameters in this study and the reported values for EOS PEEK HP3. This is considered to be a result of variation in manufacturing parameters as well as the significance of the anisotropy of the samples; as the samples were all produced in the x-y plane, there was no investigation into the effect of material anisotropy.

However, it is important to emphasise the comparability of the tests conducted on laser sintered materials and the reported values for injection moulded PEEK:

As discussed in **section 2.4**, for laser sintered materials the manufactured orientation can result in a 20%/45% decrease in the reported tensile strength of laser sintered nylon and EOS PEEK HP3 respectively [52,58]. In addition, the surface roughness has a significant impact on failure initiation in laser sintered polymers as the partially sintered particles on the surface of the manufactured sample would lead to localised stress concentrations. Consequently, the differences in testing methodologies and sample characteristics mean that the direct comparison of the mechanical properties of injection moulded and laser sintered materials are not reliable; however, the results provide an indication of the

relative strength of the materials, and act to outline possible limitations of the process/mechanical performance.

Figure 64 shows the improvement in material properties using EOS PEEK HP3 over conventional SLS materials. The thermal and mechanical properties of EOS PEEK HP3 are far superior to previous selectively laser sintered polymers and closer to that of higher performance injection moulded PEEK blends.

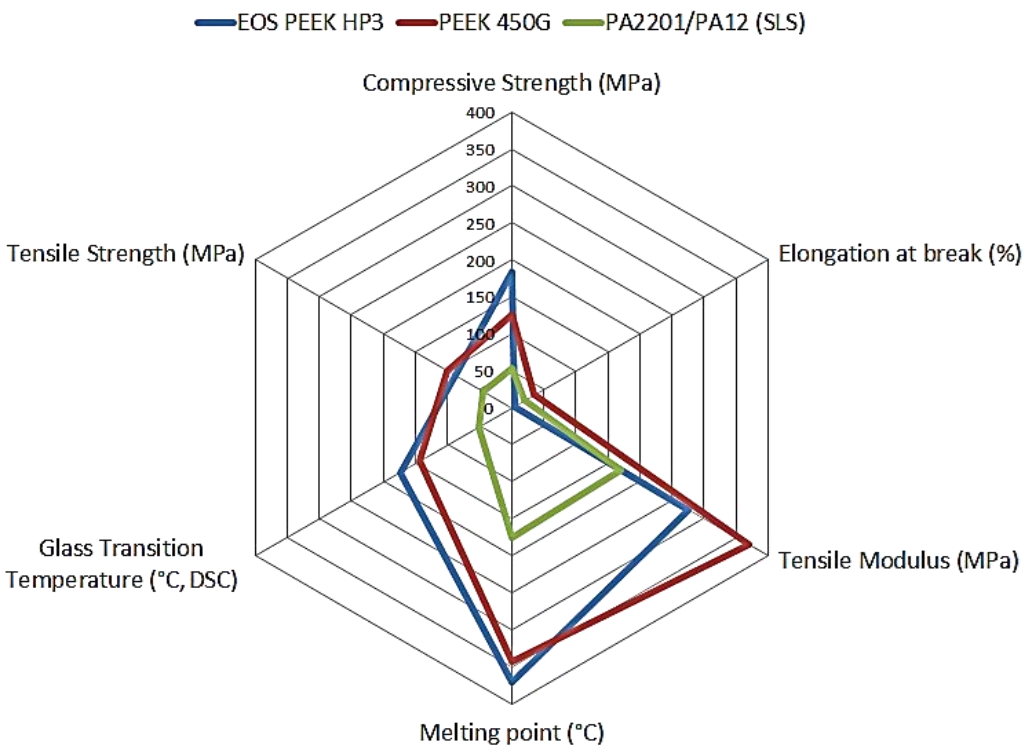

Figure 64: The comparative properties of EOS PEEK HP3

6.7. Friction and Wear Properties

This section investigates the wear and frictional properties of EOS PEEK HP3. EOS PEEK HP3 has been reported to demonstrate "excellent wear resistance[7]"; however, there is very little documented evidence of this.

In polymers, the mechanism of wear has been shown to be significantly affected by surface roughness. In **section 6.3** it was shown that the surface roughness of manufactured EOS PEEK HP3 was relatively high (Sa = 20µm), meaning that the asperities should have a significant effect on the material wear.

To establish the lubricated and unlubricated tribological properties of EOS PEEK HP3, samples were tested using a High Frequency Reciprocating Rig (HFRR) at various speeds and loads; the test parameters are shown in **Table 17**. To allow preferential wear of the EOS PEEK HP3 sample, a high stiffness steel ball was used and measurements of friction were made over a four hour period.

Table 17: HFRR test parameters (Steel vs. EOS PEEK HP3)

		Loading Mass (max. contact pressure)		
		300g (94.8MPa)	**500g** (112.3MPa)	**1kg** (141.5MPa)
Frequency (max sliding speed)	**25Hz** (157mm/s)	UL	UL	UL, L
	50Hz (314mm/s)	UL, UL®, L, L®	UL, L	
	100Hz (628mm/s)	UL		

Note: UL – Unlubricated, L – Lubricated., ® - Repeat

[7] *EOS website [cited 14th January 2014]*: http://www.eos.info/material-p

6.7.1. HFRR Results - Friction

Figure 65 shows the unlubricated HFRR results. It can be seen that following an initial period of bedding in, the coefficient of friction approaches steady state.

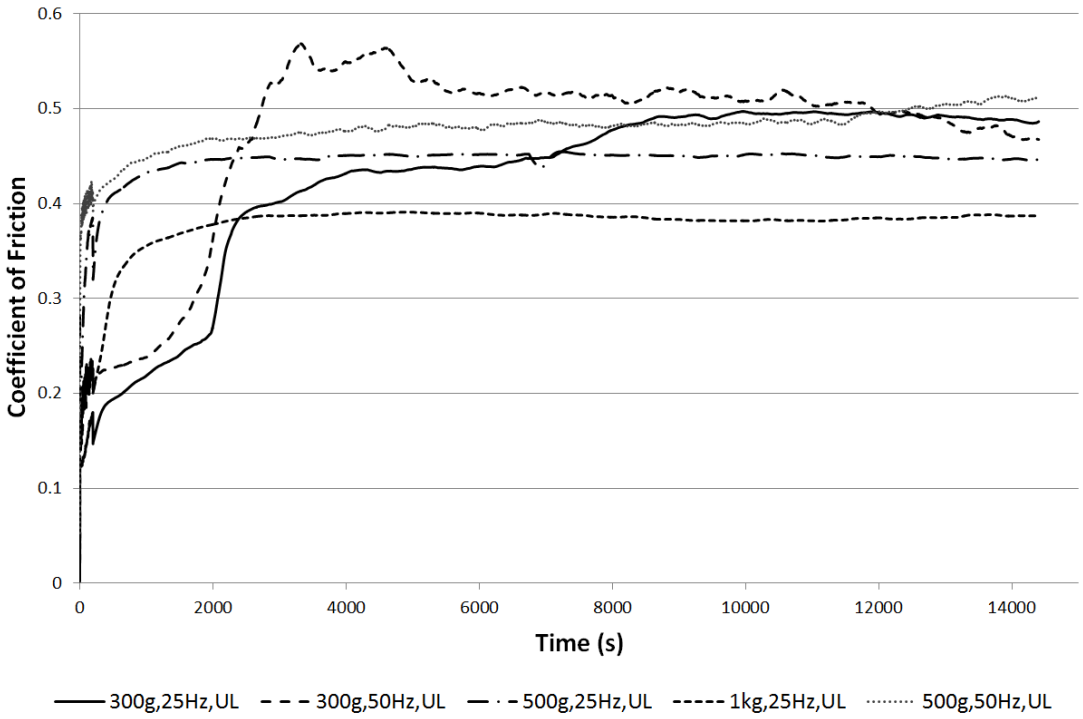

Figure 65: Coefficient of friction vs. time (Steel vs. EOS PEEK HP3 – unlubricated)

By running the samples to steady state, their tribological characteristics could be analysed to reflect the usable life of the component; it was observed that the coefficient of friction reduced with applied load, but increased with frequency. In addition, it was seen that in highly loaded unlubricated tests, the influence of adhesion became more prominent. This is apparent from the oscillation in the coefficient of friction trace. Moreover, as adhesion is related to the contact area, deformation of the asperities on the polymer surface resulted in an increase in the 'real contact area'; increasing adhesion.

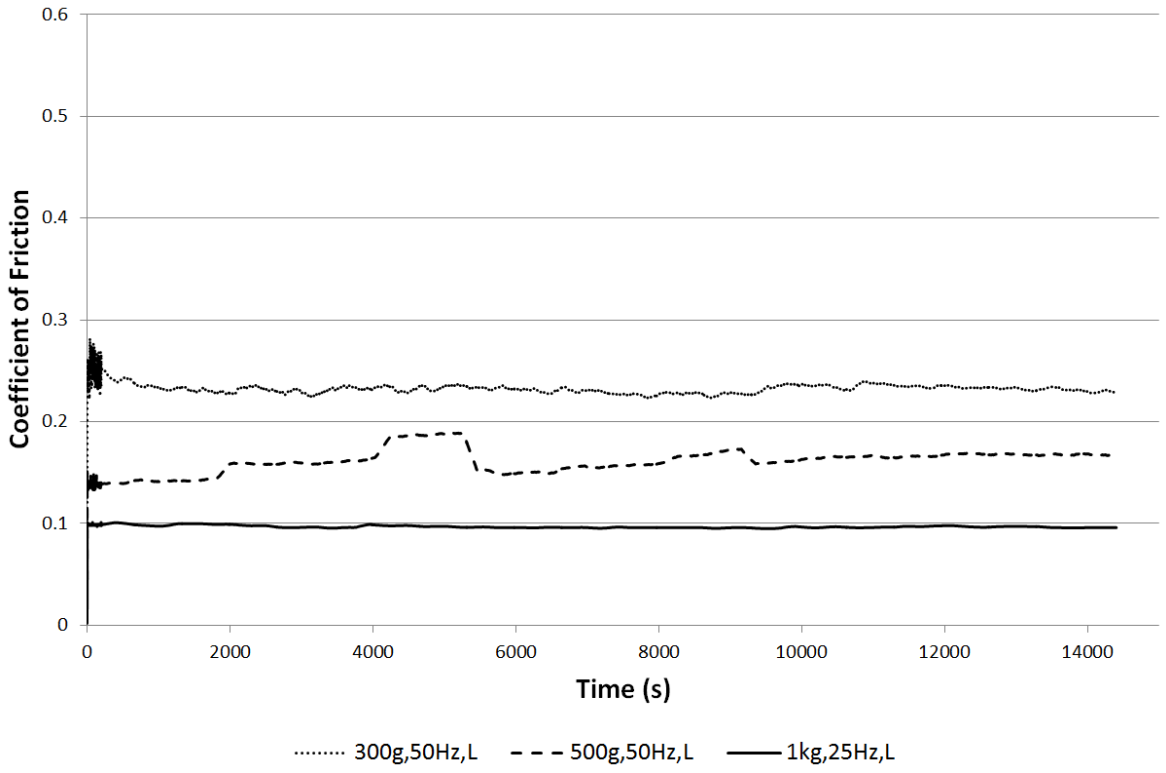

Figure 66: Coefficient of friction vs. time (Steel vs. EOS PEEK HP3 – lubricated)

Figure 66 shows the lubricated[8] HFRR results. The bedding in period that was seen in the unlubricated tests (**Figure 65**) was not as prominent in the lubricated tests. Furthermore, it was observed that the coefficient of friction was much lower in the lubricated tests (approximately 50%). This reduction in the coefficient of friction was attributed to reduced adhesion and the lubricant film supporting the load; reducing the contact stress on the material. Moreover, under high loads, the increase in contact pressure would result in a significant increase in lubricant viscosity. In as much as viscosity is a measure of a fluids resistance to flow; this increase greatly enhanced the

[8] *Castrol, Product Data – Castrol Manual EP 80W [Internet]. [cited 2013 July 13]. p. 1–2. Available from:* http://datasheets.bp.com/bpglis/FusionPDS.nsf/0/0822197B4F516F45802577F5004F7F21/$file/BPXE-8C4U29_0.pdf

lubricant's ability to support load without being squeezed out of the contact zone. This could be seen by the reduction in coefficient of friction with load.

6.7.2. HFRR Results - Wear

Following HFRR testing the generated wear scars were examined. There was little wear debris and the wear scars were significantly smaller than those observed on injection moulded PEEK (**Chapter 5**). The wear scars for the 50Hz, 500g tests are shown below (**Figure 67**).

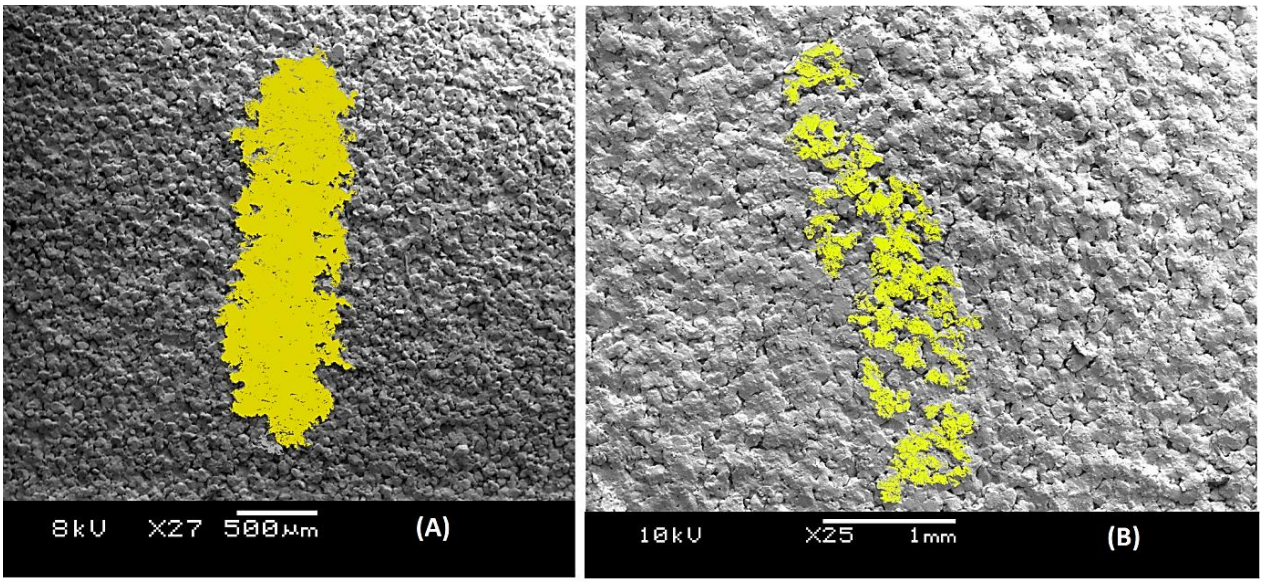

Figure 67: Apparent wear scars for A) unlubricated (1.45 mm^2), B) lubricated (0.96 mm^2)

Table 18 gives the wear areas calculated for the lubricated and unlubricated tests. The wear was seen to be proportional to both speed and load for all test conditions.

Table 18: EOS PEEK HP3 apparent wear area (mm^2) vs. load and frequency

			Loading Mass (max. contact pressure)		
			300g (94.8MPa)	**500g** (112.3MPa)	**1kg** (141.5MPa)
Frequency (max sliding speed)	**25Hz** (157mm/s)	**Unlubricated**	1.26	1.31	1.40
		Lubricated	-	-	1.04
	50Hz (314mm/s)	**Unlubricated**	1.32	1.45	-
		Lubricated	0.93	0.96	-
	100Hz (628mm/s)	**Unlubricated**	1.48	-	-

In lubricated tests, wear was low and only observed on the asperities of the material (**Figure 67**). However, in unlubricated tests the wear area was more significant and the effects of sliding speed and load on the surface of the material could be observed (**Figure 68** and **Figure 69**).

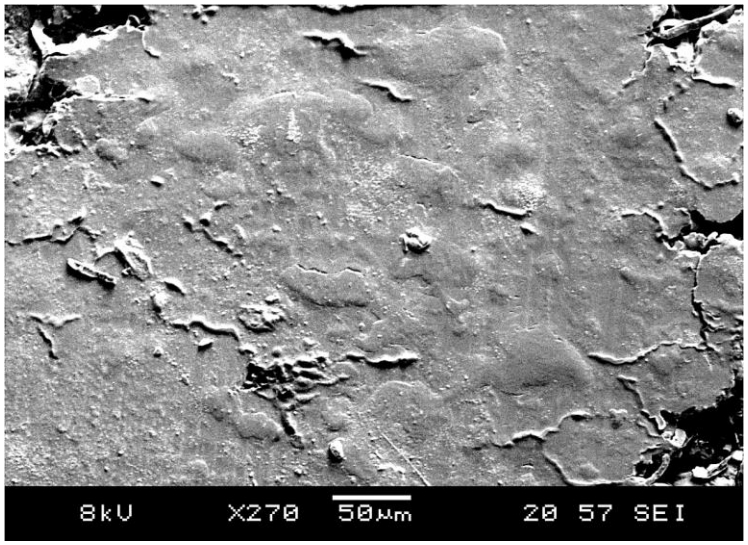

Figure 68: Smearing of the material in unlubricated testing (500g, 50Hz)

Figure 68 shows the unlubricated wear surface. Preferential asperity wear and the consequential smearing of asperity material, as the harder counterface ploughed through the softer material increased with load. This also significantly reduced the surface roughness of the material, but increased the wear scar area.

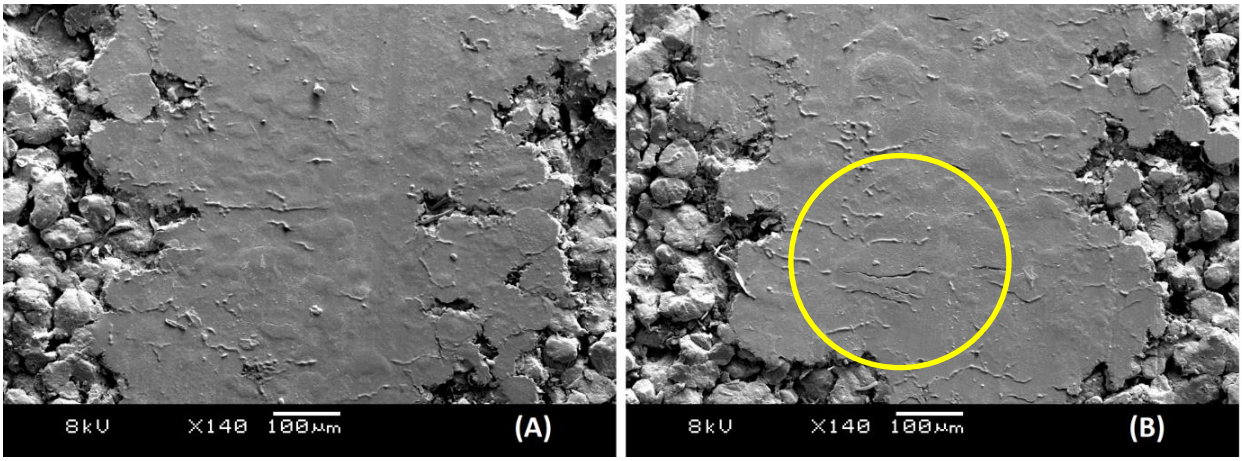

Figure 69: Unlubricated wear (500g, 50Hz), A) sliding velocity = max, B) sliding velocity = min

Fatigue tearing in the deformed region could be seen (**Figure 69**). This was more prominent under high load and at the ends of contact; namely when the sliding velocity approached $0mms^{-1}$ (**Figure 69b**). This increase was associated with reduced sliding speeds and increased adhesive wear. However, in the centre of the wear scar where the sliding velocity was at maximum, fretting lines could be seen (**Figure 69a**). These were more prominent with higher sliding speeds and also increased load.

In contrast, surface smearing was not seen in lubricated tests, and wear was less sensitive to both frequency and load.

Figure 70 shows the preferential asperity wear following unlubricated testing. It was observed that in all lubricated tests, due to the high roughness of test surface, the

lubricant film thickness was incapable of preventing asperity wear. However, following testing, the surface of the material was effectively polished reducing the surface roughness of the material and improving its wear characteristics.

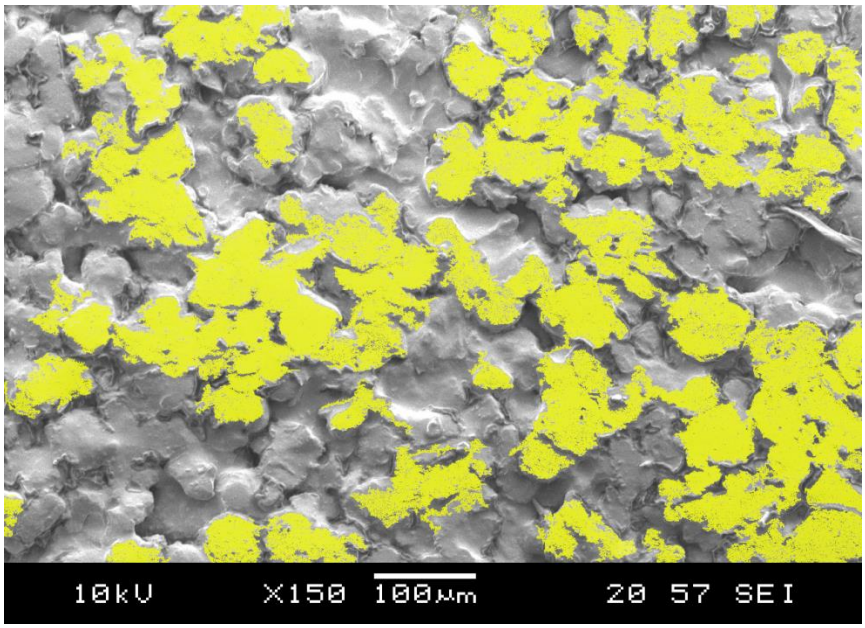

Figure 70: Asperity wear in lubricated tests (500g, 50Hz)

Micro pitting (~4µm diameter) was observed on the lubricated wear surface **Figure 71**. This was only detected in highly loaded tests; associated with the highest contact pressures. The impact of this on the tribological properties of the surface was minimal, as asperity wear dominated the contact.

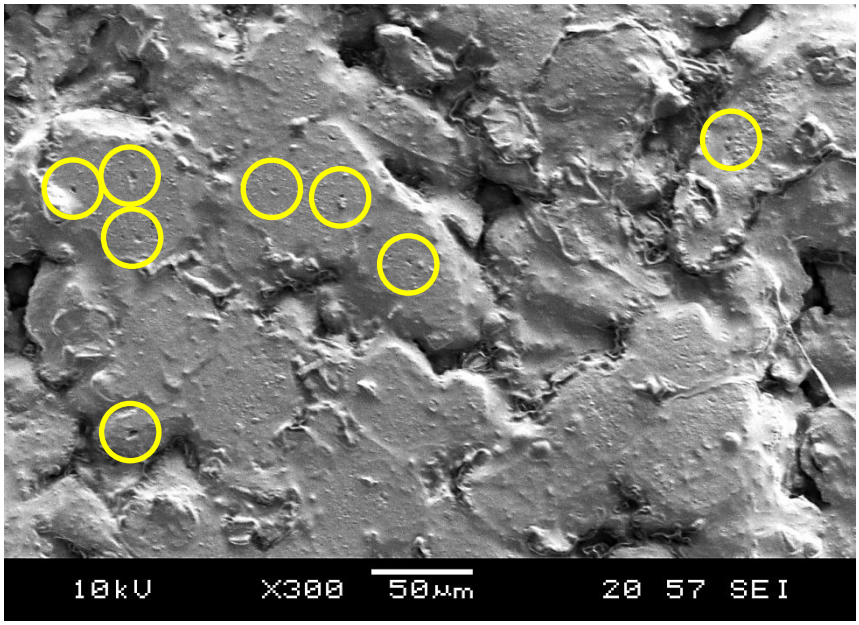

Figure 71: Lubricated wear showing micro-pitting on the worn surface (1kg, 25Hz)

6.8. Carbon Reinforced Selectively Laser Sintered PEEK

Developments have also been made into the production of carbon fibre reinforced (CFR) laser sintered PEEK. Reinforcement has been shown, in some cases, to improve both the strength and tribological properties of an injection moulded polymer [40,94]. However, the use of reinforcement to improve the tribological properties of SLS polymers has not been investigated.

HFRR samples were manufactured by Paramount Industries, USA, using an EOSINT P800 (EOS Electro Optical Systems 2011a) high temperature laser sintering system to include 10% carbon fibre reinforcement (**Figure 72**).

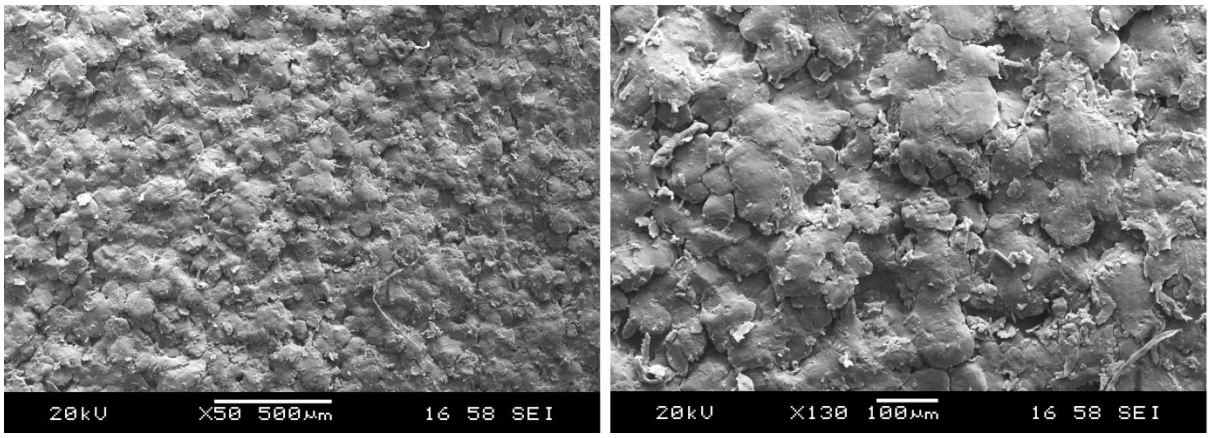

Figure 72: SEM image showing the un-run surface of CFR PEEK HP3

Table 19 gives the published properties of CFR PEEK HP3. It can be seen that the properties are comparable to EOS PEEK HP3 but the tensile strength is significantly higher.

Table 19: The reported properties of CFR PEEK HP3

Material	CFR PEEK HP3
Tensile Strength, Ultimate (ASTM D 638)	110.3 ± 1.5 MPa
Elongation at Break (ASTM D 638)	2.2-2.5%
Compressive Strength (ASTM D 635)	161.27 MPa
Glass Transition Temperature (DSC)	156 °C
Specific Gravity (ASTM D 792)	1.29 g/cc
Melting point (ASTM D 3418)	371 °C

Reinforcement typically acts to strengthen a polymer; however, the influence of this on material wear depends on a number of factors.

Firstly, it can be seen that there was very little fibre directionality associated with the laser sintered CFR PEEK HP3 (**Figure 72**); typically in injection moulded materials, the flow of the molten plastic/fibre mix into the mould results in a preferential directionality

in the material, reducing the friction and noise of a reinforced polymer [29]. In addition, in laser sintered CFR PEEK HP3 there was no over-moulded/tribological layer on the outside of the material, therefore the abrasion wear due to the exposed reinforcement is felt immediately.

Furthermore, exposure of fibres in a matrix can result in those fibres becoming dislodged from the material; in a closed tribosystem this will dramatically increase the amount of 3rd body abrasive wear seen on the material.

Table 20 shows the test parameters used for testing CFR PEEK HP3.

Table 20: HFRR test parameters (Steel vs. CFR PEEK HP3)

		Loading Mass (max. contact pressure)	
		300g (94.2MPa)	**1kg** (140.7MPa)
Frequency (max sliding speed)	**25Hz** (157mm/s)	UL	UL, L
	50Hz (314mm/s)	UL	-

Note: UL – Unlubricated, L – Lubricated.

It can be seen that, when compared to unreinforced EOS PEEK HP3, the coefficient of friction traces were much more erratic (**Figure 73**). Despite this the values for steady state coefficient of friction, when reached, were lower. Additionally, it was seen that the coefficient of friction again reduced with load.

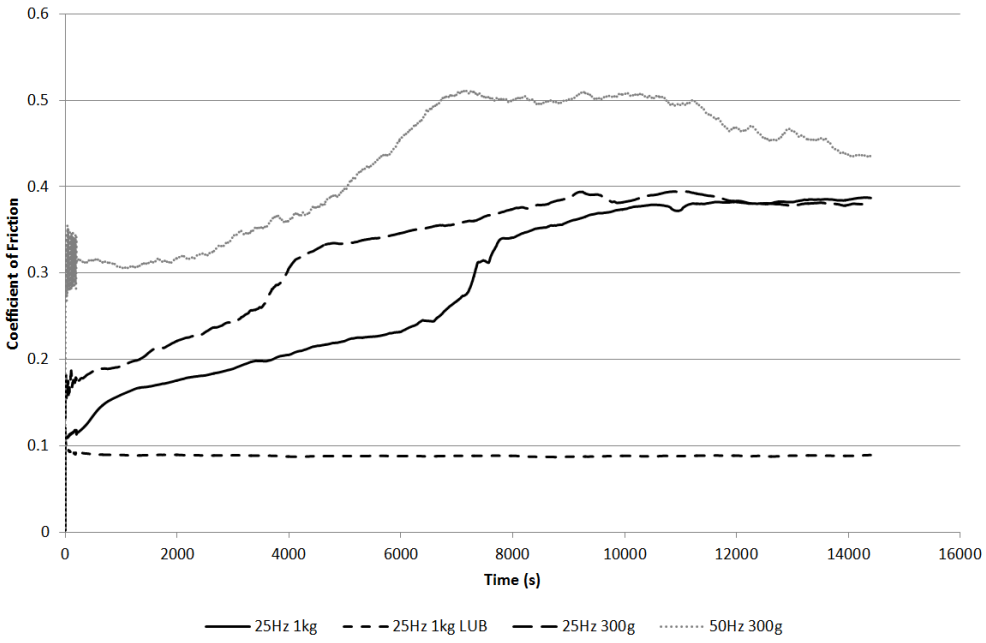

Figure 73: Coefficient of friction vs. time (Steel vs. CFR PEEK HP3)

The wear scar for the 1kg, 25Hz test is shown in **Figure 74**. It was observed that the unlubricated wear scar area was significantly smaller for the reinforced material. This was attributed to the reduction in smearing.

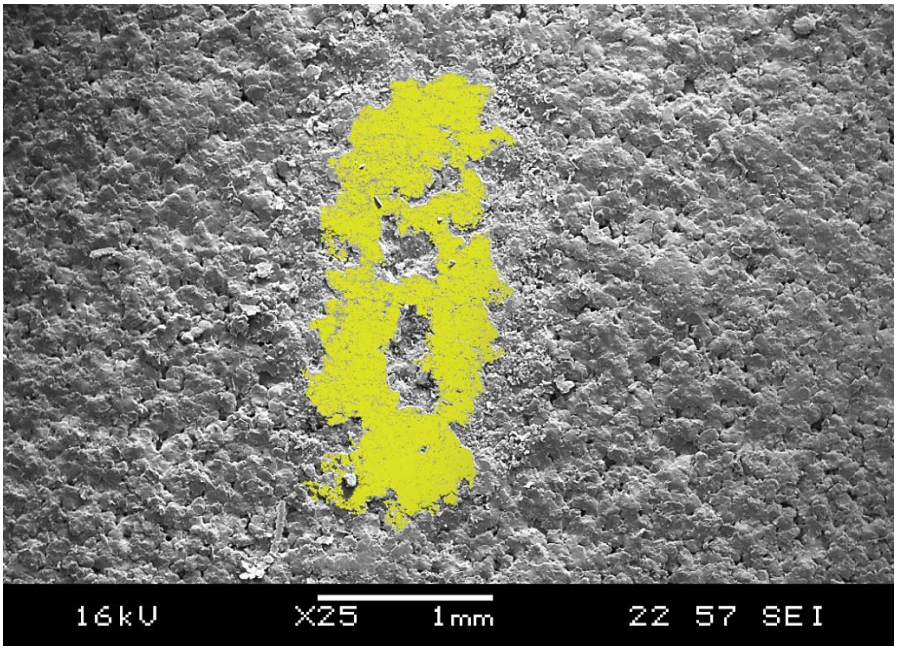

Figure 74: Wear scar CFR SLS PEEK (1kg, 25Hz)

On close examination it was observed that the wear scar it could be seen that the fibres in the matrix were exposed (**Figure 75**). The exposure of these fibres, and their removal and abrasive tendencies when contained in the contact region, resulted in significant amounts of scuffing/fretting.

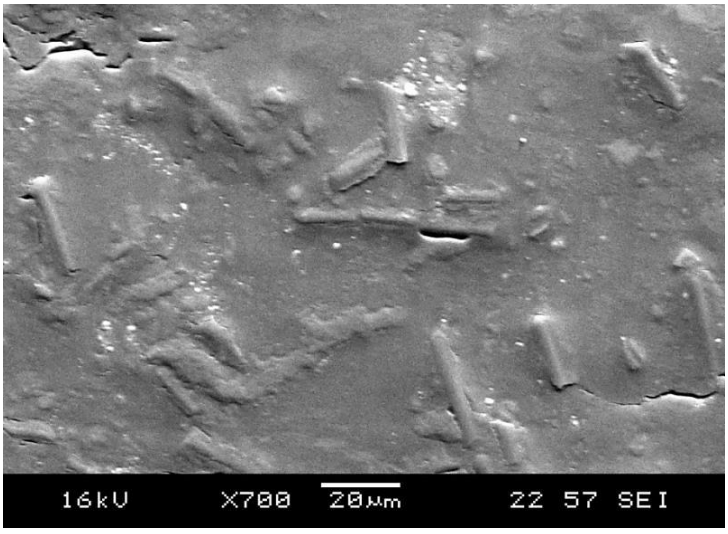

Figure 75: Carbon Fibre reinforcement exposed in the wear scar

This scuffing/fretting increased the amount of wear debris produced (**Figure 76**). Removed fibres could be seen along with significant amounts of abrasive wear debris.

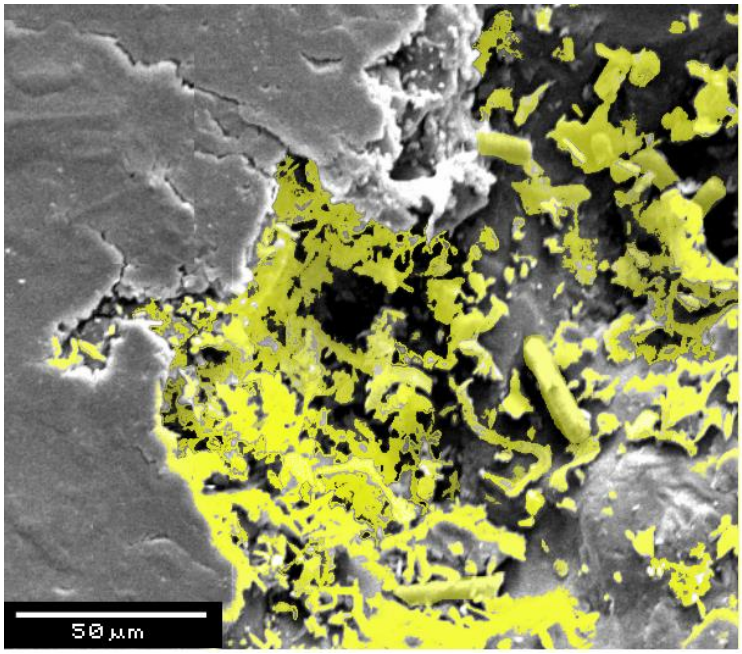

Figure 76: Wear debris in unlubricated CFR PEEK HP3

It was also observed that in the highly loaded and high speed tests, the coefficient of friction reduced towards the end of the test. This reduction in the coefficient of friction was associated with the exposed fibres in the matrix orientating to the direction of sliding. This is shown in **Figure 77**; it can be seen that at the ends of contact, the fibres showed no preferential orientation, however in the central portion of the wear scar, the fibres appear to have orientated to the direction of sliding.

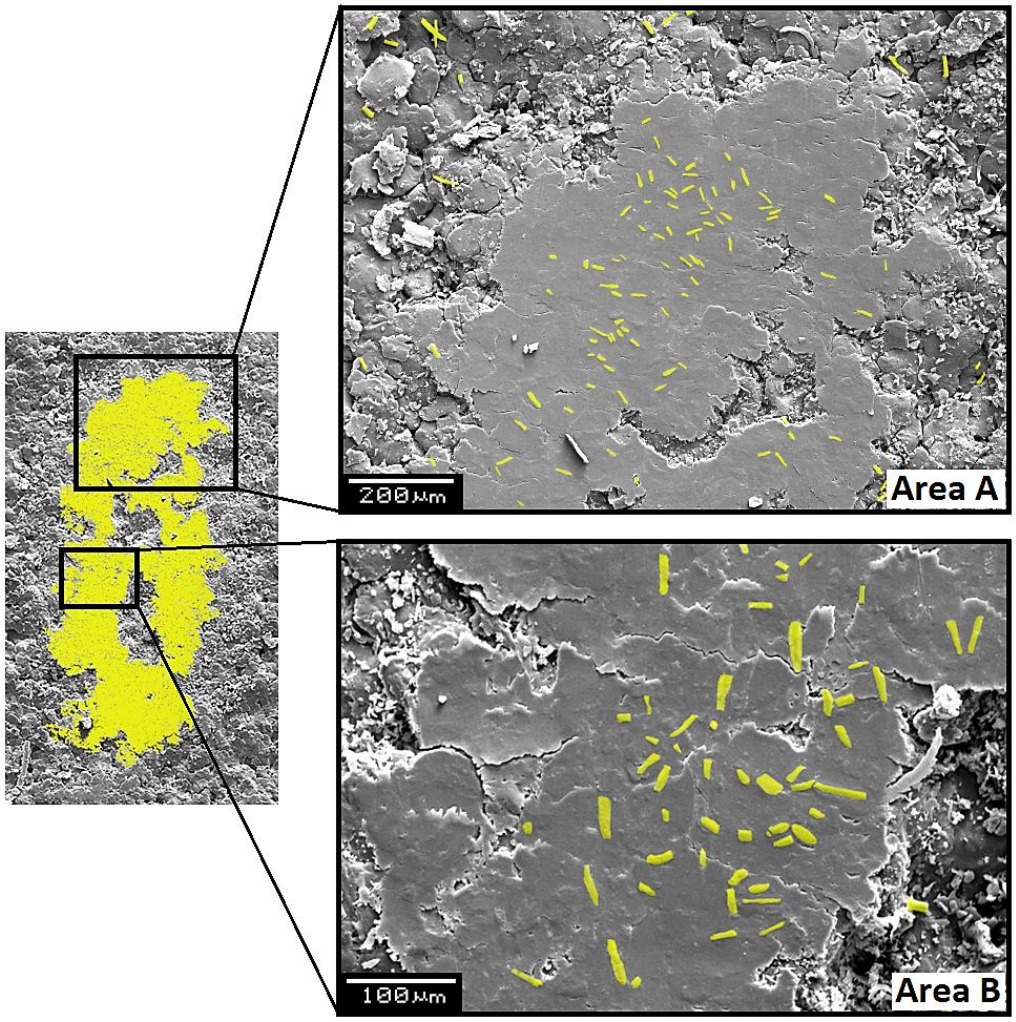

Figure 77: Fibre orientation within the wear scar

6.9. Conclusions

Traditionally, the properties of a laser-sintered material would be expected to be significantly worse than those of high performance injection-moulded polymers. However, it has been shown that the performance of EOS PEEK HP3 is significantly higher than for previous laser-sintered materials and comparable with high performance injection-moulded materials.

From visual examination it was observed that the roughness of the material was determined by partially sintered particles on the surface.

The failure mechanisms observed varied depending on the method of loading; secondary fractures were observed in tensile testing whereas delamination of the material could be seen at higher loads in compressive testing. The surface of the failed compressive strength samples showed partially sintered powder in the bulk of the material, further examination showed that the bulk of the material was approximately 4% porous with these pores being approximately 24nm in diameter. This should be evaluated to improve the material properties and refine processing parameters, as this was not immediately apparent from tensile failures.

Limited plasticity was observed in mechanical testing, with failure occurring along the partially sintered particle boundaries in the material. In addition, the low elongation to break of EOS PEEK HP3 shows that the material is more brittle than PEEK 450G and PA 2201/PA12.

The coefficient of friction and wear of EOS PEEK HP3, as determined by HFRR testing, were significantly lower than for injection moulded PEEK 450G (**chapter 5**). It was observed that the wear of EOS PEEK HP3 was dominated by surface asperity contact, with spreading of surface material and asperity wear dominating unlubricated and lubricated wear mechanisms respectively.

In unlubricated contact, high sliding velocities and contact pressures resulted in scuffing/fretting in the centre of the wear scar, whereas high loads at the ends of contact resulted in significant surface tearing fatigue. In lubricated contact, the impact of speed was less significant, although micro-pitting was also seen in highly loaded contact.

By reinforcing SLS PEEK, it was shown that the wear area reduced. However, the wear debris increased due to increased abrasion. It was also observed that the exposed fibres would orientate to the direction of sliding in high speed and high load tests, reducing both friction and wear.

Although the tribological properties of SLS PEEK are comparable to high performance injection moulded materials, the mechanical strength of the material and the small amount of plasticity during failure may limit its application to non-conformal machine elements.

Overall, the use of EOS PEEK HP3 for impact loading is not recommended as the brittle tendencies may lead to sudden failure. However, design optimisation methods to allow for the distribution of load across a surface are recommended to improve the systemic performance.

As with any material, the specific design requirements may vary with application. Thus, further analysis to replicate the precise operational conditions may be needed. However, this chapter outlines the fundamental mechanical, thermal and physical characteristics of the material and can be used to give an indication of the suitability of HT-SLS materials for mechanical applications.

Chapter 7

THE SUITABILITY OF LASER SINTERED PEEK FOR GEAR APPLICATIONS

7.1. Introduction

The main benefits of additive layer manufacture (ALM) lie in those areas where conventional manufacturing methods reach their limitations; it enables the manufacture of components to be design-driven rather than production driven.

However, the results in **chapter 6** have outlined that despite the tribological performance of EOS PEEK HP3 being good, the mechanical strength of the material and the small amount of plasticity demonstrated during failure may limit its application to machine elements.

This section of the thesis reports on the direct application of the laser sintered material EOS PEEK HP3 to power transmission gears. Specific efforts are made to establish the materials reaction to bending failure.

Finally, the results of this investigation are used in parallel with those obtained in **chapter 6** to establish an optimised gear geometry for high performance laser sintered polymer gears.

7.2. Materials Production

Traditionally, injection moulded polymer gears for power transmission have been produced with a steel central hub; this prevented failures in the coupling between the shafts and allowed the gear to be appropriately located. However, due to the difficulty of sintering around a steel input coupling, the design of the gear body was altered to accommodate the stresses on the polymer; preventing any failures occurring at the body itself.

Two design iterations were developed (**Figure 78**):

- Removal of the steel hub, instead producing the internal keyway as a feature of the gear itself.
- Multiple face external couple.

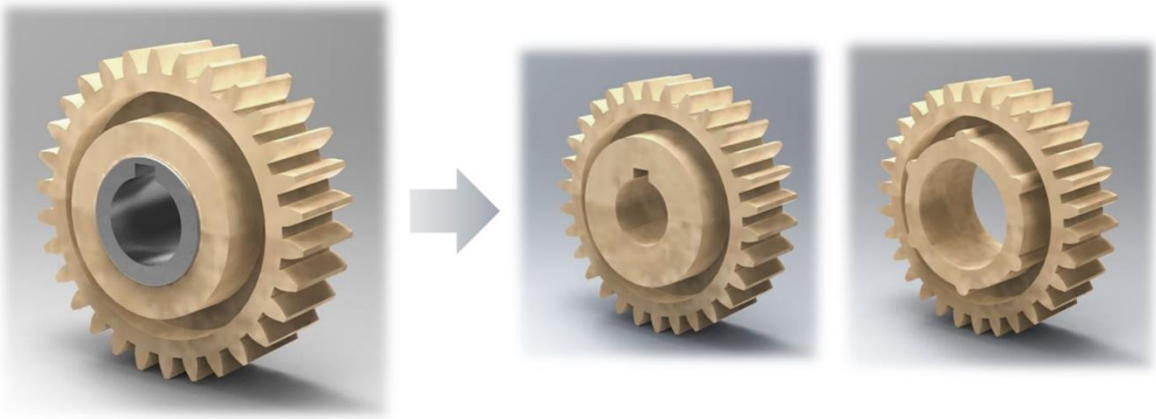

Figure 78: Keyway re-design to account for removal of the steel hub.

The designs were analysed using finite element methods for a nominal input torque and material (**Figure 79**). The resultant stress volume; calculated for a nominal threshold stress of 2.3 MN/m^2; allowed the two design iterations to be compared.

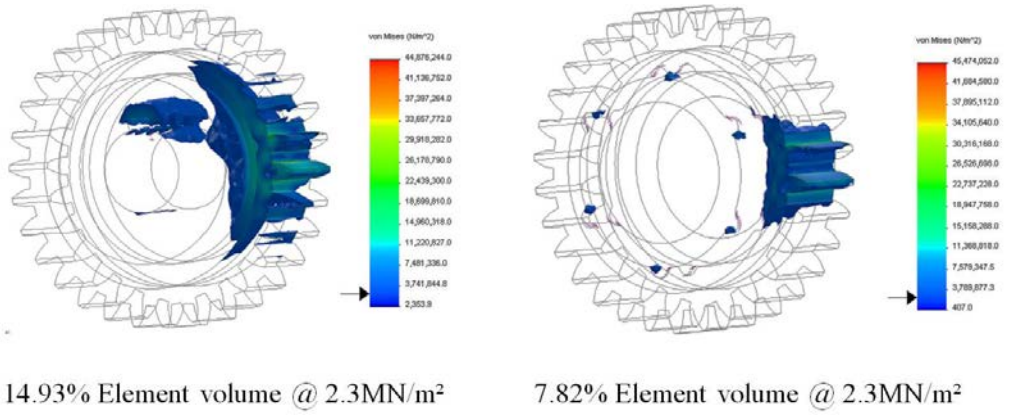

Figure 79: Finite Element Analysis results for design selection of shaft coupling

It can be seen that the incorporation of multiple locating faces act to transfer the torque more effectively to the gear teeth, reducing the stress at the locating face.

Figure 80 shows the developed test geometry.

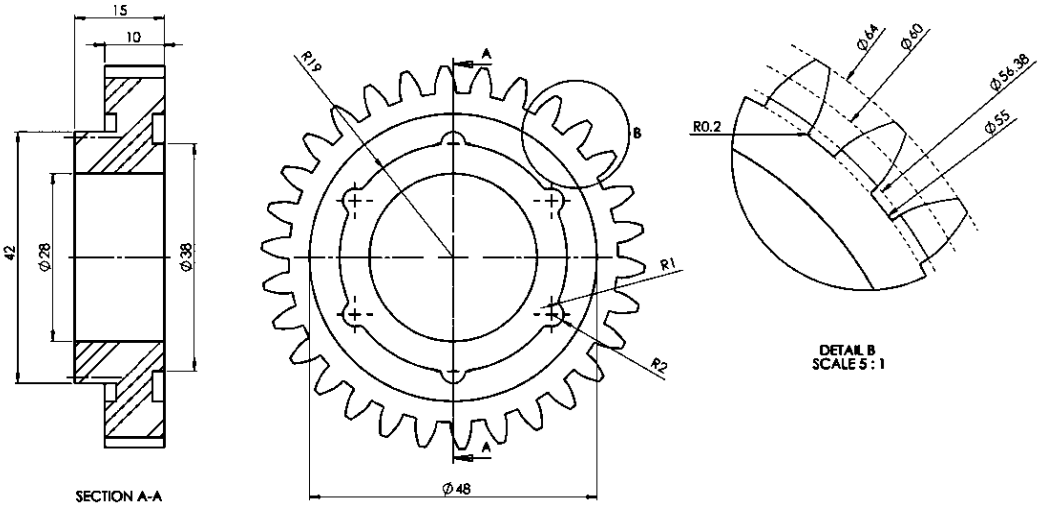

Figure 80: Manufactured gear geometry showing locating faces

Once the test geometries were developed, the resulting design was given to the Centre for Additive Layer Manufacturing (CALM) at the University of Exeter and Produced on an EOSINT P 800 laser sintering system (**Figure 81**).

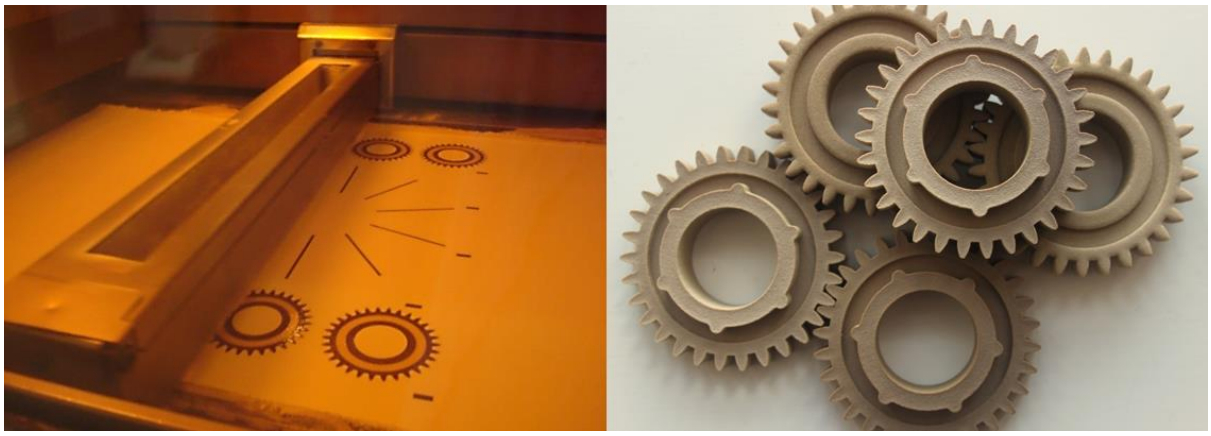

Figure 81: Test gears produced on the EOSINT P800 laser sintering machine

7.3. Test Methods

The MK II gear test rig was modified to allow the new gear hub design to be mounted to the gear test rigs; **Figure 82** shows an exploded view of the hub assembly.

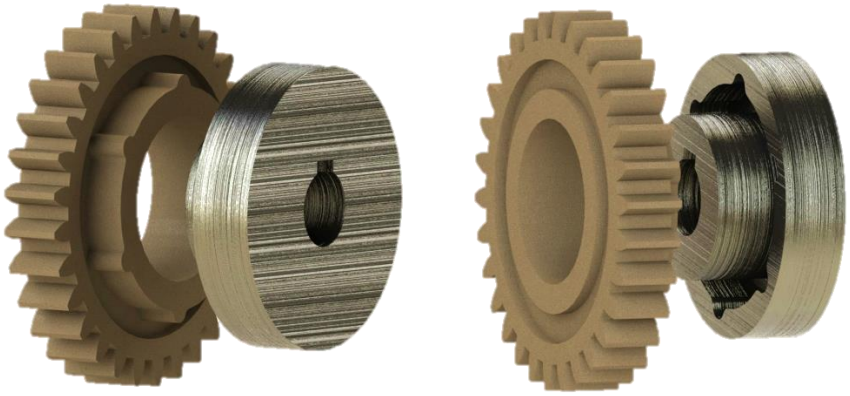

Figure 82: Hub assembly

The test gears were placed on the shafts in the gear test rig and tests were run for a range of loads and speeds, shown in **Table 21**. In addition, lubricated tests were conducted to

establish the contribution of lubricant on the wear and tribological properties of the material.

Table 21: Gear test conditions

Test No.	Test	Lubricated	Load, Speed
1	Steel vs. HP3	✓	8.2Nm, 1500rpm
2	Steel vs. HP3	✓	12.2Nm, 1000rpm
3	Steel vs. HP3	✓	8.2Nm, 1000rpm
4	Steel vs. HP3	✗	8.2Nm, 1000rpm
5	Steel vs. HP3	✗	8.2Nm, 500rpm
6	Injection moulded PEEK vs. HP3	✗	8.2Nm, 1000rpm
7	HP3 vs. HP3	✗	8.2Nm, 1000rpm
8	HP3 vs. HP3	✓	8.2Nm, 1000rpm

Test parameters were identified to promote bending failure in the gear teeth. The results of the proposed investigation were then to be used in parallel with the tribological results obtained in **chapter 6** to establish an optimised gear geometry for high performance laser sintered polymers.

7.4. Results

EOS PEEK HP3 gears were analysed to assess the response of the material to bending fatigue and the influence of polymer gear kinematics on the tribological performance of the contact.

7.4.1. Gear Failure

It was observed that bending fatigue was the predominant form of failure in the EOS PEEK HP3 gears. However, samples were shown to be sensitive to changes in both load and speed, with lubrication significantly improving lifetime for a given load.

Lubrication increased the life of the EOS PEEK HP3 gears. However, for an equivalent torque, lubrication would not reduce the transmitted load. Therefore, the reduction in bending failures suggested that the failure was significantly affected by the lubricant dampening the tooth contact.

Figure 83: Root failures in dry running EOS PEEK HP3 (test 7 and test 5)

Figure 83 shows the failed gear geometry. Individual teeth were plucked from the body of the gear. Closer examination of both the broken tooth and the gear body revealed two distinct regions of failure (**Figure 84**).

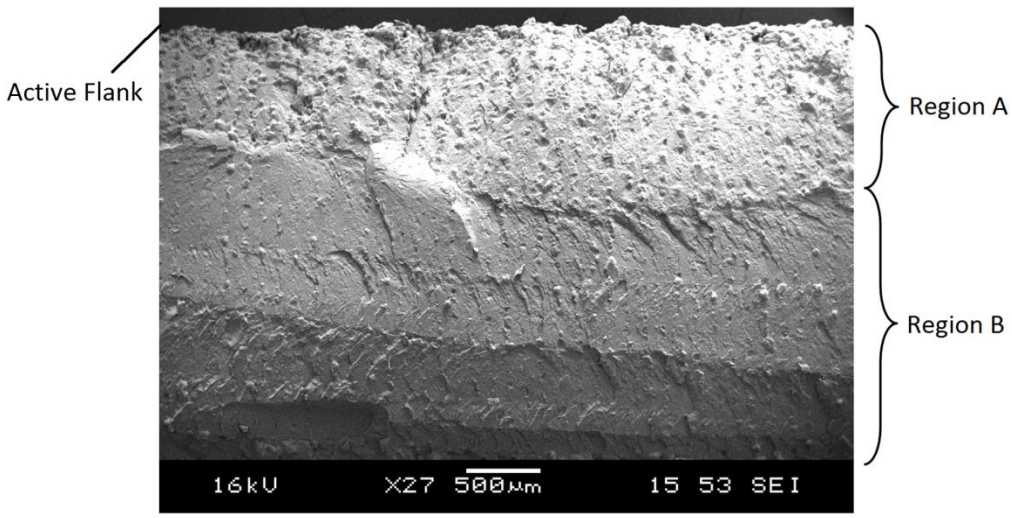

Figure 84: Regions of failure: Region A, inter-granular progressive failure; Region B, surface fracture showing distinct tooth mesh progression

Progressive failure was seen to progress up to 1.5mm into the material before tooth fracture occurred. It could also be seen that the failure typically originated in the centre of the tooth flank and propagated outwards, and that the progressive region was less well defined in highly loaded tests.

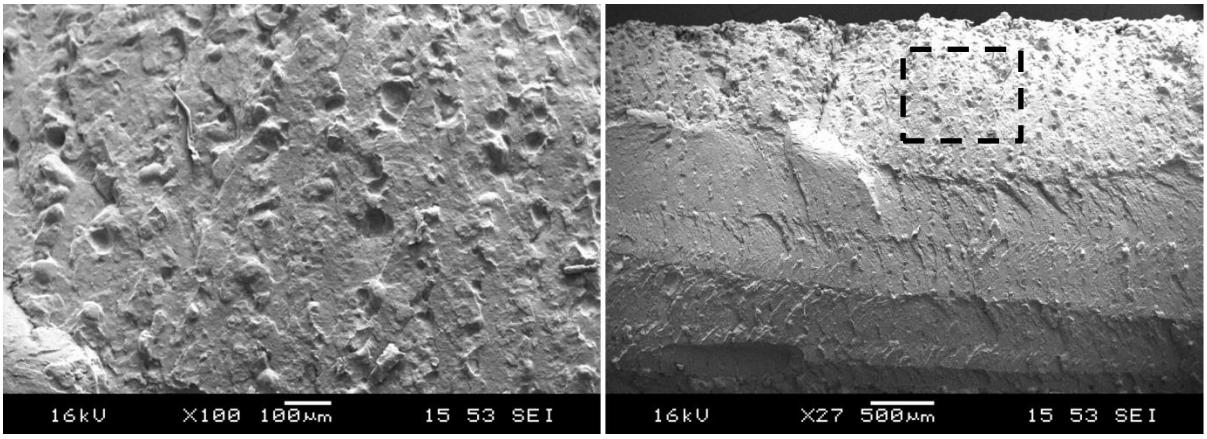

Figure 85: Failure surface, progressive (following stress path defined by the partially sintered material in the component

Figure 85 shows partially sintered material on the failure surface. It could be seen that the partially sintered material was more apparent in the progressive region of the failure. Consequently, it was believed that the stress path, in the region of progressive failure, was governed by the partially sintered powder boundaries in the material.

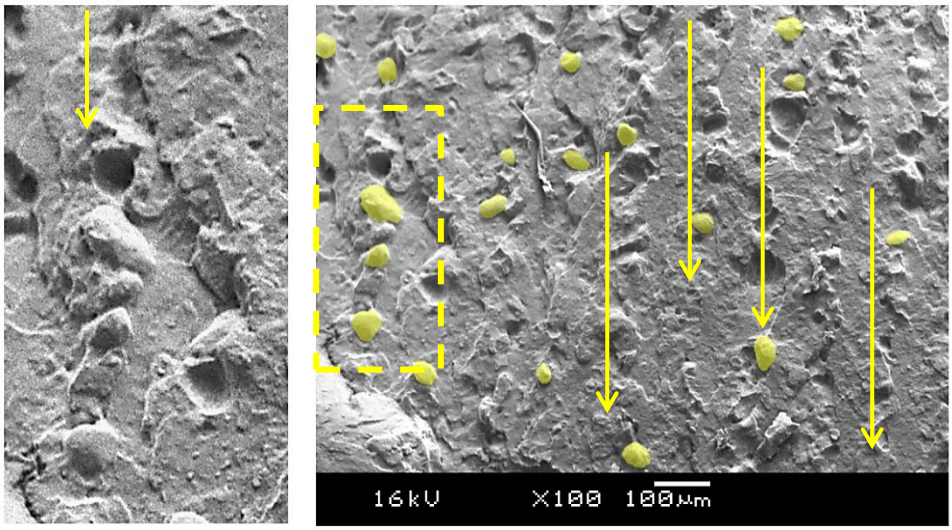

Figure 86: Partially sintered material on the fractured surface

From **Figure 86**, the partially sintered material on the fractured surface could be seen to follow the manufactured plane direction; concentrated to the area adjoining the planes. This suggested that the partially sintered material and, as a consequence, the porosity was isolated to the interface between the manufactured layers where the sintering process was not fully formed.

Similar observations were made in the flexure tests discussed in **section 6.4**.

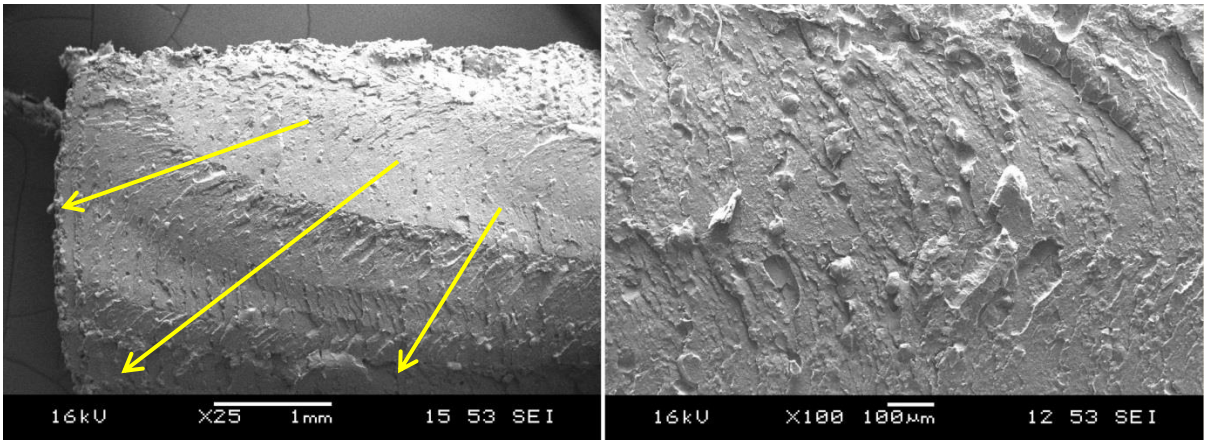

Figure 87: Failure surface (bending failure) showing the direction of failure progression

Figure 87 shows the brittle progression of the failure from the centre of the gear tooth. It could be seen that the failure surface was similar in appearance to those seen in tensile, fracture and flexure testing (**section 6.4**). However, the failure surface did still show progression governed by the tooth loading.

Furthermore, partially sintered material could again be seen on the fractured surface. However, the crack path did not progress between the manufactured planes, instead demonstrating brittle failure associated with single event bending.

The mechanical strength of EOS PEEK HP3, as discussed in **chapter 6**, was limited by the degree of sintering in the bulk of the material. It has been shown that the predominant form of failure seen in the EOS PEEK HP3 test gears was bending fatigue with two regions of failure identified from the failed surface. Therefore, despite the failure surface being similar in appearance to that obtained through mechanical testing, the progression of the failure, as a consequence of the dynamic loading effects, was not observed in the (one-off-load-event) mechanical testing discussed in **chapter 6**.

7.4.2. Gear Wear

To provide accurate tooth wear profiles at various stages of the test, surface replication techniques were used using CharmFlex®Putty hydrophilic vinyl polysiloxane vinyl impression material (Denkist, Inc., South Korea); the test was stopped, putty was formed against the tooth in question, and removed once it was able to hold this form before continuing the test. The overall time taken in this process was less than three minutes meaning thermal effects on the progressive transfer of material and on the tribological properties of the lubricant were deemed negligible.

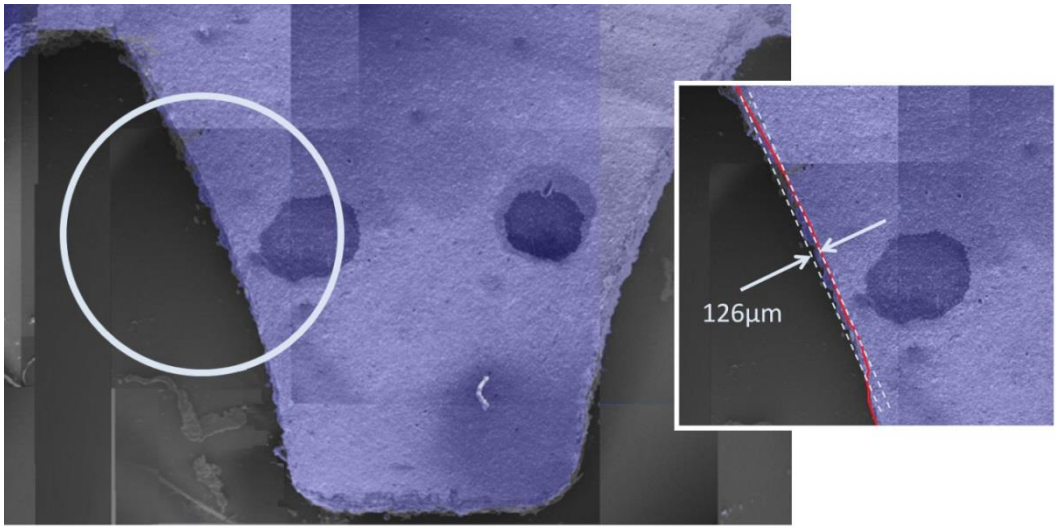

Figure 88: Differential wear measurement using replicated surface profiles

Figure 88 shows the superimposed tooth profiles. Wear measurements could be made to show the progression of wear on the gear tooth profiles. It should be noted that as the test gear geometry was a 1:1 ratio (Ref. **Section 4.5.4.1**) the non-hunting characteristics of the mesh meant that the wear presented by a single tooth mesh could be studied on each tooth up to the point that tooth breakage occurs. Consequently, the tooth profile and the measured wear at the end of the test could be averaged for each tooth mesh.

Figure 89 shows the progression of wear vs. test duration for the tested EOS PEEK HP3 gears.

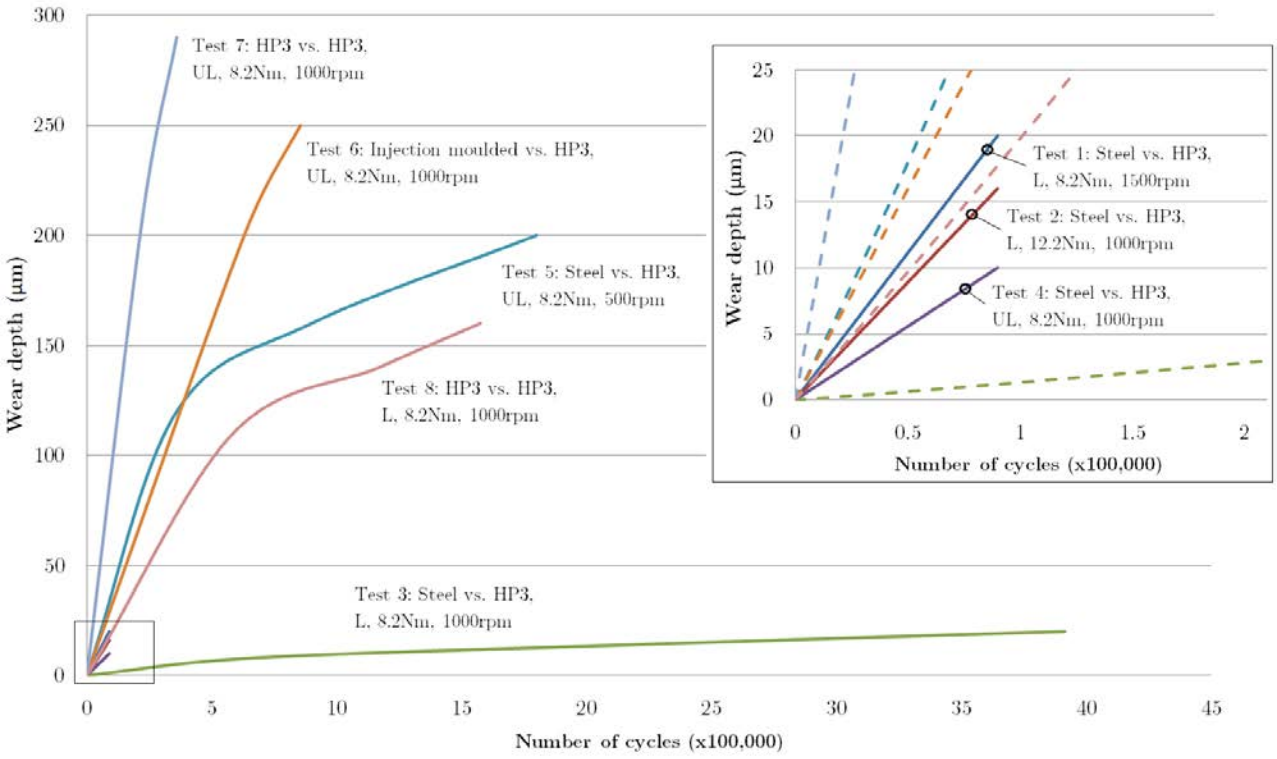

Figure 89: Wear depth vs. number of cycles for the tested EOS PEEK HP3 gears

It was observed that sudden failure occurred following very little wear, suggesting that the impact of wear was minimal in the initiation of tooth failures.

7.4.2.1. Un-lubricated Wear

In **chapter 6**, the tribological properties of EOS PEEK HP3 were shown to be desirable. The tribological responses of the material to both load and speed were good, demonstrating low wear. In unlubricated tests, spreading of asperity material was seen to reduce the material surface roughness dramatically.

However, as discussed throughout this thesis, despite simulated tribological contacts providing an indication of material performance, gear contact is a complex and the only way to accurately specify a material for gearing is through application.

Unlubricated EOS PEEK HP3 gears showed significant amounts of scuffing on the gear flanks, increasing towards the extremities of contact where sliding velocities were highest (**Figure 90**).

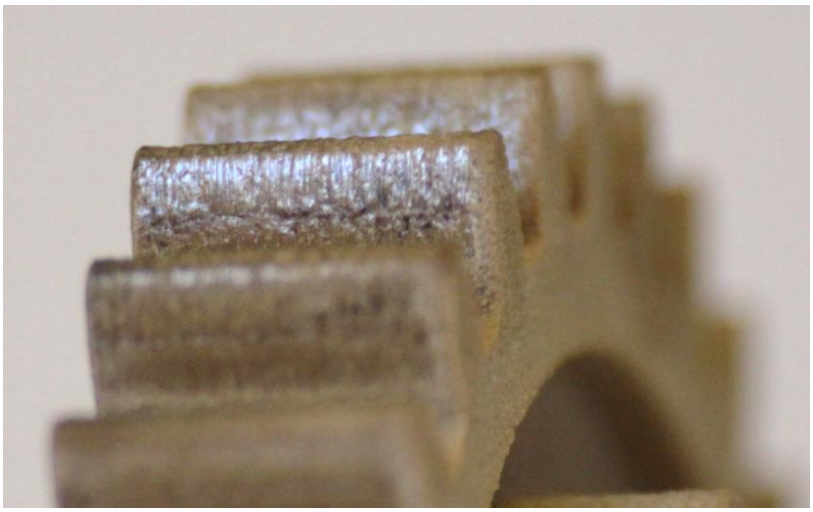

Figure 90: scuffing on addenda of gear tooth

Upon closer examination topographical variations along the gear profile could be seen. **Figure 91** shows the raised pitch line observed in the driven EOS PEEK HP3 gears. It could be seen that the raised pitch line is a result of material build up due to the sliding velocity direction, and debris contained within the contact region. In addition, surface fatigue could be seen around the pitch point due to the high localised contact stress.

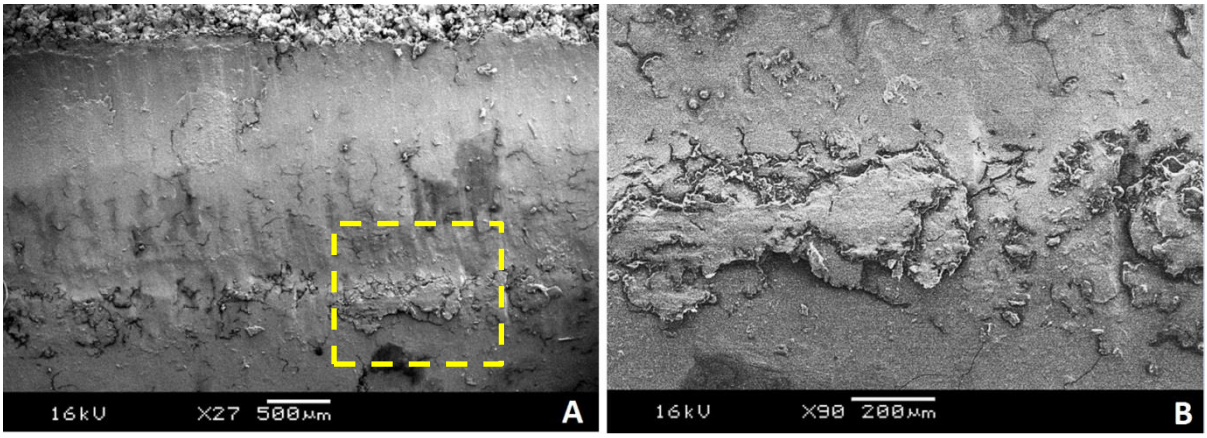

Figure 91: Raised profile on the pitch line of the driven EOS PEEK HP3 gear

Material build up could also be seen at the end of the mesh (**Figure 92**). This is similar to the observations seen in fretting tests (**section 6.7.2.**).

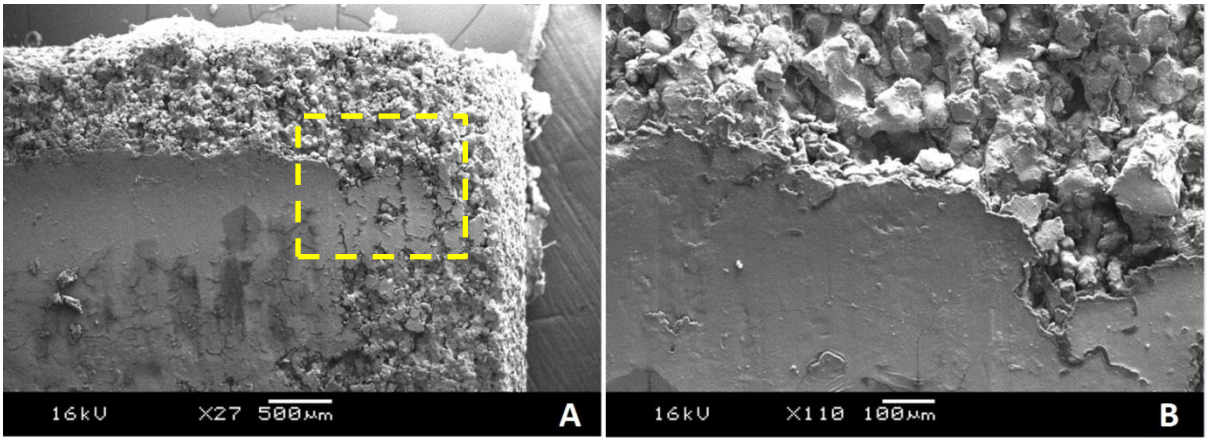

Figure 92: material build-up and smearing can be seen at the end of mesh

However, in contrast to the fretting tests, the worn profile was significantly affected by misalignment due to manufacturing inaccuracies.

During the initial bedding in period, the wear was mainly abrasion; however, the influence of adhesion became more significant as the temperature increased.

When running the EOS PEEK HP3 gears against steel, the impact of adhesive wear was significant. It was observed that polymer material would be transferred onto the conforming steel gear (**Figure 93**). The transfer layer was significantly affected by the rotational speed, being much more prominent in low speed contacts, and stabilising as the test progressed.

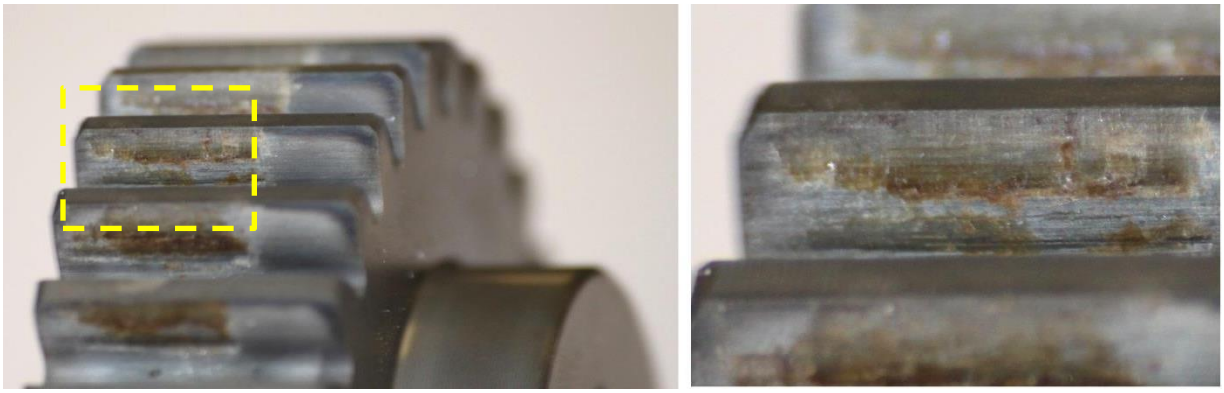

Figure 93: Polymer transfer to the metal counterface (unlubricated)

Figure 94 shows the transferred polymer on the steel gear. It is possible to see that the film was thicker towards the pitch line of the gear, with the metal gear itself showing very little wear. The formation of a polymer transfer layer effectively improved the tribological properties of the contact, reducing the surface roughness of the steel counterface and the resulting abrasive wear.

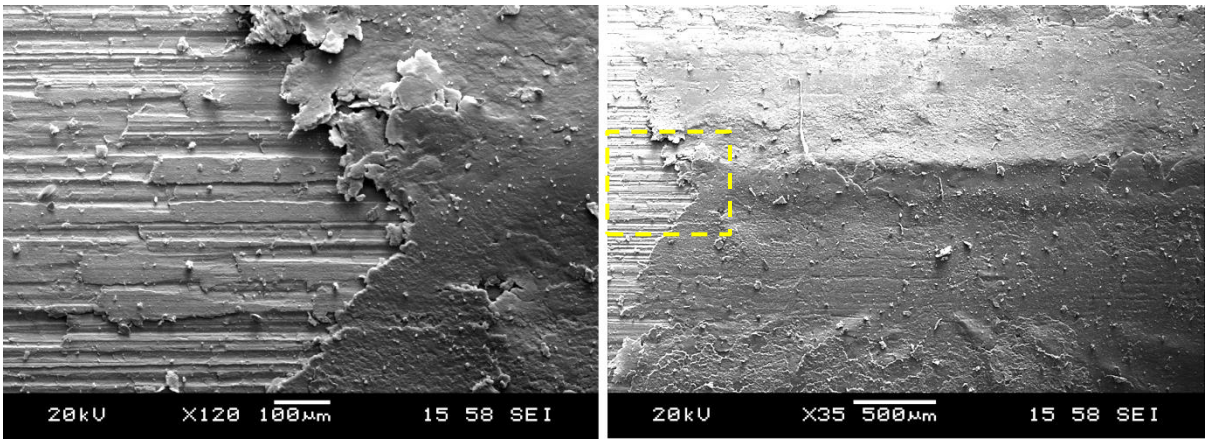

Figure 94: SEM image of polymer transfer to metal counterface

The degree of material transfer seen in the unlubricated tests of EOS PEEK HP3 was significantly more than observed in **section 6.7.2.** It was concluded that the increased material transfer was a result of the increased counterface roughness improving the durability of the transferred material. In addition, the adhesive debris that was not formed as material transfer was contained within the contact in tribological testing, therefore preventing wear from progressing further into the material, and acting to abrade any transferred material off of the counterface.

When running EOS PEEK HP3 against PEEK 450G the counterface was inherently more compliant. This can be seen by the profiling of the EOS PEEK HP3 gear tooth where the tip became rounded due to the extension in the path of contact (**Figure 95B**).

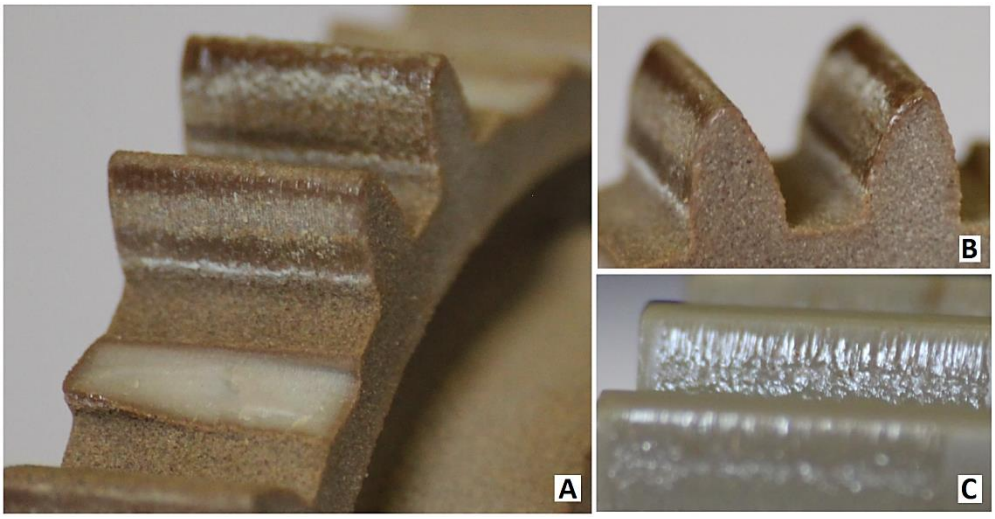

Figure 95: Abrasive transfer of PEEK 450G to laser sintered material a) polymer transfer, b) rounding of tooth profile due to deflection of counterface c) scuffing on PEEK 450G

In addition, material transfer from the PEEK 450G to the EOS PEEK HP3 gear can be seen, with preferential wear occurring on the injection moulded material due to the abrasive action of the laser sintered material (**Figure 95C** and **Figure 96**). It was observed that, although there was a small amount of transfer around the pitch point, the main mechanism of wear was abrasion as the EOS PEEK HP3 asperities and debris ploughed through the injection moulded material.

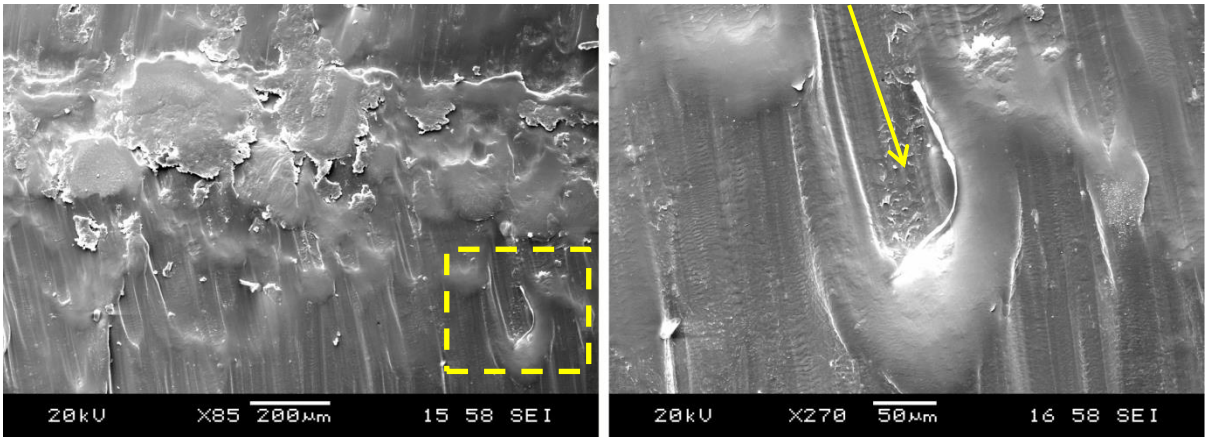

Figure 96: Worn PEEK 450G gear tooth

Figure 97 shows the transferred material seen on the EOS PEEK HP3 gear. The thickness of the film was consistent along the tooth profile, although larger amounts were observed around the pitch point.

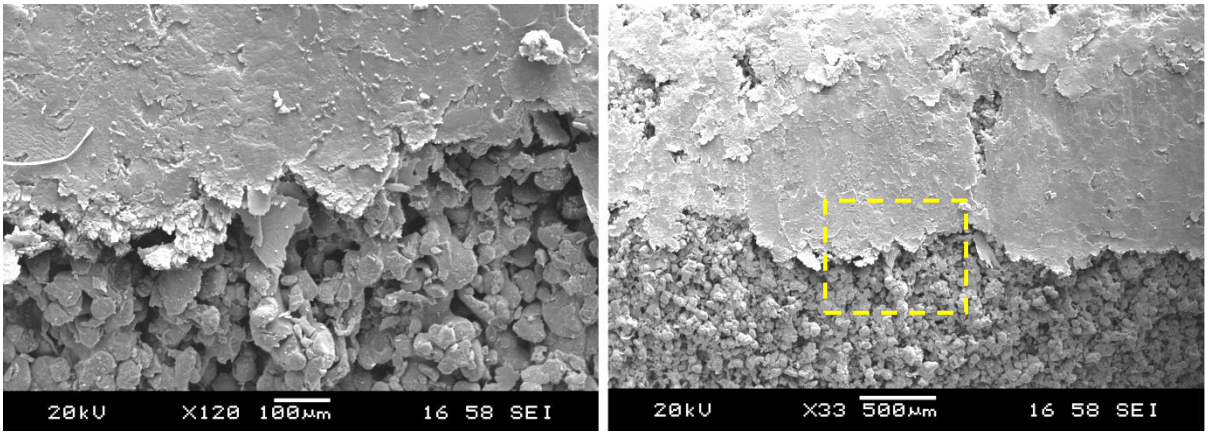

Figure 97: SEM image of PEEK 450G transfer to EOS PEEK HP3 gear

It was observed that there very little surface damage occurred on the EOS PEEK HP3 gear once the transfer film was formed on the surface (**Figure 98**). However, removal of this transfer and the subsequent exposure of the laser sintered material again increased abrasion.

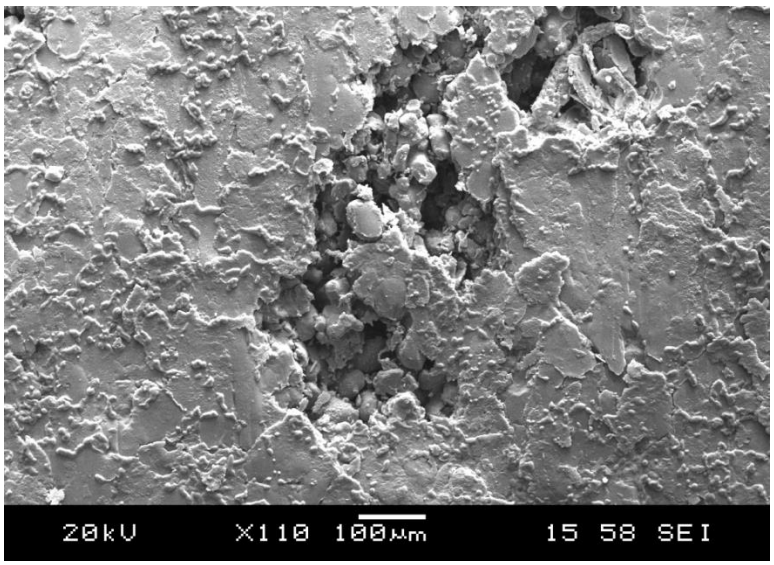

Figure 98: Surface transfer removed from surface of EOS PEEK HP3 gear

7.4.2.2. Lubricated Wear

Lubrication was shown to significantly improve the fundamental tribological properties of EOS PEEK HP3 (**section 6.7**). However, lubrication has also been shown to considerably increase the work of adhesion as the energy required to bring two surfaces into contact is much higher; therefore the formation of adhesive junctions is more difficult, reducing the transferred material. Moreover, as the transferred material was shown to significantly affect the tribological performance of the unlubricated gear contact, the tribological performance of the contact may be reduced.

Figure 99 shows the worn surfaces. It can be seen that there is no obvious transfer layer formed on the steel counterface. Furthermore, the surface of the steel gear showed evidence of wear with metallic material apparent on the surface of the polymer.

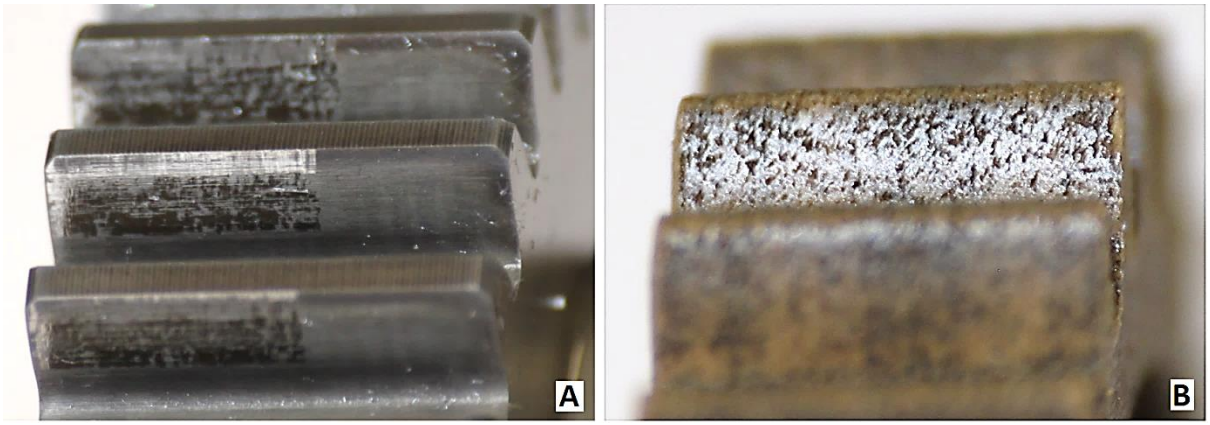

Figure 99: Lubricated wear of: A) steel and; B) EOS PEEK HP3, gear teeth.

To characterise the metallic material seen on the surface of the EOS PEEK HP3 gear, energy dispersive spectroscopy (EDS) was used. From the EDS, significant amounts of both iron and silicon were observed (**Figure 100**).

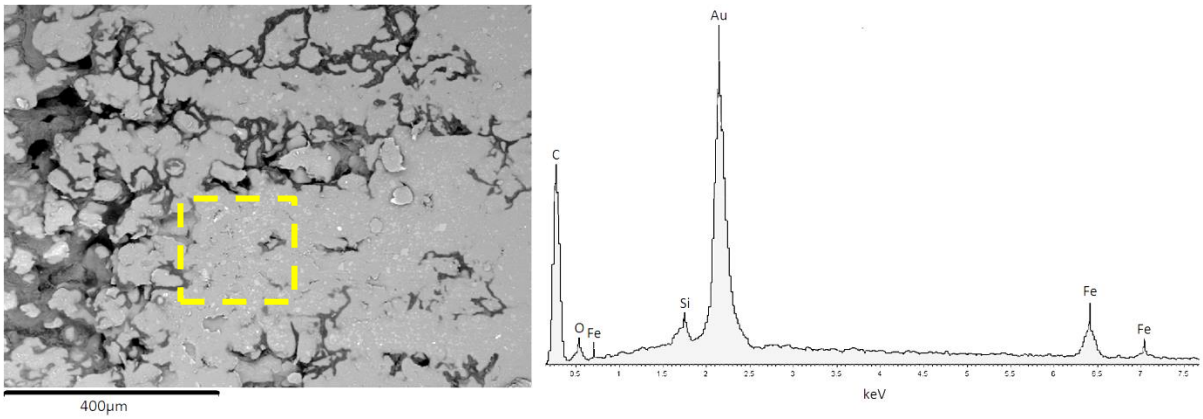

Figure 100: Measured EDS spectrum on the surface of the EOS PEEK HP3 gear[9]

Figure 101 shows the location of the ferrous material on the surface of the EOS PEEK HP3 gear; the majority of which is in the located in the cavities of the unworn surface although significant amounts was also seen on the worn surface.

[9] Gold coating for SEM imaging can be seen in the EDS spectrum

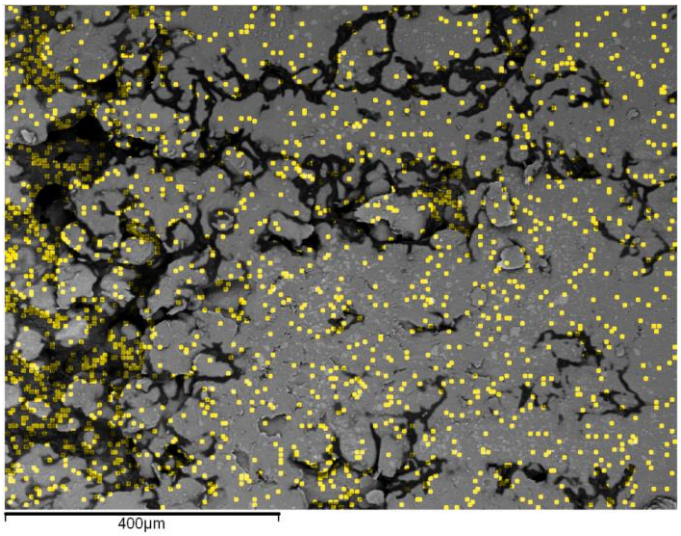

Figure 101: The location of the Iron material on the surface of the EOS PEEK HP3 gear

The metallic particles embedded in the polymer were seen to appear following an initial period of running. **Figure 102** shows the surface of a worn steel gear tooth. Asperity wear could be seen. In addition, the wear was more severe where sliding velocities were highest.

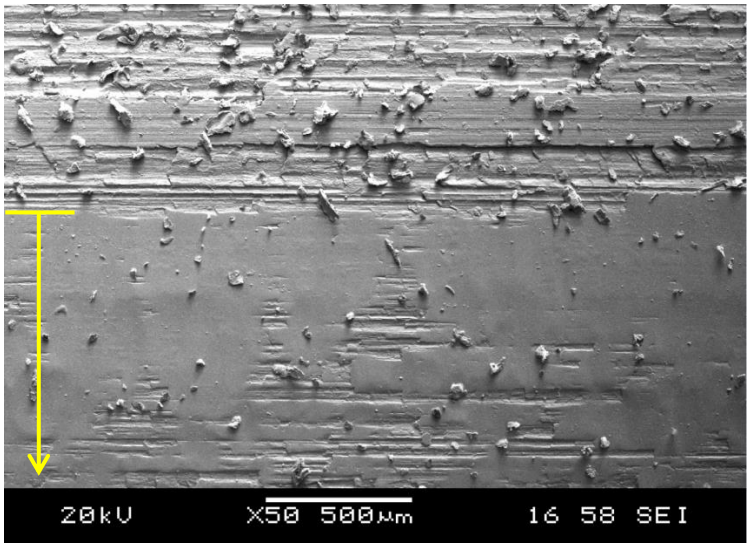

Figure 102: SEM image of worn metal gear tooth

It was concluded that the high contact pressures initiated surface fatigue of the material asperities on the steel gear. Consequently, particles were removed from the surface of the steel gear teeth and suspended in the lubricant. These particles were subsequently caught in the surface asperities and embedded into the surface of the polymer gear. The abrasive action of these metallic particles as the gears meshed increased the wear on the steel gear, effectively polishing the surface of the gear teeth and reducing the surface roughness (**Figure 103**).

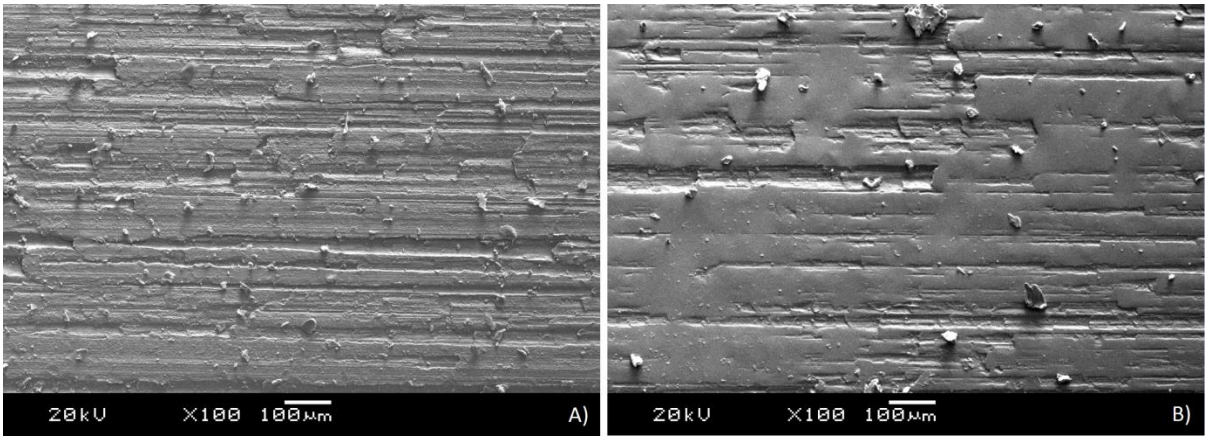

Figure 103: effective polishing of steel counterface. A) un-run surface, b) run surface

The surface of the EOS PEEK HP3 gear teeth showed very little evidence of abrasion or tooth profiling, with a reduction in smearing of asperity material (**Figure 104**).

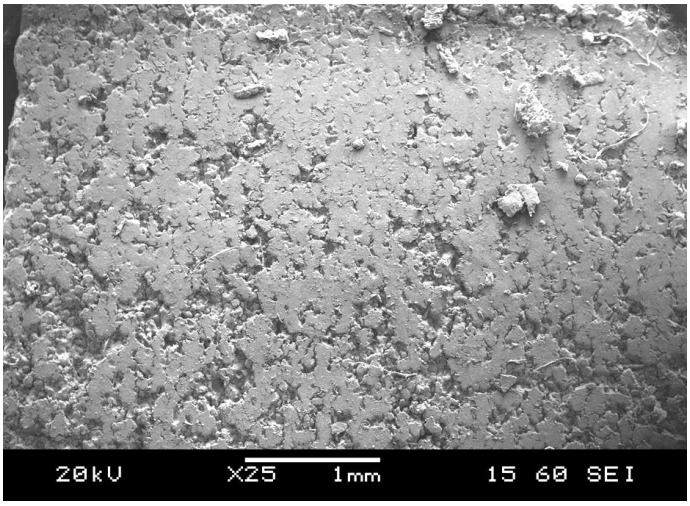

Figure 104: lubricated wear on EOS PEEK HP3 gear tooth

Following prolonged running, small scale pitting (approximately 30µm) was observed at the first point of single tooth contact (**Figure 105**). This was due to the low material compliance resulting in high contact stresses.

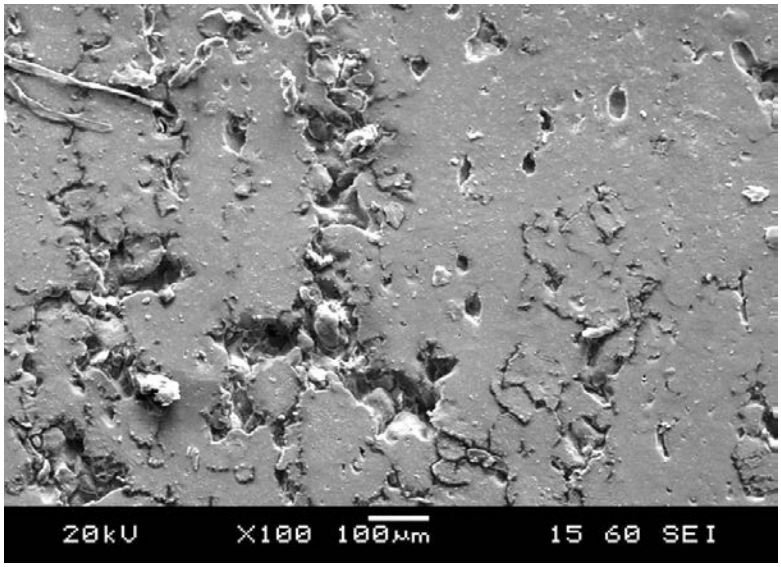

Figure 105: small scale pitting occurring at first point of contact due to the low material compliance leading to high contact stresses

Larger scale macro-pitting was observed at the pitch point of the meshing EOS PEEK HP3 gears (**Figure 106**).

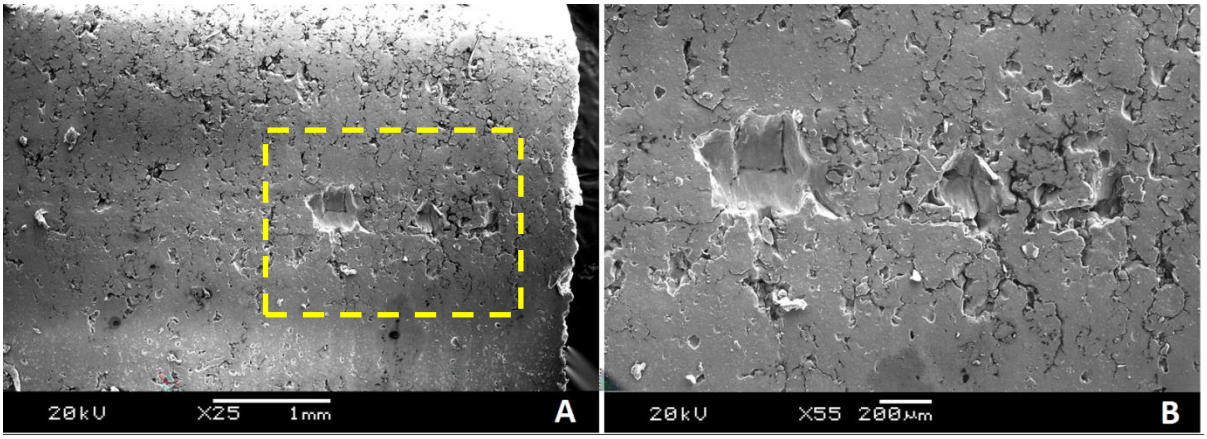

Figure 106: Severe localised pitting can be seen on the pitch line in the lubricated test

This was seen to occur after 3,000,000 cycles and was based on surface fatigue propagating through the partially sintered particle boundaries, resulting in the removal of surface material (**Figure 107**).

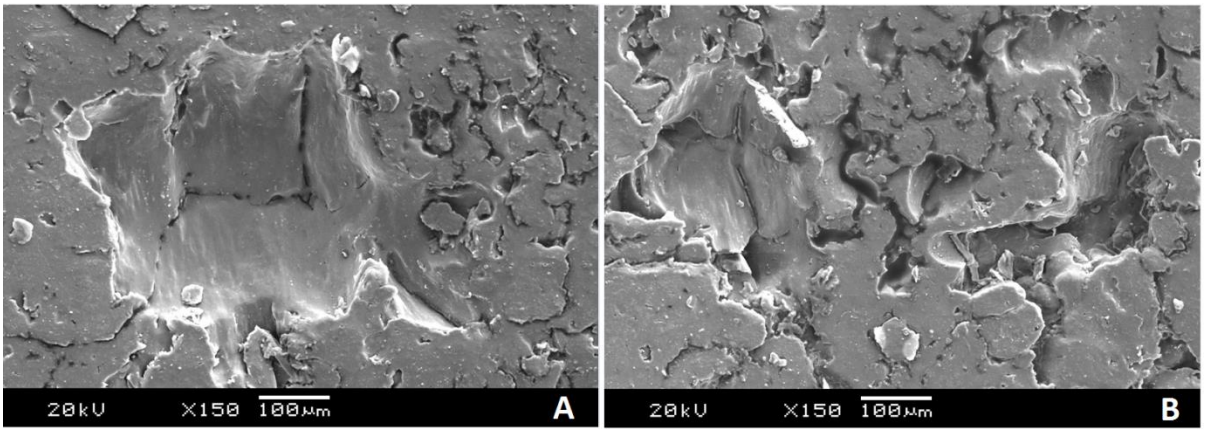

Figure 107: Pitting damage seen at pitch line in the lubricated tests

It was observed that the partially sintered material boundaries on the surface of the material were also visible in the bulk of the material (**Figure 107A**). The progression of the failure into the bulk of the polymer followed a similar mechanism to that seen in

bending fatigue; the progression of a failure into the surface of the material from cyclic stresses and lubrication effects is concentrated on the partially sintered particle boundaries, thus the eventual removal of material is based on this process.

However, it was also observed that the removed areas, although hemispherical, were larger than a single un-sintered particle. On closer examination, it was seen that the progression of the failure was based on progression through the particle boundaries between the manufactured layers.

The significance of this partially sintered material on porosity was shown to be small; however, the removal of these particles can dramatically alter the wear mechanisms observed.

7.5. Conclusions from Gear Testing

Generally, when specifying a polymer for mechanical applications such as gearing, good flexural strength, stiffness and shear strength to resist tooth deflection and tooth root failures should all be considered. In addition, depending on lubrication conditions, consideration should also be given to the frictional properties, and the impact of lubricant on the fatigue properties of the surface.

This section of the thesis reported on the direct application of the laser sintered material EOS PEEK HP3 to power transmission gears, specifically looking at the occurrence and mechanism of bending failure.

It has been shown that the predominant form of failure seen in the EOS PEEK HP3 test gears was bending fatigue. Limited plasticity was seen in failure, although regions of progressive failure and fast fracture could be identified from the failed surface. In addition, the failure stress path, in the region of progressive failure, was governed by the partially

sintered particle boundaries in the material; showing a similar failure response to the flexure testing seen in **chapter 6**.

The tribological characteristics of the worn surfaces were also similar to those seen in **chapter 6**, with EOS PEEK HP3 showing low levels of wear despite the surface roughness of the parts. In addition, it was observed that the surface roughness of the EOS PEEK HP3 gears reduced during bedding in; effectively optimising the tooth profile to the conforming gear face.

Wear mechanisms observed in dry running EOS PEEK HP3 gears included, adhesion, fatigue, fretting and spreading of asperity material. However, when running the EOS PEEK HP3 gears against steel it was observed that polymer material would be transferred onto the conforming steel gear. This transfer layer was much more prominent in the low speed contacts and reduced the abrasion seen in the contact.

In addition material transfer from the PEEK 450G to the EOS PEEK HP3 gear could be seen, with preferential wear occurring on the injection moulded material due to the abrasive action of the laser sintered material.

In the lubricated tests reduced adhesion was observed; no visible transfer layer formed on the steel counterface. In contrast, the surface of the steel gear showed evidence of wear, with metallic material apparent on the surface of the polymer. In addition, the life of the EOS PEEK HP3 gears was increased as the lubricant acted to dampen the impact tooth loading.

After prolonged running, evidence of surface fatigue was seen in the lubricated EOS PEEK HP3 gears, this later propagated into large scale pitting around the pitch point of the gear. The material porosity was found to have a significant effect on the durability of

the material; the failure path, for both bending and contact fatigue, propagated along the particle boundaries, between the manufactured layers.

It was concluded that limitations in the transmissible speed and load were due to the partially sintered particles in the bulk of the material, and the exposed partially sintered particles on the surface. Therefore optimisation of the sintering process and the component geometry would be required to improve durability of the manufactured part.

However, for high power, the low material ductility and toughness means that the increased shock loads will have a significant effect on the bending strength and fatigue properties of the material. Consequently, although the technology was feasible for low power transmission, the performance characteristics of the material when applied to mechanical contacts remain inferior to their injection moulded counterparts.

7.6. Geometry Optimisation

In an attempt to improve the transmissible power levels of EOS PEEK HP3 gears, the results of this investigation were used in parallel with those obtained in **chapter 6** to establish an optimised University of Birmingham gear geometry for high performance laser sintered polymers.

It has been shown that bending fatigue is the predominant failure mechanism in highly loaded laser sintered EOS PEEK HP3 gears. In addition, it has been shown that the tribological response of the material to high contact pressures and sliding velocities are good.

In high compliance polymer gears the path of contact is extended, meaning the load is shared and the contact ratio is increased; reducing the contact stress on the gear teeth

(**chapter 4**). However, EOS PEEK HP3 has a relatively high stiffness; therefore deflection and load sharing effects are less significant.

The mechanical tests in **chapter 6** outlined the low degree of plasticity seen in the failed EOS PEEK HP3 samples. This, coupled with the tooth bending observations seen in the applied gear testing, outlined that geometrical tooth optimisation should be based on improving the bending strength of the gear.

To do this, stub-root gear design methodology has been applied; reducing the overall tooth height. Furthermore, the application of a full fillet radius, generated from the lowest point of tooth contact, will minimise stress concentrations in the root.

Further reductions to the bending stress in the gear root can be made through increasing the pressure angle of the gear teeth, thereby increasing the thickness of the gear tooth at the root, or by increasing the facewidth to offset the fine pitch.

Moreover, the increased radius of curvature of the high pressure angle gears will: reduce the contact stresses, reducing material wear; increase the entrainment velocity, thereby increasing the film thickness between the meshing teeth - reducing tooth wear and heat generation; and reduce the average sliding speed, reducing abrasive wear of the surface.

However, the increased pressure angle will reduce the contact ratio (from 1.654 to 1.474), meaning the transmitted load will be carried by a single tooth, for a longer period during each meshing cycle. In addition, the bottom land is reduced as the pressure angle is increased. This means that the root fillet will almost simultaneously be subject to tensile stress during tooth engagement and a compressive stress as the preceding tooth is loaded. However, stub-root designs move the root diameter up, increasing bottom land and the associated stress razors.

To reduce the impact of low manufactured accuracy and impact loading on the gear meshing characteristics, geometrical alterations can be incorporated into the optimised gear. Small amounts of tip relief, to prevent manufactured tolerances impacting on contact below theoretical lowest point of single tooth contact should be applied.

Profile crowning has also been used to compensate for misalignment in metallic gear sets. However, in laser sintered materials large geometrical lead variations mean that crowning will improve load distribution and prevent contact occurring on the edge of the gear flank.

The manufacturing constraints on injection moulded polymer gears have meant that many forms of profile optimisation are not used. For instance, lead crowning to improve the gear contact position is not used as it results in problematic removal from the mould.

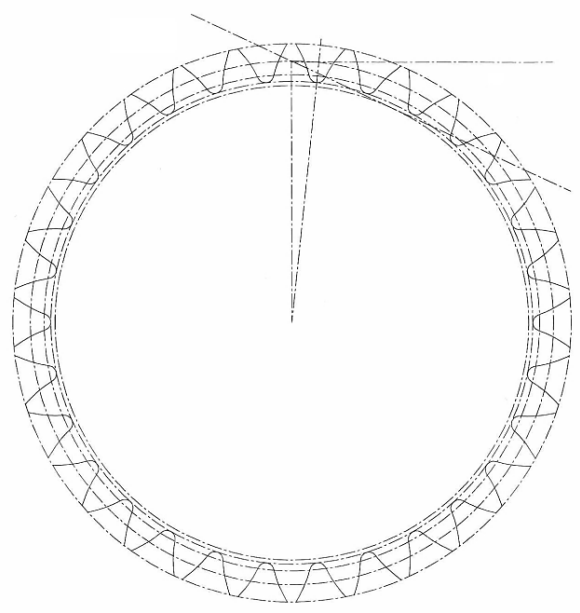

Figure 108: Optimised University of Birmingham gear geometry

Figure 108 shows the optimised University of Birmingham gear geometry. The geometry is based on a 30 teeth, 25° pressure angle, stub-root (full fillet) design with 100µm of crowning. The full geometrical specification is shown in **Table 22**.

Table 22: University of Birmingham laser sintered gear geometry

Number of teeth	30
Normal module	2.000
Normal diametral pitch	12.700
Normal pressure angle	25.00°
Reference centre distance	60.000
Root diameter (mm)	55.239
Tip diameter (mm)	64.000
Pitch diameter (mm)	60.000
Basic rack radius coefficient	0.391
Contact ratio	1.474
Basic rack addenda coefficient	1.040
Basic rack dedenda coefficient	1.150
Tip relief diameter (mm)	61.327
Parabolic tip relief amount (mm)	0.200
Crowning amount (mm)	0.300

The optimised geometry developed here will be used to analyse the effectiveness of a laser sintered polymer for application to power transmission. However, future developments to incorporate cooling holes/internal features to assist with temperature control, define shrinkage rates so that manufactured geometry is manufactured to tighter tolerances, and to investigate asymmetric tooth profiles, could also be made.

Geometrical optimisation methods discussed should be coupled with refinements to the laser sintering process to produce a fully sintered, non-porous structure capable of transmitting high levels of torque.

To conclude, the application of EOS PEEK HP3 to machine elements is desirable; the design flexibility enables the manufacture of components to be design-driven rather than production driven, allowing the design to be tailored for a specific application. Furthermore, despite the limited plasticity shown in the material failure, the mechanical

properties of laser sintered EOS PEEK HP3 demonstrate significant improvements over previously recorded laser sintered polymers and it has been shown that the wear performance of the material is comparable with injection moulded PEEK.

Chapter 8

CONCLUSIONS AND FUTURE WORK

8.1. Chapter Conclusions and Summaries

The application of polymers to machine elements is an emerging area of research; the use of high performance polymers in certain applications significantly reduces the weight, and the requirement of lubrication. However, despite the use of mechanical polymers increasing, there is still a stigma following the use of the material. In addition, the quantification of the material properties and the effect these have on the mechanical performance, under a specific application, are not well understood.

This section will summarise the main conclusions from this programme of work and recommendations for future work to improve the understanding and the transmissible power of polymer machine elements.

8.1.1. Chapter 5

The simplification of polymer gear contact, through the use of fretting and twin disc tests, allows the materials response to the conditions found at the gear tooth interface to be separated from dynamic issues, such as deflection. Thus gear tooth optimisation can be made to determine those conditions for which the material responds best.

It has been shown that the wear of PEEK was dominated by surface fatigue, adhesion and the subsequent ploughing of the counterface through the material. An increase in the coefficient of friction was also observed, a consequence of the high temperatures induced in the closed tribosystem, significantly affecting the occurrence of adhesion.

It was found that fundamental tribological testing of PEEK demonstrated similar failure mechanisms to those observed in polymer gear contact, such as, fatigue at low sliding velocities and fretting at higher speeds.

However, the severity of the test conditions was difficult to control; pressure profiles were based on tooth loading for gears and a constant load for HFRR tests. Therefore, to enable appropriate maximum loads and sliding speeds to be modelled, the maximum tested PV values (pressure x velocity) were up to 60% higher than the maximum values for a perfectly stiff gear.

The wear mechanisms of PEEK running against itself in non-conformal, unlubricated, rolling-sliding contact have been investigated over a range of loads and slip-ratios to determine the effect of temperature and roll/slide interactions on the tribological properties of PEEK.

Overall, the possibility of using PEEK in low slip ratio conditions, for both low and high loads, has been demonstrated, with high temperature operation being possible despite an increase of wear. It has been shown that wear, friction and temperature increase as the slip ratio and the load are increased. However, the wear rates are significantly lower than for other polymers tested using the twin-disc configuration. Failure mechanisms observed on the contact surfaces included surface melting and contact fatigue failures, particularly in the more severe high slip-ratio, high load conditions.

The reduction of load and slip-ratios has been shown to help reduce the generated temperature, and its associated effects around the pitch-point and the region of premature contact. Thus, the possibility of optimising polymeric gear tooth geometry to reduce the slip-ratio away from the pitch point will potentially increase the service life and reduce the occurrence of those wear mechanisms shown in the high slip-ratio tests.

The use of simplified geometry has provided an indication of a materials performance for a specific gear application, with similar wear responses being shown and appropriate sliding speeds and loads being achievable. Therefore the use of these results in conjunction with the design process, can aid in the development of more effective, highly loaded, polymeric gear systems. However, the kinematics of a polymeric gear are complex and to fully understand a material response to the loading conditions found direct gear testing is recommended.

8.1.2. Chapter 6

Traditionally, the properties of a laser-sintered material would be expected to be significantly worse than those of high performance injection-moulded polymers. However, it has been shown that the performance of EOS PEEK HP3 is significantly higher than for previous laser-sintered materials and comparable with high performance injection-moulded materials.

From visual examination it was observed that the roughness of the material was determined by partially sintered particles on the surface.

The failure mechanism observed varied depending on the method of loading; secondary fractures were observed in tensile testing whereas delamination of the material could be seen at higher loads in compressive testing. The surface of the failed compressive strength

samples showed partially sintered powder in the bulk of the material, further examination showed that the bulk of the material was approximately 4% porous with these pores being approximately 24nm in diameter. This should be evaluated to improve the material properties and refine processing parameters as this was not immediately apparent from tensile failures.

Limited plasticity was observed in mechanical testing, with failure occurring along the partially sintered particle boundaries in the material. In addition, the low elongation to break of EOS PEEK HP3 shows that the material is more brittle than PEEK 450G and PA 2201/PA12.

The coefficient of friction and wear of EOS PEEK HP3, as determined by HFRR testing, were significantly better than for injection moulded PEEK 450G (**chapter 4**). It was observed that the wear of EOS PEEK HP3 was dominated by surface asperity contact, with spreading of surface material and asperity wear dominating unlubricated and lubricated wear mechanisms respectively.

In unlubricated contact, high sliding velocities and contact pressures resulted in scuffing/fretting in the centre of the wear scar, whereas high loads at the ends of contact resulted in significant surface fatigue. In lubricated contact, the impact of speed was less significant, although micro-pitting was also seen in highly loaded contact.

By reinforcing SLS PEEK, it was shown that the wear area reduced. However, the wear debris increased due to increased abrasion. It was also observed that the exposed fibres would orientate to the direction of sliding in high speed and high load tests, reducing both friction and wear.

Despite the tribological properties of SLS PEEK being comparable to high performance injection moulded materials, the mechanical strength of the material and the small amount of plasticity during failure may limit its application to non-conformal machine elements.

Overall, the use of EOS PEEK HP3 for impact loading is not recommended as the brittle tendencies may lead to sudden failure. However, design optimisation methods to allow for the distribution of load across a surface are recommended to improve the systemic performance.

As with any material, the specific design requirements may vary with application. Thus, further analysis to replicate the precise operational conditions may be needed. However, this chapter outlines the fundamental mechanical, thermal and physical characteristics of the material and can be used to give an indication of the suitability of HT-SLS materials for mechanical applications.

8.1.3. Chapter 7

Generally, when specifying a polymer for mechanical applications such as gearing, good flexural strength, stiffness and shear strength to resist tooth deflection and tooth root failures should all be considered. In addition, depending on lubrication conditions, consideration should also be given to the frictional properties, and the impact of lubricant on the fatigue properties of the surface.

This section of the thesis reported on the direct application of the laser sintered material EOS PEEK HP3 to power transmission gears, specifically looking at the occurrence and mechanism of bending failure.

It has been shown that the predominant form of failure seen in the EOS PEEK HP3 test gears was bending fatigue. Limited plasticity was seen in failure, although regions of progressive failure and fast fracture could be identified from the failed surface. In addition, the failure stress path, in the region of progressive failure, was governed by the partially sintered particle boundaries in the material; showing a similar failure response to the flexure testing seen in **chapter 6**.

The tribological characteristics of the worn surfaces were also similar to those seen in **chapter 6**, with EOS PEEK HP3 showing low levels of wear despite the surface roughness of the parts. In addition, it was observed that the surface roughness of the EOS PEEK HP3 gears reduced during bedding in; effectively optimising the tooth profile to the conforming gear face.

Wear mechanisms observed in dry running EOS PEEK HP3 gears included, adhesion, fatigue, fretting and spreading of asperity material. However, when running the EOS PEEK HP3 gears against steel it was observed that polymer material would be transferred onto the conforming steel gear. This transfer layer was much more prominent in the low speed contacts and reduced the abrasion seen in the contact.

In addition material transfer from the PEEK 450G to the EOS PEEK HP3 gear could be seen, with preferential wear occurring on the injection moulded material due to the abrasive action of the laser sintered material.

In the lubricated tests reduced adhesion was observed; no visible transfer layer formed on the steel counterface. In contrast, the surface of the steel gear showed evidence of wear, with metallic material apparent on the surface of the polymer. In addition, the life of the EOS PEEK HP3 gears was increased as the lubricant acted to dampen the impact tooth loading.

After prolonged running, evidence of surface fatigue was seen in the lubricated EOS PEEK HP3 gears, this later propagated into large scale pitting around the pitch point of the gear. The material porosity was found to have a significant effect on the durability of the material; the failure path, for both bending and contact fatigue, propagated along the particle boundaries, between the manufactured layers.

It was concluded that limitations in the transmissible speed and load were due to the partially sintered particles in the bulk of the material, and the exposed partially sintered particles on the surface. Therefore optimisation of the sintering process and the component geometry would be required to improve durability of the manufactured part.

However, for high power, the low material ductility and toughness means that the increased shock loads will have a significant effect on the bending strength and fatigue properties of the material. Consequently, although the technology was feasible for low power transmission, the performance characteristics of the material when applied to mechanical contacts remain inferior to their injection moulded counterparts.

8.1.4. Summary

This thesis has outlined testing methods for both laser sintered and injection moulded PEEK for the simulation of polymeric gear contact. This has allowed development of optimised gear tooth geometry to determine the effectiveness of a laser sintered polymer for application to power transmission.

8.2. Future Work

The mechanical and tribological performance of laser sintered PEEK has been shown to be a significant improvement over existing laser sintered polymers and comparable with

injection moulded PEEK. However, the low level of plasticity shown in the material failure limits the transmissible loads.

The following sections outline suggested areas for future work to help improve the understanding of laser sintered polymers, and increase the transmissible gear loads. To do this, material optimisation, testing methods and specific application based problems will be summarised.

8.2.1. Material Optimisation

The surface of the failed compressive strength samples showed partially sintered powder in the bulk of the material, further examination showed that the bulk of the material was approximately 4% porous with these pores averaging 24nm in diameter.

It was concluded that in future, geometrical optimisation methods discussed should be coupled with refinements to the laser sintering process to produce a fully sintered, non-porous structure capable of transmitting high levels of torque.

However, the manufacturing method will always display a degree of anisotropy. Therefore components should be manufactured to ensure that, flexural loads are applied normal to the manufactured plane, and longitudinally in tension.

Future work should also investigate other selectively laser sintered polymers and provide an analytical study into the reduction in material strength through porosity.

8.2.2. Mechanical and Tribological Testing

To improve the understanding of the mechanical and tribological response of EOS PEEK HP3 and other selectively laser sintered polymers, further investigations are proposed. The

continued research in this area will allow further material specific affects to be understood.

Possible future areas of development include:

- The use of lower viscosity lubricants and water lubrication: As the lubricant used in this investigation had a relatively high viscosity, the contact loads were significantly dampened. However, with higher viscosity lubricants the efficiency of transmission will reduce.
- Polished vs un-polished wear properties: As transfer was shown to significantly reduce the abrasive wear seen in EOS PEEK HP3 gears, the influence of counterface roughness on the formation of a more durable transfer should be investigated for unlubricated contact vs. steel.
- Noise emissions: to better understand the tribological response of the material during contact.
- Wear debris characterisation: Further investigations into material wear debris should be made to improve the understanding of the predominant wear mechanisms.
- Fundamental adhesion characterisation vs. temperature for EOS PEEK HP3 to understand the influence of temperature on the frictional properties of the material.
- Twin disc/rolling tests: To investigate the influence of rolling fatigue on material wear.

8.2.3. Gear Design

It is understood that for polymeric gear application, the only way to confidently specify a material is through physical testing. Therefore, the developed laser sintered gear design

methodologies should be used in combination with physical testing to ensure the feasibility of the material for the application.

The optimised geometry developed here can be used to analyse the effectiveness of a laser sintered polymer for application to power transmission. However, future developments to incorporate cooling holes/internal features to assist with temperature control, define shrinkage rates so that manufactured geometry are produced to tighter tolerances, and to investigate asymmetric tooth profiles, should be made.

In addition, further quantification of the thermal properties of laser sintered gears should be made, and the influence of increased temperatures on the long term running fatigue of the material investigated.

References

[1] J.W. Humphrey, J.P. Oleson, A.N. Sherwood., Greek and Roman technology: a sourcebook: annotated translations of Greek and Latin texts and documents., Routledge, 2003.

[2] C. Huygens, Horologium oscillatorium: sive, De motu pendulorum ad horologia aptato demonstrationes geometricae, 1673.

[3] F. Ferfecki, H. A, Polymer Gear Development to Improve Efficiency and NVH Performance of an Engine Mass Balance System, in: SAE World Congr., Detroit, 2011.

[4] L. Snyder, At the "PEEK" of the Polymer Food Chain, Gear Technol. (2010) 22–28.

[5] K. Dearn, S.N. Kukureka, D. Walton, Engineering polymers and composites for machine elements, in: S.K. Sinha B.J. Briscoe Ed. Polym. Tribol., Imperial College Press, London, 2009: pp. 470–505.

[6] Corus, Plc., Corporate governance, London, 2006.

[7] D. V Rosato, D. V Rosato, M.G. Rosato, N.R. Schott, Plastics Engineering, Manufacturing & Data Handbook, 2001.

[8] D. Walton, C.J. Hooke, K. Mao, A.R. Breeds, S.N. Kukureka, A new look at testing and rating non-metallic gears, in: Proc. 3rd World Congr. Gearing Power Transm., Paris, 1992: p. 683.

[9] R.B. Seymour, Engineering polymers sourcebook, McGraw-Hill, New York, 1990.

[10] J. Brandup, E. Immergut, E. Grulke, Polymer handbook, 4th ed., John Wiley & sons, inc, 1999.

[11] K.D. Dearn, An investigation into tribological and performance related aspects of polymeric gearing, PhD thesis: University of Birmingham, 2008.

[12] R.O. Ebewele, Polymer science and technology, CRC Press, 2000.

[13] T.J. Hoskins, K.D. Dearn, Y.K. Chen, S.N. Kukureka, The wear of PEEK in rolling–sliding contact – Simulation of polymer gear applications, Wear. 309 (2014) 35–42.

[14] A.B. Cropper, The failure mode analysis of plastic gears, PhD Thesis: University of Birmingham, 2003.

[15] T. Sınmazçelik, T. Yılmaz, Thermal aging effects on mechanical and tribological performance of PEEK and short fiber reinforced PEEK composites, Mater. Des. 28 (2007) 641–648.

[16] S.M.Y.& E.H.A. S. K. Bhatejaa, Radiation-induced crystallinity changes in linear polyethylene: long-term aging effects in pressure-crystallized ultra-high molecular weight polymer, J. Macromol. Sci. Part B Phys. 29 (1990) 1–10.

[17] C. Hooke, S. Kukureka, P. Liao, M. Rao, Y. Chen, The friction and wear of polymers in non-conformal contacts, Wear. (1996).

[18] N.. Wright, S.. Kukureka, Wear testing and measurement techniques for polymer composite gears, Wear. 251 (2001) 1567–1578.

[19] K.D. Dearn, T.J. Hoskins, D.G. Petrov, S.C. Reynolds, R. Banks, Applications of dry film lubricants for polymer gears, Wear. (2012).

[20] T.L. Orberle, Properties Influencing Wear of Metals, J. Met. 3 (1951) 438–439.

[21] I.M. Hutchings, Tribology — Friction and wear of engineering materials, Tribol. Int. 25 (1992) 357.

[22] B. Briscoe, Wear of polymers: an essay on fundamental aspects, Tribol. Int. 14 (1981) 231–243.

[23] K.A. Laux, C.J. Schwartz, Influence of linear reciprocating and multi-directional sliding on PEEK wear performance and transfer film formation, Wear. 301 (2013) 727–734.

[24] H. Koike, K. Kida, E.C. Santos, J. Rozwadowska, Y. Kashima, K. Kanemasu, Self-lubrication of PEEK polymer bearings in rolling contact fatigue under radial loads, Tribol. Int. 49 (2012) 30–38.

[25] S. Bahadur, The development of transfer layers and their role in polymer tribology, in: Wear, 2000: pp. 92–99.

[26] P.L. Menezes, Kishore, S. V. Kailas, M.R. Lovell, Friction and transfer layer formation in polymer-steel tribo-system: Role of surface texture and roughness parameters, Wear. 271 (2011) 2213–2221.

[27] E.E. Nunez, A.A. Polycarpou, The effect of surface roughness on the transfer of polymer films under unlubricated testing conditions, Wear. 326-327 (2015) 74–83.

[28] W. Wieleba, The mechanism of tribological wear of thermoplastic materials, Arch. Civ. Mech. Eng. VII (2007).

[29] T.J. Hoskins, K.D. Dearn, S.N. Kukureka, D. Walton, Acoustic noise from polymer gears – A tribological investigation, Mater. Des. 32 (2011) 3509–3515.

[30] A.C. Moore, D. Tabor, Some mechanical and adhesive properties of indium, J. Appl. Phys. 3 (1952) 299.

[31] J.K. Lancaster, Basic mechanisms of friction and wear of polymers, Plast. Polym. 41 (1973) 297–306.

[32] J.K. Lancaster, Abrasive wear of polymers, Wear. 14 (1969) 223–239.

[33] Y. Chen, S. Kukureka, C. Hooke, The wear and friction of short glass-fibre-reinforced polymer composites in unlubricated rolling-sliding contact, J. Mater. Sci. (1996).

[34] D.H. Gordon, S.N. Kukureka, The wear and friction of polyamide 46 and polyamide 46/aramid-fibre composites in sliding–rolling contact, Wear. 267 (2009) 669–678.

[35] H. Ruckdäschel, J. Sandler, V. Altstädt, . On the friction and wear of carbon nanofiber-reinforced PEEK-based polymer composites, Tribol. Interface …. (2008).

[36] R. Schroeder, F.W. Torres, C. Binder, a. N. Klein, J.D.B. de Mello, Failure mode in sliding wear of PEEK based composites, Wear. (2012) 1–10.

[37] S. Nak-Ho, N.P. Suh, Effect of fiber orientation on friction and wear of fiber reinforced polymeric composites, Wear. 53 (1979) 129–141.

[38] T.C. Ovaert, H.S. Cheng, Counterface topographical effects on the wear of polyetheretherketone and a polyetheretherketone-carbon fiber composite, Wear. 150 (1991) 275–287.

[39] S. Kukureka, Y. Chen, C. Hooke, P. Liao, The wear mechanisms of acetal in unlubricated rolling-sliding contact, Wear. 185 (1995) 1–8.

[40] S.. Kukureka, C.. Hooke, M. Rao, P. Liao, Y.. Chen, The effect of fibre reinforcement on the friction and wear of polyamide 66 under dry rolling–sliding contact, Tribol. Int. 32 (1999) 107–116.

[41] A. Avanzini, G. Donzella, A. Mazzù, C. Petrogalli, Wear and rolling contact fatigue of PEEK and PEEK composites, Tribol. Int. 57 (2012) 22–30.

[42] M. Buggy, A. Carew, The effect of thermal ageing on carbon fibre-reinforced polyetheretherketone (PEEK), J. Mater. Sci. 29 (1994) 1925–1929.

[43] M. Berer, Z. Major, G. Pinter, Elevated pitting wear of injection molded polyetheretherketone (PEEK) rolls, Wear. 297 (2013) 1052–1063.

[44] S. Kono, Increase in power density of plastic gears for automotive applications, PhD Thesis: University of Birmingham, 2003.

[45] B. Bhushan, Adhesion and stiction: Mechanisms, measurement techniques, and methods for reduction, J. Vac. Sci. Technol. B Microelectron. Nanom. Struct. 21 (2003) 2262.

[46] G. Jintang, Tribochemical effects in formation of polymer transfer film, Wear. 245 (2000) 100–106.

[47] J. Greses, C.M. Stotko, EOS innovations for e-manufacturing : High performance polymers and integrated quality management system, in: Innov. Dev. Virtual Phys. Prototyp., CRC Press, 2011: pp. 659–663.

[48] D. Drummer, D. Rietzel, F. Kühnlein, Development of a characterization approach for the sintering behavior of new thermoplastics for selective laser sintering, Phys. Procedia. 5 (2010) 533–542.

[49] M. Vasquez, B. Haworth, N. Hopkinson, Optimum sintering region for laser sintered nylon-12, Proc. Inst. Mech. Eng. Part B J. Eng. Manuf. 225 (2011) 2240–2248.

[50] G.V. Salmoria, J.L. Leite, R. a. Paggi, a. Lago, a. T.N. Pires, Selective laser sintering of PA12/HDPE blends: Effect of components on elastic/plastic behavior, Polym. Test. 27 (2008) 654–659.

[51] B. Van Hooreweder, D. Moens, R. Boonen, J. Kruth, P. Sas, On the difference in material structure and fatigue properties of nylon specimens produced by injection molding and selective laser sintering, Polym. Test. 32 (2013) 972–981.

[52] U. Ajoku, N. Saleh, N. Hopkinson, R. Hague, P. Erasenthiran, Investigating mechanical anisotropy and end-of-vector effect in laser-sintered nylon parts, Proc. Inst. Mech. Eng. Part B J. Eng. Manuf. 220 (2006) 1077–1086.

[53] R.D. Goodridge, C.J. Tuck, R.J.M. Hague, Laser sintering of polyamides and other polymers, Prog. Mater. Sci. 57 (2012) 229–267.

[54] EOS, Material Data Sheet (preliminary) EOS PEEK HP3, 49 (n.d.) 1–2.

[55] M. Schmidt, D. Pohle, T. Rechtenwald, Selective Laser Sintering of PEEK, CIRP Ann. - Manuf. Technol. 56 (2007) 205–208.

[56] M.A. Beard, O.R. Ghita, J. Bradbury, S. Flint, K.E. Evans, Material characterisation of Additive Manufacturing components made from a polyetherketone (PEK) high temperature thermoplastic polymer, in: Innov. Dev. Virtual Phys. Prototyp., CRC Press, 2011: pp. 329–332.

[57] O.R. Ghita, E. James, R. Trimble, K.E. Evans, Physico-chemical behaviour of Poly (Ether Ketone) (PEK) in High Temperature Laser Sintering (HT-LS), J. Mater. Process. Technol. 214 (2014) 969–978.

[58] O. Ghita, E. James, R. Davies, S. Berretta, B. Singh, S. Flint, et al., High Temperature Laser Sintering (HT-LS): An investigation into mechanical properties and shrinkage characteristics of Poly (Ether Ketone) (PEK) structures, Mater. Des. 61 (2014) 124–132.

[59] R. Drago, Fundamentals of gear design, Butterworths, 1988.

[60] E. Letzelter, M. Guingand, J. de Vaujany, P. Schlosser, A new experimental approach for measuring thermal behaviour in the case of nylon 6/6 cylindrical gears, Polym. Test. 29 (2010) 1041–1051.

[61] H. Düzcükoğlu, R. Yakut, E. Uysal, The Use of Cooling Holes to Decrease the Amount of Thermal Damage on a Plastic Gear Tooth, J. Fail. Anal. Prev. 10 (2010) 545–555.

[62] K. Terashima, N. Tsukamoto, N. Nishida, J. Shi, Development of Plastic Gear for Power Transmission: Abnormal Wear on the Tooth Root and Tooth Fracture near Pitch Point, Bull. JSME. (1986).

[63] D. Koffi, R. Gauvin, H. Yelle, Heat generation in thermoplastic spur gears, J. Mech. Trans. Autom DEs ASME. 107 (1985) 31–37.

[64] M. Karimpour, K.D. Dearn, D. Walton, A kinematic analysis of meshing polymer gear teeth, Proc. Inst. Mech. Eng. Part L J. Mater. Des. Appl. 224 (2010) 101–115.

[65] K. Mao, W. Li, C.J. Hooke, D. Walton, Friction and wear behaviour of acetal and nylon gears, Wear. 267 (2009) 639–645.

[66] M. Rao, C.J. Hooke, S.N. Kukureka, P. Liao, Y.K. Chen, The effect of PTFE on the friction and wear behavior of polymers in rolling-sliding contact, Polym. Eng. Sci. 38 (1998) 1946–1958.

[67] H. İmrek, Performance improvement method for Nylon 6 spur gears, Tribol. Int. 42 (2009) 503–510.

[68] A. Breeds, S. Kukureka, K. Mao, D. Walton, C. Hooke, Wear behaviour of acetal gear pairs, Wear. 166 (1993) 85–91.

[69] K. Mao, A numerical method for polymer composite gear flash temperature prediction, Wear. 262 (2007) 1321–1329.

[70] E. Hatchmann, E. Strickle, Design of Plastic Gears, in: Soc. Plast. Eng. Annu. Technol. Conf., 1968: p. 512.

[71] K. Terashima, N. Tsukamoto, N. Nishida, Development of plastic gears for power transmission: design on load-carrying capacity, Bull. JSME. (1986).

[72] D. Walton, Y. Shi, A comparison of ratings for plastic gears, Arch. Proc. Inst. …. 203 (1989) 31–33.

[73] S. Senthilvelan, R. Gnanamoorthy, Damage Mechanisms in Injection Molded Unreinforced, Glass and Carbon Reinforced Nylon 66 Spur Gears, Appl. Compos. Mater. 11 (2004) 377–397.

[74] M. Kurokawa, Y. Uchiyama, S. Nagai, Performance of plastic gear made of carbon fiber reinforced poly-ether-ether-ketone, Tribol. Int. 32 (1999) 491–497.

[75] M. Kurokawa, Y. Uchiyama, S. Nagai, Performance of plastic gear made of carbon fiber reinforced poly-ether-ether-ketone: Part 2, Tribol. Int. 33 (2000) 715–721.

[76] H. Giesche, Mercury Porosimetry: A General (Practical) Overview, Part. Part. Syst. Charact. 23 (2006) 9–19.

[77] M.. Jenkins, Crystallisation in miscible blends of PEEK and PEI, Polymer (Guildf). 42 (2001) 1981–1986.

[78] J. Atkinson, J. Hay, M. Jenkins, Enthalpic relaxation in semi-crystalline PEEK, Polymer (Guildf). 43 (2002) 731–735.

[79] P.K. Meuleman, D. Walton, K.D. Dearn, D.J. Weale, I. Driessen, Minimization of transmission errors in highly loaded plastic gear trains, Proc. Inst. Mech. Eng. Part C J. Mech. Eng. Sci. 221 (2007) 1117–1129.

[80] E. Sukjit, K.D. Dearn, Enhancing the lubricity of an environmentally friendly Swedish diesel fuel MK1, Wear. 271 (2011) 1772–1777.

[81] L. Shen, T. Liu, P. Lv, Polishing effect on nanoindentation behavior of nylon 66 and its nanocomposites, Polym. Test. 24 (2005) 746–749.

[82] H. Hertz, Über die Berührung fester elastischer Körper, J. Für Die Reine U. Angew. Math. 92 (1882) 156–171.

[83] J. White, The design and evaluation of polymer composite spur gears, PhD Thesis: University of Birmingham, 1999.

[84] D. Walton, A.B. Cropper, D.J. Weale, P.K. Meuleman, The efficiency and friction of plastic cylindrical gears. Part 1: the influence of materials, Proc. Inst. Mech. Eng. J. 216 (2002) 75–92.

[85] H. Blok, The flash temperature concept, Wear. 6 (1963) 3509–3515.

[86] Victrex, Material Data Sheet Victrex ® PEEK 450G, (n.d.) 1–2.

[87] F.E. Kennedy, X. Tian, Dissipative Processes in Tribology, Proceedings of the 20th Leeds-Lyon Symposium on Tribology held in the Laboratoire de Mécanique des Contacts, Institut National des Sciences Appliquées de Lyon, Elsevier, 1994.

[88] P.J. Rae, E.N. Brown, E.B. Orler, The mechanical properties of poly(ether-ether-ketone) (PEEK) with emphasis on the large compressive strain response, Polymer (Guildf). 48 (2007) 598–615.

[89] G.M.K. Ostberg, J.C. Seferis, Annealing effects on the crystallinity of polyetheretherketone (PEEK) and its carbon fiber composites, App. Polym. Sci. 33 (1986) 29–33.

[90] S. Mukherjee, S.A. Jabarin, Aging characteristics of orientated poly(ethyleneterephthalate), Polym. Eng. Sci. 35 (1995) 1145–1154.

[91] H. Zarringhalam, C. Majewski, N. Hopkinson, Degree of particle melt in Nylon-12 selective laser-sintered parts, Rapid Prototyp. J. 15 (2009) 126–132.

[92] EOS, Material Data Sheet EOS PA2201/PA12, 49 (n.d.) 1–2.

[93] M.P. Sepe, Dynamic Mechanical Analysis for Plastics Engineering, William Andrew Publishing/Plastics design library, 1998.

[94] J. Sandler, P. Werner, M. Shaffer, Carbon-nanofibre-reinforced poly (ether ether ketone) composites, Compos. Part A …. 33 (2002) 1033–1039.

List of Figures